FOLDING STUDIES OF OVINE PRION PROTEINS

By

Kai-Chun Chen

A DISSERTATION

Submitted to
Michigan State University
in partial fulfillment of the requirement
for the degree of

DOCTOR OF PHILOSOPHY

Physiology

2010

ABSTRACT

FOLDING STUDIES OF OVINE PRION PROTEINS

By

Kai-Chun Chen

Several studies on scrapie in sheep have shown that the propensity for the conversion of a naturally occurring protein PrP from its normal cellular form (PrP^{C}) to a virulent scrapie form (PrP^{Sc}), both *in vitro* and *in vivo*, correlates with susceptibility to the disease. Since scrapie results from the PrP^{C}-to-PrP^{Sc} conversion, the PrP^{Sc} precursor occurring in PrP folding should play a key role in modulating disease occurrence. Susceptibility to classical scrapie correlates strongly with specific polymorphisms at positions 136, 154, and 171 in ovine prion proteins (ovPrPs). Therefore, I hypothesized that these polymorphisms affect scrapie susceptibility by modulating the structure and population of the PrP^{Sc} precursor. This hypothesis led to two sub-hypotheses: *First*, folding and unfolding of ovPrPs proceed through an intermediate. *Second*, this intermediate is the precursor of PrP^{Sc}.

In this dissertation, I examined whether an intermediate state occurs in ovPrP (un)folding using a continuous-flow mixing method. Four PrP variants, comprising residues 94-233 of full-length ovPrP and correlated with differing susceptibilities to classical scrapie in sheep, were studied. An initial lag phase in refolding and unfolding kinetics indicates the presence of a native-like intermediate. I found that the relative populations and structural stability of the folding intermediates in these variants

correlate with their propensities for classical scrapie. Variants susceptible to classical scrapie appear to have a larger population and higher structural stability in their intermediate states than do resistant variants. This could give susceptible variants more opportunities to undergo the PrP^{C}-to-PrP^{Sc} conversion and oligomerize. Therefore, I argue that the observed folding intermediate is the precursor of PrP^{Sc}. A model for amyloid formation is proposed:

$$\textit{Conformational folding of } PrP^{C}\text{: } N \leftrightarrow I \leftrightarrow U$$

$$\text{Assembly of } PrP^{Sc} \text{ oligomers: } (PrP^{Sc})_n + I \rightarrow (PrP^{Sc})_{n+1}$$

where *N*, *I*, and *U* represent native, intermediate, and unfolded states, respectively.

Contrary to earlier studies on human PrP, I was unable to resolve any kinetic intermediate under refolding conditions within the dead-time of our instrument (~90 μs). Thus, I postulate that the folding kinetics of ovPrPs differs from the kinetics of human PrPs, which could reflect structural differences in their respective intermediates.

Residues (136, 154, and 171) involved in genetic modulation are distant in the primary structure. Since ovPrP variants exhibit differing population and structural stability in their intermediate state, the polymorphism may modulate structural conversion through long-range interactions on the intermediate species. Consistent with this idea, a peptide model that is not involved in genetic modulation shows that local interactions in the vicinity of the disulfide bond do not suffice for the formation of a folding intermediate.

To Bill and My Family

ACKNOWLEDGEMTS

First and foremost, I would like to thank my advisor Dr. William Wedemeyer, who brought me into this exciting field, and provided me with his total trust. I would also like to thank my collaborator Dr. Heinrich Roder, who is my life-saver. Without their continuous scientific and spiritual support, this work would never be done.

I want to acknowledge my committee members, including Drs. Kathleen Gallo, David Kreulen, Vilma Yuzbasiyan-Gurkan, and Birgit Zipser for their guidance and encouragement. I will always remember the time they spent on my second preliminary exam. Thanks for making me talk and connect to the outside world.

I appreciate the help from the MSU Physiology department, especially from Richard Brandt, Kim Crain, and Dr. Arthur Weber. They always tried to solve problems for me even before I recognized them. I acknowledge Terry Ball, Yi-Heng Sen, and Drs. Daniel Jones, Jon Kaguni, Lisa Lapidus, Min-Hao Kuo, Xue Li, Denise Mills, Jose-Luis Gallegos-Perez, Dean Shooltz, John Wang, Ming Xu, and Honggao Yan for their scientific support. I also thank supports from The Lim Pen-Yuan Cultural and Educational Foundation and my previous educators in Taiwan.

I want to express many thanks to my friends for going through the stress and depression with me along the whole PhD program. Ahlen, Chin-Mei, Chun-I, Feng, Guillermo, Hui-Wen, Joyce, Shuyi, Weining, Yi, Yvette, and many other people, I hope that absorbing those negative emotions has not caused permanent damage to your mental health.

Last but not least, I want to send bunches of appreciation to my family. I thank my parents for their continuous loving nags. I acknowledge the warmth transmitted by the daily phone calls from my lovely sisters. I also appreciate my brother in-law Hari for his long-standing support.

TABLE OF CONTENTS

LIST OF TABLES

LIST OF FIGURES

LIST OF ABBREVIATIONS

AD: Alzheimer's disease

Ala (A): Alanine

ALS: Amyotrophic lateral sclerosis

ANS: 8-Anilinonaphthalene-1-sulfonic acid

Arg (R): Arginine

Asp (D): Aspartic acid

BSE: Bovine spongiform encephalopathy (mad cow disease)

CD: Circular dichroism

CI2: Chymotrypsin inhibitor 2

CJD: Creutzfeldt-Jacob disease

CNS: Central nervous system

CWD: Chronic wasting disorder

Cys: Cystine (disulfide bond)

ER: Endoplasmic reticulum

fCJD: Familial CJD

FFI: Fatal familial insomnia

FSE: Feline spongiform encephalopathy

Gln (Q): Glutamine

GSS: Gerstmann-Straussler-Scheinker diseases

GuHCl: Guanidine hydrochloride

HD: Huntington's disease

HDX: Hydrogen/deuterium exchange

His: Histidine

I_{α}: Intermediate state

IPTG: Isopropyl β-D-1-thiogalactopyranoside

Leu (L): Leucine

LRS: Lymphoreticular system

MALDI-TOF-MS: Matrix-assisted laser-desorption/ionization time-of-flight mass spectrometry

Met (M): Methionine

N: Native folded state

NATA: *N*-acetyl tryptophan amide

NBS: *N*-bromo-succinamide

Ni-NTA: Nickel-nitrilotriacetic acid

ORF: Open reading frame

OvPrP: Ovine prion protein

PD: Parkinson's disease

Phe (F): Phenylalanine

PMD: Protein misfolding disorder

Prion: The infectious agent that is believed to cause TSEs. It denotes to 'small proteinaceous infectious particle'

Pro (P): Proline

PrP: Prion protein

PrP^{C}: The normally occurring cellular form of a PrP

PrP^{Sc}: An abnormal form of a PrP that is involved in prion disease. Its conformation differs from PrPC, and its aggregate is associated with infectivity in prion diseases

RP-HPLC: Reverse-phase high-performance liquid chromatography

TCEP: Tris-(2-carboxyethyl) phosphine hydrochloride

TMT: Transmissible mink encephalopathy

Trp (W): Tryptophan

TS: Transition state

TSE: Transition state ensemble

TSE: Transmissible spongiform encephalopathy

Tyr (Y): Tyrosine

Phe (F): Phenylalanine

Pro (P): Proline

U: Unfolded state

UV: Ultraviolet

Val (V): Valine

Chapter 1. Introduction to Prion Diseases

Prion diseases, also termed transmissible spongiform encephalopathies (TSEs), are a group of fatal neurodegenerative diseases including scrapie in sheep and goats, bovine spongiform encephalopathy in cattle (mad cow disease), chronic wasting disorder (CWD) in deer and elk, fatal familial insomnia (FFI), Gerstmann-Straussler-Scheinker diseases (GSS), as well as Creutzfeldt-Jacob disease (CJD) in humans (Table 1). Based on the etiologies, TSE can be classified as sporadic, inherited, and acquired. The pathologic changes include vacuolation, neuronal death, and astrocytosis in the central nervous system (CNS)(*1*). Despite intensive studies, the means of treatment and diagnosis are still limited by our current knowledge of its pathogenesis.

Table 1.1. Prion diseases in humans and animals(*2-3*)

Disease	Host	Etiology
Kuru	humans	infection through cannibalism
Iatrogenic CJD	humans	transmitted through neurosurgical procedures or administration of pituitary tissue extracts
Variant CJD	humans	infection from bovine prions
Familial CJD	humans	germline mutations
FFI	humans	germline mutations
Sporadic CJD	humans	somatic mutations or spontaneous PrP^{C}-to-PrP^{Sc} conversion (uncertain)
Classical Scrapie	sheep	infection in genetically susceptible sheep
Atypical Scrapie	sheep	sporadic (uncertain)
BSE (bovine spongiform encephalopathy)	cattle	infection with contaminated meat and bone meal (MBM)
TMT (transmissible mink encephalopathy)	mink	infection with prions from sheep or cattle
FSE (feline spongiform encephalopathy)	cats	infection with contaminated bovine tissues or MBM
CWD (chronic wasting disease)	deer, elk	unknown

1.1. Protein-only hypothesis.

The identity of TSE infectious agent had been puzzling for decades. Based on its resistance to ultraviolet (UV) irradiation, Alper and Griffith suggested that this agent is solely composed of proteins and might be able to self-replicate(*4-5*). However, further evidence did not appear until twenty years later. In the 1980s, Prusiner *et al.* isolated this agent with high purity, and reported three observations supporting the '*protein-only hypothesis*': *First*, this agent is resistant to procedures that attack nucleic acids. *Second*, treatments that modify proteins can diminish scrapie infectivity. *Third*, this agent is smaller than a virus, a spiroplasma-like organism, or a parasite. The name 'prion' was coined to denote this agent as 'a small proteinaceous infectious particle'(*6*).

Purified prions were used to identify the cDNA clone encoding the entire open reading frame (ORF) of a prion protein (PrP)(*7*). A chromosomal gene encoding PrP was subsequently identified(*8*). The entire ORF of *Prnp* genes is contained within a single exon, suggesting that alternative splicing seems unlikely to explain the two PrP isoforms(*7-8*). A later study suggested that the normal cellular form (PrP^{C}) and the virulent scrapie form (PrP^{Sc}) share the same primary structure; therefore, the pathogenic conversion of PrP seems to involve either posttranslational modifications or conformational changes(*9*). Although earlier studies suggested that posttranslational modifications are not involved in the pathogenic conversion(*10*), emerging evidence indicates that covalent differences might exist in these two isoforms(*11-12*). By contrast, dramatic structural changes have been observed upon PrP^{C} to PrP^{Sc} conversion(*13-15*).

Substantial evidence supports the *protein-only hypothesis*. *First*, prion infectivity is reduced by antibody against PrP(*16-18*). *Second*, prions from inherited diseases are infectious to experimental animals(*19*). *Third*, mice lacking PrP^{C} do not support conversion to PrP^{Sc}(*20*). *Fourth*, the scrapie agent is able to induce propagation of infectivity in neuroblastoma cells(*21-22*).

Since the *protein-only hypothesis* suggests that prion diseases result from the structural conversion of PrP^{C} to PrP^{Sc}(*6*), its final proof can be archived only if conversion of a pure PrP^{C} to a form that causes prion diseases can be carried out *in vitro*. Caughey *et al*. have developed the first successful *in vitro* conversion assay, termed as cell-free conversion methods. Although it generates misfolded proteins similar to PrP^{Sc}, these preparations are not infectious(*23-24*). Another important *in vitro* conversion system, termed as protein-misfolding cyclic amplification assay (PMCA), has been developed by Soto *et al*.. In this method, PrP^{Sc} amplification is carried out via cycles of incubation and sonication (Figure 1.1)(*25*). The *de novo* generated PrP^{Sc} has been proved to be infectious when brain homogenates were used as PrP^{C} and PrP^{Sc} sources; nevertheless, cofactors have been suggested to involve in this conversion process(*25-27*). A recent advance in this field is that structural conversion has been carried out using recombinant PrP^{C} purified from *E. coli*. Wang *et. al.* have shown that prions with relatively high infectivity can be generated using recombinant PrP^{C} in the presence of lipid and RNA in PMCA method(*27*). A very recent report provides compelling evidence for the protein-only hypothesis. Kim *et al.* have observed that PrP^{Sc} infectivity can be propagated using either

the full-length or the C-terminal domain of a recombinant PrP^{C} in the absence of cofactors in PMCA method(*28*). However, the *de novo* generated PrP^{Sc} exhibits much lower infectivity, as compared to the previous preparation in the presence of lipid and RNA, suggesting that these cofactors facilitate, instead of determine, the structural conversion process(*28*).

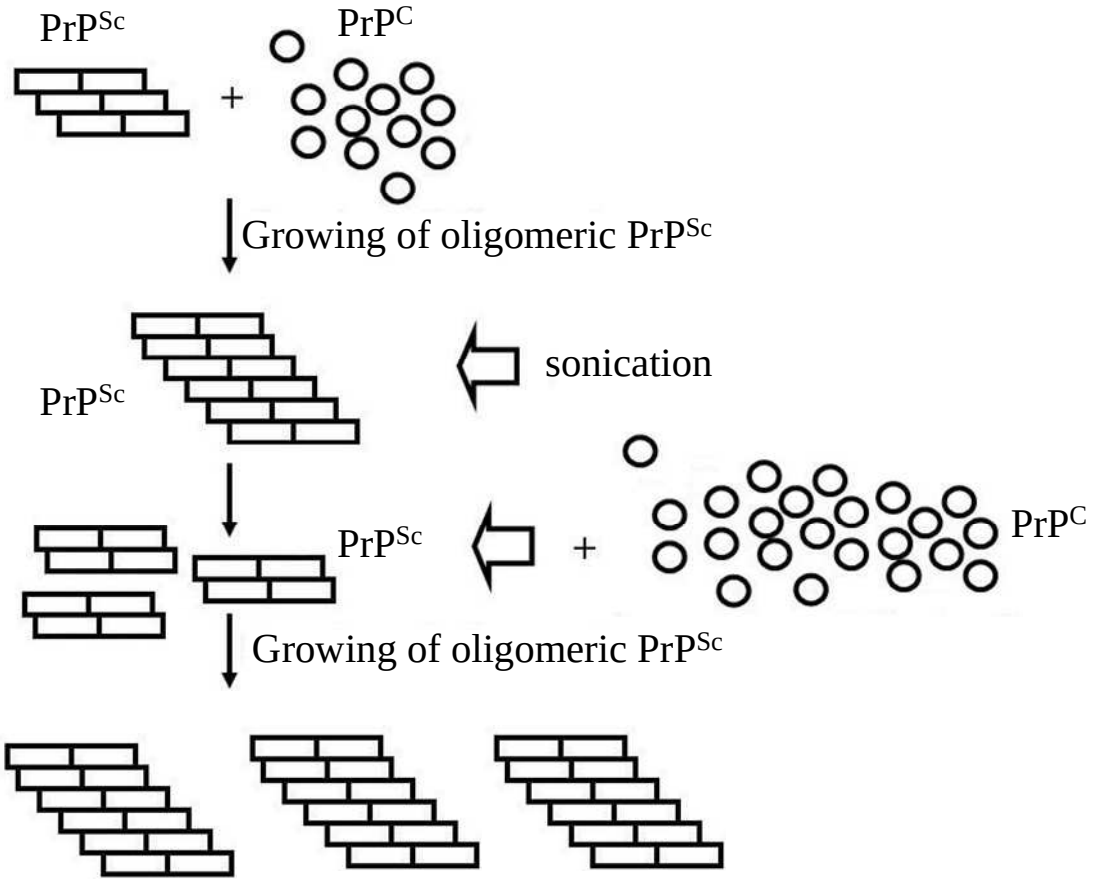

Figure 1.1. Prion amplification by PMCA. PrP^{C} is first incubated with minute amount of PrP^{Sc} to induce formation of PrP^{Sc} polymers. Sonication is then applied to break the newly formed PrP^{Sc} polymers to generate new growth 'seeds' for subsequent conversion.

Although PrP^{Sc} is associated with infectivity(*29*), and aggregates thereof have been suggested to be neurotoxic(*30-32*), growing evidence has challenged the latter idea. *First*, inoculation of prion does not cause neuronal death in PrP null ($Prnp^{0/0}$) mice, indicating that PrP^{C} expression is a prerequisite for prion-induced neurotoxicity(*20, 33-34*). *Second*, PrP^{Sc} is barely or not detected in some prion diseases, and the pathological changes in the brain region are not always associated with PrP^{Sc} accumulation(*35-38*). *Third*, PrP^{Sc} accumulation can occur without developing neurotoxicity even in the presence of PrP^{C}(*39-40*).

1.2. PrP27-30. PrP^{Sc} exhibits partial resistance to proteinase K digestion. The proteinase-resistant core is composed of ~142 residues and has an apparent molecular mass of ~27-30 kDa; thus, it is designated as PrP27-30. Unlike PrP^{Sc}, PrP^{C} is sensitive to PK digestion(*41*) (Figure 1.2).

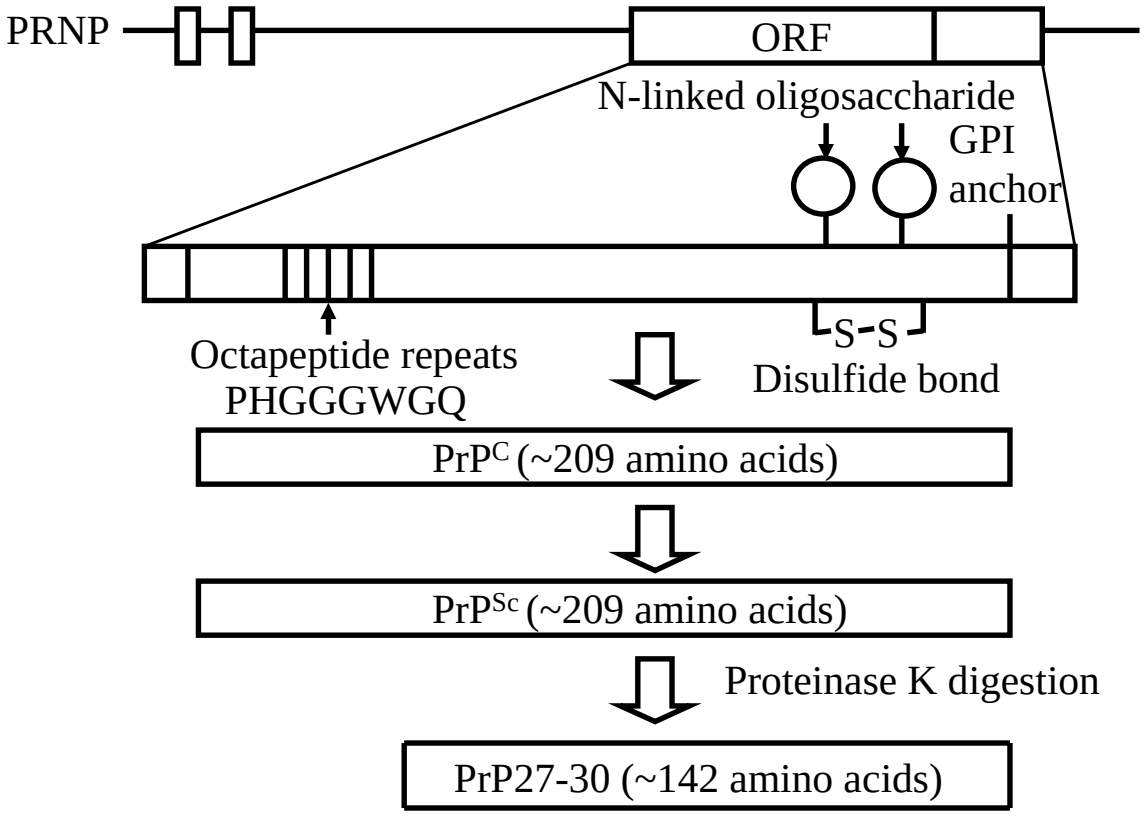

Figure 1.2. PrP isoforms.

1.3. Conformations of PrP^C and PrP^{Sc}. PrP^C is composed of an unstructured N-terminal domain and a globular C-terminal domain (residues ~120-233) of known structure, comprising three α-helices, a short two-stranded antiparallel β-sheet, and a disulfide bond (Cys182-Cys217) linking helices 2 and 3 (Figure 1.3)(*42-46*). Relatively little is known about the structure of PrP^{Sc}, except that it appears to have significantly more β-sheet and slightly less α-helix (17-30% α-helix; 43-54% β-sheet) compared to PrP^C (47% α-helix; 3% β-sheet)(*13-15*).

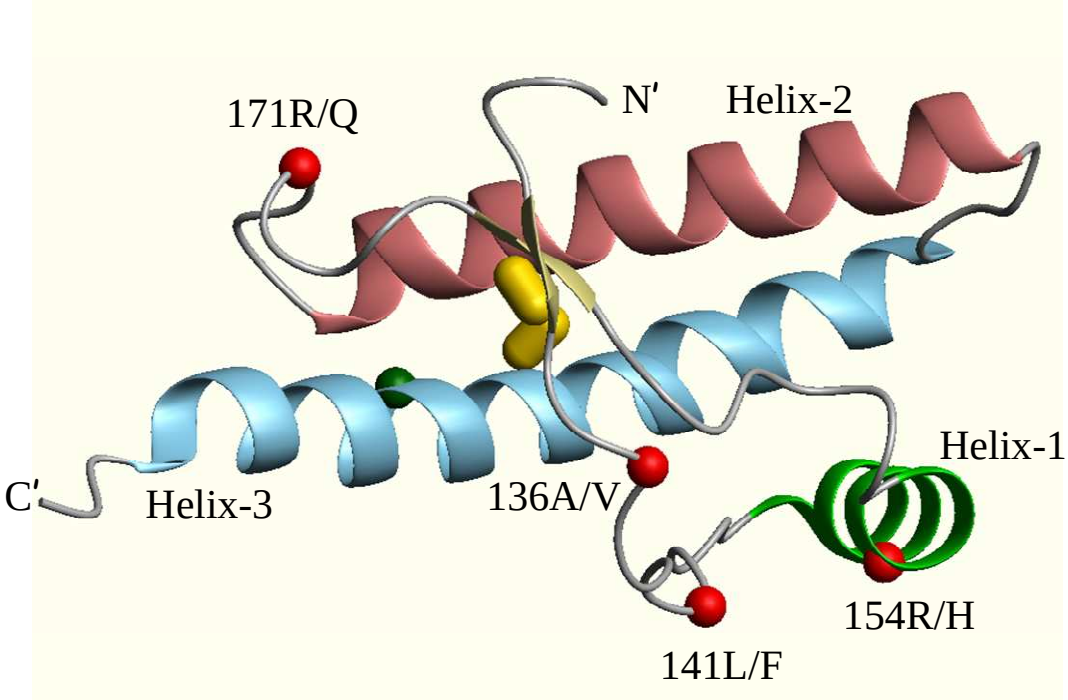

Figure 1.3. Ribbon representation of the structure of ovPrP (residue 126-233). Helix 1 is shown in green; helix 2 is shown in mauve; helix 3 is shown in blue. The antiparallel β-sheet is shown in yellow; the disulfide bridge is shown in gold. The residues involved in genetic modulation in sheep scrapie are shown in red. Sheep numbering is used here. Figure was drawn with MOLMOL(*47*). For interpretation of the references to color in this and all other figures, the reader is referred to the electronic version of this dissertation.

Three structural models for PrP^{Sc} have been proposed. *(i) β-helical model* (Figure 1.4.A). Based on electron crystallography and molecular modeling, Govaerts *et al.* proposed the trimeric β-helical model of PrP27-30(*48*). By refolding residues 89-174 into a left-handed β-helical fold(Figure 1.4.A1), PrP form a trimer as the fundamental unit of a fibril with helices 2 and 3 mostly preserved (Figure 1.4.A2)(*48*). To initiate a fibril, PrP^{Sc} trimers

stack on one another through hydrogen bonds in the direction perpendicular to the β-strands, thus constructing a cross-β architecture (Figure 1.4.A3)(*48*). The C-terminal α-helices and the N-linked glycans provide an external coating similar to PrP^{C} (Figure 1.4.A3), which might explain the absence of host immune response against PrP^{Sc}(*48*). Consistent with this model, an antibody study observed that secondary structure changes occur in α-helix 1, whereas α-helices 2 and 3 remain largely conserved during the PrP^{C}-to-PrP^{Sc} conversion(*49*). *(ii) Spiral model*. (Figure 1.4.B) Based on molecular dynamics simulations, DeMarco *et al.* proposed that the core of the β-structure in the prion protofibril is composed of a three-stranded sheet E1-E3 (E1: 116-119; E2: 129-132; E3: 160-164), and an isolated strand E4 (135-140), with retention of all three native α-helices(*50*) (Figure 1.4.B1). Oligomerization occurs by docking PrP^{Sc} monomers through E4 to E1 (Figure 1.4.B2); protofibrils grow in a spiral-like manner (Figure 1.4.B3)(*50*). *(iii) Parallel and in-register β-structure model*. (Figure 1.4.C) Contrast to the above two models, Surewicz *et al*. proposed that PrP^{C} to PrP^{Sc} conversion involves refolding of the entire α-helical domain (Figure 1.4.C1) based on the analyses of hydrogen/deuterium exchange and site-directed spin labeling(*51*). In this model, the β-sheet core is composed of residues ~160-220, which forms a single-molecule layer that stack on top of one another with parallel, in-register alignment of β-strands to form amyloid(*51*) (Figure 1.4.C2).

Figure 1.4. Comparison of structural models for PrP^{Sc} and amyloid. (A) *β-helical model.* A1: Model for monomeric PrP27-30. Structural conversion involves residues 89-174, whereas C-terminal helices of monomeric PrP^{C} remain intact. A2: Trimeric PrP27-30 forms the fundamental unit for building up a fibril. A3: Two trimeric PrP27-30 are linked through hydrogen bonds. Glycans and C-terminal α-helices extend away from the center of the structure. Figure was adopted and modified from Govaerts, C. et al. (2004) *Proc. Natl. Acad. Sci. U S A.* **101**, 8342-8347. (B) *Spiral model*. B1: Monomeric PrP^{Sc}. All three native α-helices remain intact during structural conversion. B2: Propagation of a protofibril occurs by docking PrP monomers through E4 to E1. B3: A protofibril grows in a spiral-like manner. Figure was adopted and modified from DeMarco, M. et al. (2004) *Proc. Natl. Acad. Sci. U S A.* **101**, 2293-2298. (C) *Parallel and in-register β-structure model*. C1: Monomeric PrP^{Sc}. Structural conversion involves a major part of helices of a monomeric PrP^{C}. C2: Individual monomers stack on top of one another to form amyloid. Figure was adopted and modified from Cobb, N.J. et al (2007) *Proc. Natl. Acad. Sci. U S A.* **104**, 18946-18951.

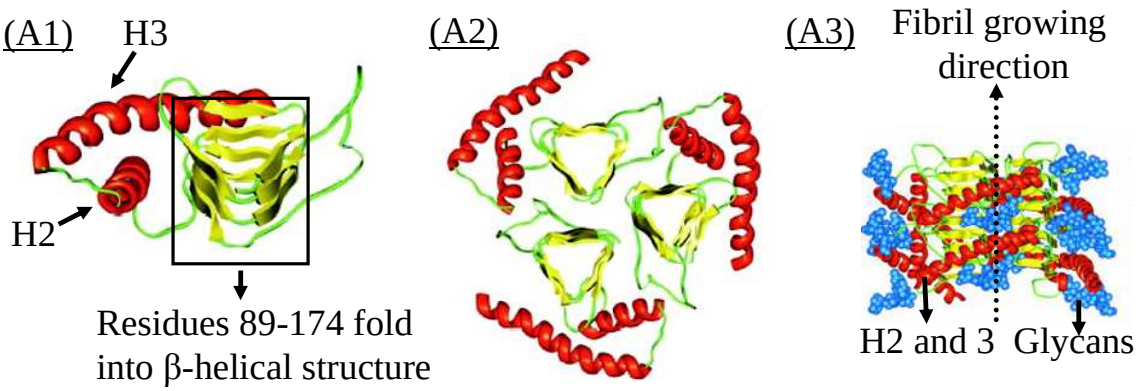

Figure 1.4. (cont'd)

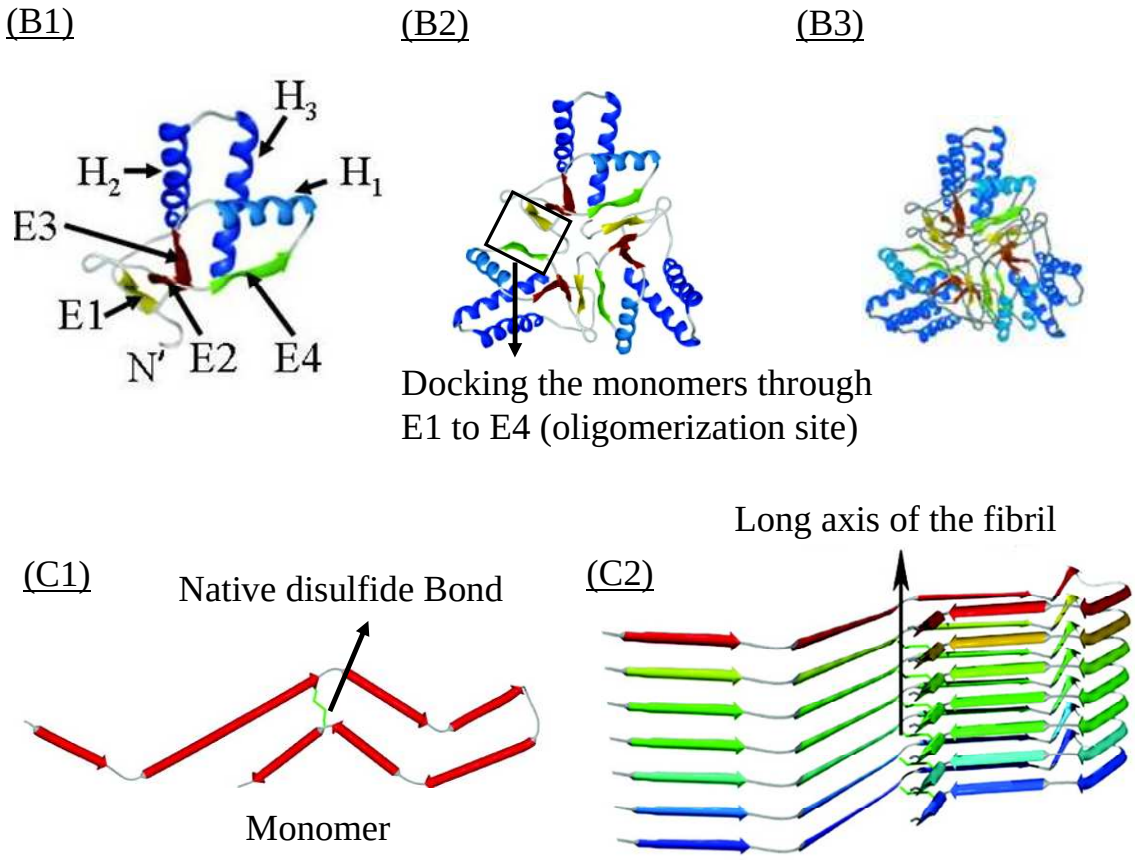

1.4. Theoretical models for structural conversion. Two theoretical models have been proposed for the PrP^{C}-to-PrP^{Sc} conversion(*1, 52*). The *refolding model* suggests that the PrP^{C} is in equilibrium with a partially folded intermediate PrP^{*} (Figure 1.5). A high activation energy barrier prevents spontaneous conversion of PrP^{C} to PrP^{Sc}. When PrP^{*} interacts with exogenously introduced PrP^{Sc}, it refolds under the effect of PrP^{Sc}, and adopts the PrP^{Sc} conformation. In this model, the driving force for structural conversion is monomeric PrP^{Sc}. However, this model has a chicken-and-egg problem. For example, it cannot explain the existence of PrP^{Sc} found in patients who have never been exposed to

exogenous PrP^{Sc}, as in inherited prion diseases. Proponents of the refolding model suggest that the concentration of PrP^{*} for the mutant PrP is higher than that for the wild-type PrP, and is sufficient to initiate aggregation without a preexisting PrP^{Sc} seed, leading to *de novo* formation of PrP^{Sc}. For illustration, the reaction may occur as $PrP^{*} + PrP^{*} \rightarrow (PrP^{Sc})_2$. In contrast to the refolding model, the *nucleation model* proposes that PrP^{C} itself is the precursor of PrP^{Sc}. PrP^{C} and PrP^{Sc} are in a reversible equilibrium, with PrP^{C} strongly favored by free energy. PrP^{Sc} monomer is stable only when it is added onto a PrP^{Sc} aggregate (Figure 1.5). In other words, the structural conversion is driven by oligomeric PrP^{Sc}. This model suggests that infectivity is encoded in the highly ordered PrP^{Sc} aggregate, instead of monomeric PrP^{Sc}, since the latter exists ubiquitously(*52*). The key differences between these two models are: (i) whether a kinetic folding intermediate PrP^{*} is formed, (ii) the identity of the precursor to PrP^{Sc}, and (iii) the driving force for structural conversion.

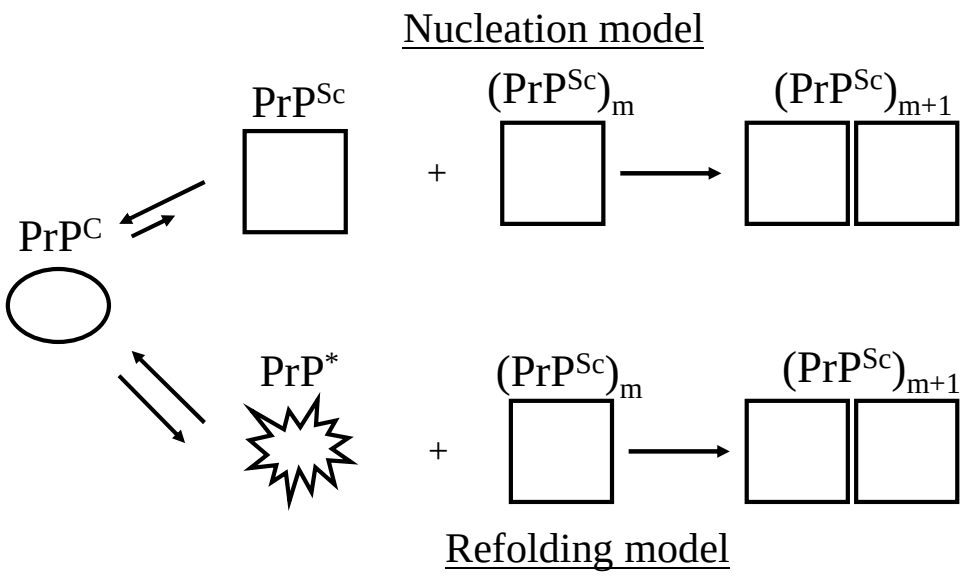

Figure 1.5. Two models for conformational conversion of PrP^{C} to PrP^{Sc}. The *refolding model* (upper panel) indicates that a partially folded intermediate PrP^{*} is the precursor of PrP^{Sc}. This conversion process can be expressed as $(PrP^{C} \leftrightarrow PrP^{*}) + (PrP^{Sc})_{m} \rightarrow (PrP^{Sc})_{m+1}$. The *nucleation model* (lower panel) indicates that PrP^{C} itself is the precursor of PrP^{Sc}. This conversion process can be expressed as $(PrP^{C} \overset{\rightarrow}{\leftarrow} PrP^{Sc}) + (PrP^{Sc})_{m} \rightarrow (PrP^{Sc})_{m+1}$.

1.5. Prion strain and species barrier. One of the most puzzling phenomena is that prions exist in different *strains* that exhibit distinct neuropathology, incubation time, and specific neuronal target areas(*52*). Conformational stability(*53*), glycosylation patterns(*54*), and cleavage sites for proteinase K digestion(*55-57*) have been shown to differentiate strain types, suggesting that strain-specific information is encoded in PrP^{Sc} structure.

Transmission of prions across species often delay the onset of disease, or prevent it altogether(*1, 58-59*). Such effects are usually reduced and finally stabilized in further passage(*60*). This phenomenon has been referred as the *'species barrier'*. Early studies argue that the species barrier is determined by the degree of the differences in the primary structure of donor and recipient PrPs. However, growing evidence suggests that the conformation of the donor prion strain and the primary structure of the recipient PrP are both important in determining the species barrier(*58, 60*).

To explain the role of the primary structure of the host PrP in prion transmission, the *'conformational selection hypothesis'* was proposed. In this model, the transmission barrier is determined by the conformation of the donor prion strain and the conformational constraints imposed by the primary structure of recipient PrP(*58, 61*). If the conformation of the donor PrP^{Sc} is within the spectrum of the conformations allowed by the recipient primary structure, a low transmission barrier is expected(*61-62*). Conversely, if the primary structure of the recipient PrP does not favor to form the conformation of the donor prion, a high transmission barrier is expected. The passage can be stabilized only after a new strain showing structural compatibility has emerged(*61-62*). It is conceivable that cellular chaperone and environment could set different conformational constraints on the recipient PrP^{C}, thus modulating the range of preferred conformation.

Two theoretical models have been proposed to explain the emergence of a new strain. *First*, a new strain might be generated *de novo* during the intermolecular interaction

between the host PrP^{C} and the donor PrP^{Sc}(*61-62*). *Second*, the concept of '*substrain*' has been proposed. A substrain is a collective of interconvertible prion conformations(*63*). A strain comprises a set of substrains, with one dominant PrP^{Sc} conformation coexisting with other minor conformational states(*63*). When a prion inoculum composed of a diverse substrain population is introduced into a recipient animal, recipient PrP^{C} may preferentially interact with a specific substrain and causes the dominant conformation to shift to the PrP^{C}-favored substrain(*61-62*).

A recent report has shown that endogenous cofactors can lead to the emergence of a new strain(*63*). Consistent with the *substrain concept*, strain selection has been observed to occur within a population of diverse substrains to adapt different cell types(*63*).

1.6. Biogenesis and trafficking of PrP^{C}. The mammalian PrP gene (*Prnp*) encodes a protein of ~ 250 amino acids that contains an amino-terminal signal peptide (residues 1-22), several octapeptide repeats, a highly conserved central hydrophobic region (residues 111-134), and a C-terminal signal peptide (residues 231-254) for addition of a glycosylphosphatidylinositol (GPI) anchor(*2*).

The primary translation product of *Prnp* is subject to cleavage of amino- and carboxyl-terminal signal peptides, addition of N-linked oligosaccharide chain at two positions (Asn181 and Asn197), formation of a disulfide bond, and attachment of a GPI anchor. The mature PrP^{C} is then transported to the cell surface(*2*).

It has been reported that PrP^C cycles continuously between the plasma membrane and an endocytic compartment through clathrin-dependent mechanism(*64-65*). A small percentage (~ 1-5%) of the endocytosed molecules undergoes proteolytic cleavage near residue 110, after which the amino- and carboxyl-terminal cleavage products are externalized(*66*). Most of the endocytosed PrP^C returns to the cell surface, but a small fraction is degraded by lysosome(*65*). Some of the endocytosed molecules are subject to cleavage within the GPI anchor, and then released into the extracellular medium(*64, 66*).

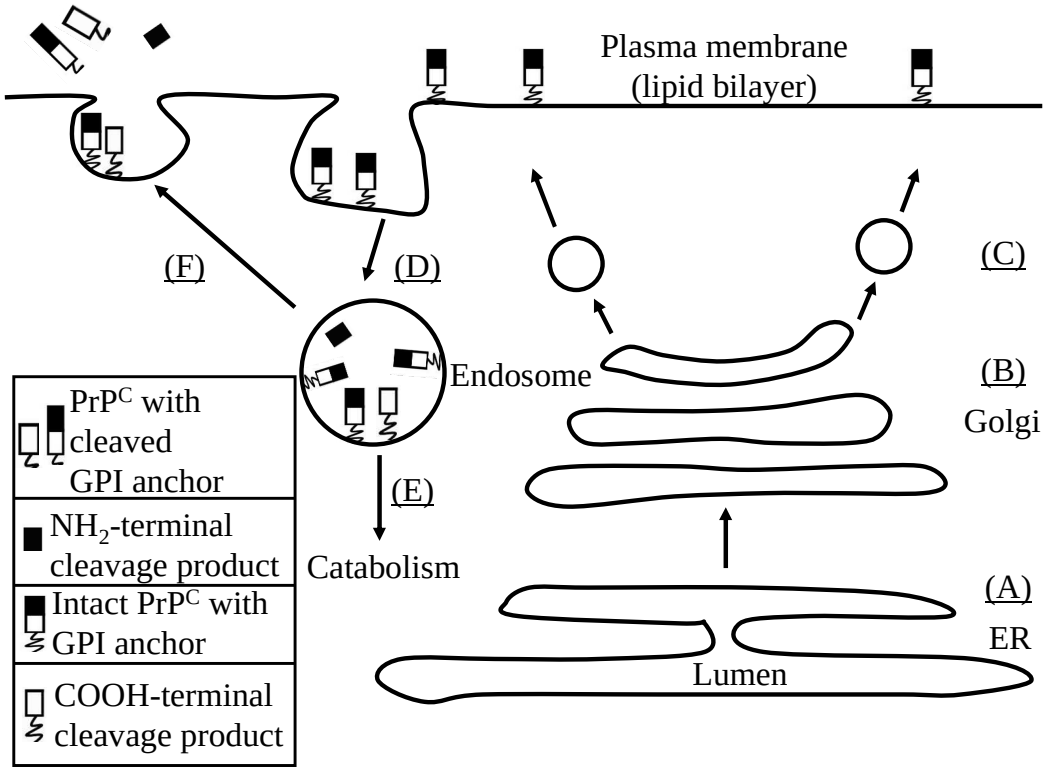

Figure 1.6. Biosynthesis and trafficking of PrP^C. (A): *In the ER*. After being synthesized, a nascent PrP^C polypeptide is subject to removal of the N-terminal signal peptide. A GPI anchor is added after the C-terminal signal peptide is removed. Glycosylation is initiated. Disulfide bond formation also occurs in the endoplasmic reticulum (ER). (B): *In the Golgi apparatus*. The N-linked oligosaccharide chains are modified in the Golgi to yield complex-type glycans. (C): Mature PrP^C is transported to the cell surface, where it is attached via its GPI anchor. (D): PrP^C is internalized through clathrin-mediated endocytosis. Most of molecules remain intact, but a small portion undergoes proteolytic cleavage along the endocytic pathway. (E): A small number of endocytosed PrP^C is degraded in lysosome. (F): PrP^C is externalized. Most of the molecules remain intact and return to the cell membrane, but some of them are released into the extracellular medium.

1.7. Proposed functions of PrP^C. PrP^C is a copper-binding cell-surface glycoprotein associated with detergent-resistant membranes, also known as lipid rafts. It is most abundant in the CNS, but also exist in other non-neuronal tissues, including spleen, lymph node, lung, heart, kidney, intestine, and skeletal muscle(*67-68*). Neither PrP^C nor its mRNA has been detected in the liver(*67*). In the brain, PrP^C is predominantly localized to the synaptic membranes(*69-70*). However, later studies challenged this observation and proposed that PrP^C distribution on the plasma membrane of neurons has no preference for synapses(*71-72*).

Mice devoid of PrP exhibit normal development and reproduction with a number of subtle abnormalities(*73-75*). However, given its highly conserved primary sequences, PrP^C seems likely to have an important physiological functions. It has been postulated that the function of PrP^C is involved only in certain conditions. Therefore, ablation of PrP^C does not affect the unchallenged experimental mice(*76*). Deletion of PrP^C may also initiate a mechanism that compensates for PrP^C deficiency(*76*).

Although the exact roles of PrP^C remain unknown, several potential functions have been proposed. *First*, PrP^C has been suggested to regulate copper metabolism(*77-79*). It has been proposed that PrP^C maintains the level of copper in the pre-synaptic cytosol and protects synaptic membrane from copper toxicity(*70, 80-82*). *Second*, PrP^C has been suggested to promote neuroprotection through its anti-Bax activity, antioxidant activity, and other signaling pathways(*76*). These functions require signaling at cell surface and/or

an undefined mechanism associated with octapeptide repeats(*76*). *Third*, PrP^{C} has been suggested to support the self-renewal of hematopoietic stem cells and to regulate neurogenesis and neural development(*83-84*).

1.8. Scrapie in sheep. Scrapie, a fatal neurological disorder occurring in sheep and goat, is a member of TSE. Classical scrapie was first reported in Europe in the 1700s, and was the first identified TSE. The neurological signs in classical scrapie include abnormalities in behavior, sensation, and movement. In 1998, an atypical type of scrapie were diagnosed in Norway. Based on PrP^{Sc} conformation and its glycosylation pattern, a new strain (Nor98) is designated for these five cases(*85*). The major clinical sign in atypical scrapie is ataxia; anxiety and loss of body condition were also observed(*85-86*). The primary structure affected in classical scrapie, the dorsal motor nucleus of the vagus, has never been involved in atypical scrapie(*85-86*).

These two types of scrapie have different epidemiology. Classical scrapie has been identified as an infectious form of TSE, and can spread through the following routes: *First*, horizontal spread can occur between two unrelated animals(*87*). *Second*, a ewe can transmit prion to her offspring through parturition and fluids(*87*). *Third*, parents can spread prion to offspring via germplasm(*87*).

By contrast, although the origin of atypical scrapie remains elusive, two observations suggest that this disease could occur sporadically. *First*, transmission between sheep in the same flock has not been identified(*85-86, 88*). There are only two reported cases

where more than one affected animals was found in the same flock(*89-90*). *Second*, the geographical distribution for atypical scrapie occurrence is more homogeneous than expected for an infectious disease(*85-86, 88*). In most cases of classical scrapie and many other acquired TSE, prion spreads from peripheral to the central nervous system (CNS) via the lymphoreticular system (LRS). However, PrP^{Sc} is barely found in the peripheral lymphoid tissues in atypical scrapie(*91-92*). Some authors suggest a possibility that PrP^{C} to PrP^{Sc} conversion occurs sporadically in the brain(*85-86, 88*), thus LRS is not necessarily needed for prion invasion. Nevertheless, this observation may reflect that atypical scrapie has alternative routes for transporting prion from the peripheral tissues to the CNS. A similar situation has been observed for prion neuroinvasion in different strains of the transmissible mink encephalopathy (TME) agent(*85-86, 88, 93*).

1.9. Genetic modulation in sheep scrapie. Polymorphisms of ovine PrPs (ovPrPs) have been associated with differing susceptibility to classical and atypical scrapie, particularly at positions 136 (A/V), 141 (L/F), 154 (H/R), and 171 (Q/R). According to surveys conducted in 15 different countries, the average allelic frequencies are 56% for $A_{136}L_{141}R_{154}Q_{171}$ (ALRQ), 30% for $A_{136}L_{141}R_{154}R_{171}$ (ALRR), 6% for $A_{136}L_{141}H_{154}Q_{171}$ (ALHQ), 5% for $V_{136}L_{141}R_{154}Q_{171}$ (VLRQ), 3% for $A_{136}L_{141}R_{154}H_{171}$ (ALRH), and 11.6% for $A_{136}F_{141}R_{154}Q_{171}$ (AFRQ)(*88*).

In classical scrapie, the variations at positions 136 (A/V), 154 (R/H) and 171 (Q/R) are involved in the genetic modulation(*88-89, 94-96*). The combination of these

polymorphisms forms five alleles: ALRQ, VLRQ, ALHQ, ALRR, and ALRH. The VLRQ allele is linked to the highest susceptibility, whereas the ALRR allele confers resistance(*88-89, 94-96*). The other three variants, ALRQ, ALRH, and ALHQ, are associated with medium to low susceptibilities. However, this scale is not absolute and exhibits prion strain-dependence(*88, 97-99*).

In atypical scrapie, the susceptibility is mainly modulated by the polymorphisms at residues 141 (L/F) and 154 (L/H). The highest susceptibility is associated with AFRQ allele. Other two haplotypes, ALHQ and ALRR, are also linked to atypical scrapie. Surprisingly, VLRQ, which renders the highest risk to classical scrapie, seems to confer resistance to atypical scrapie(*85-86, 88-89, 100-101*).

1.10. Genetic modulation in human prion diseases. Approximately 10-15% human prion diseases occurs in the familial form(*102*). Most mutations associated with human familiar prion diseases in *Prnp* gene involve the following three regions (Figure 1.7): *First*, human *Prnp* normally carries five octapeptide repeats between residues 51 to 91. Insertions of extra repeats have been linked to familial prion diseases(*103-106*). Although deletions of single repeat do not cause prion diseases(*2*), a case with two-octapeptide repeat deletion has been reported(*103*). *Second*, many point mutations have been found in the region between helices 2 and 3(*105*). *Third*, premature stop codons caused by point mutations have been reported to induce prion diseases(*105, 107*).

Polymorphisms at residue 129 between Met or Val have been reported to modulate disease susceptibility and pathogenesis in sporadic, acquired, and familial prion diseases(*108-112*). Homozygosity (129MM or 120VV) at this position appears to predispose individuals to sporadic prion diseases(*108-109*). In the cases of variant CJD, only patients with 129 MM genotype have been reported(*54, 108*). The two allelic forms also determine the phenotypes in the familial diseases caused by the pathogenic mutation at residue 178 (D178N)(*111-112*). Whereas D178N-129MM genotype is linked to FFI, D178N-129MV is associated with familial CJD (fCJD). It has been suggested that this modulation is not absolute. Several cases of fCJD have been reported in patients with D178N-129MM genotype(*113*). An explanation is that FFI and fCJD represent two extreme phenotypes of a diseases rather than two separate diseases entities(*113*).

Figure 1.7.

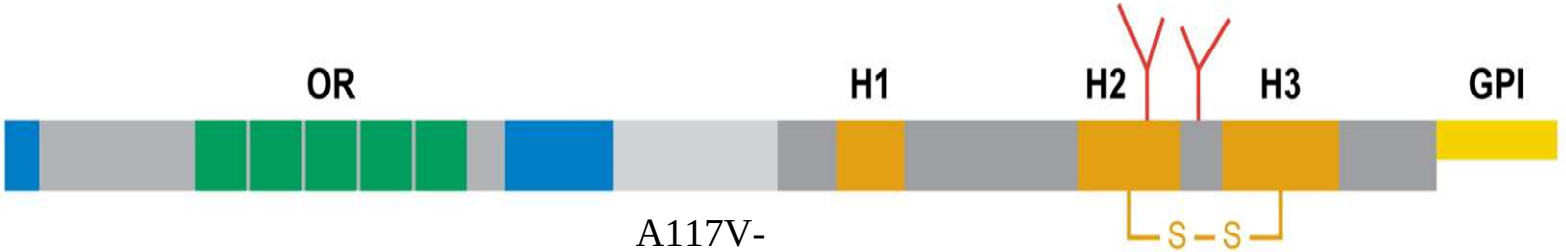

Mutations causing GSS	Octarepeat insertion	P102L-129M P105L-129V	A117V-129V G131V-129M G145*-129M	H187R-129V Q217R-129M F189S-129V D202N-129V Q212P
Mutations causing gCJD	Octarepeat insertion			D178N-129V E208H M232R V180I E200K T188K V210I T188R-129V E196K E211Q V203I
Mutations causing FFI				D178N-129M

Figure 1.7. (cont'd) Human PrP^{C} and the mutations linked to familial prion diseases. OR denotes the octapeptide repeats. H1, H2, and H3 denote helices 1, 2, and 3, respectively. Two forks on top of the protein represent potential sites for glycosylation. The sole disulfide bond (S-S) and GPI anchor are also shown in the figure. The associated polymorphisms at residue 129 are indicated. The asterisk indicates a stop codon. Figure was adopted and modified from Aguzzi, A. et al. (2008) *Annu. Rev. Neurosci.* **31**, 439-477.

1.11. Prion diseases and other protein misfolding disorders. Several neurodegenerative diseases, including prion diseases, Alzheimer's disease (AD), Huntington's disease (HD), Parkinson's disease (PD), and amyotrophic lateral sclerosis (ALS), involve protein misfolding, and thus are collectively called ***protein misfolding disorders*** (PMD). These diseases share some common features in their pathogenesis and usually involve the formation of protein aggregate in the form of fibrillar amyloid(*29*). It remains to be established whether there is a unifying mechanism to explain neuronal death occurring in these diseases.

A *'seeding nucleation'* model has been proposed to explain amyloid formation(*114*). In this theory, the rate-determining step is the slow process where nucleation of monomeric misfolded proteins occurs. Once nuclei are formed, further addition of monomers becomes very fast, resulting in a rapid polymerization phase. Although this self-seeding and propagation process seems to be common for PMDs, transmissibility has been observed only in prion diseases.

Several studies have shown prion-like transmission in animal models of AD(*115-119*); nevertheless, many of these results are conflicting(*52, 118, 120*). It has been argued that the recipient animals used in some of the studies are highly susceptible to amyloidosis, and spontaneous amyloidosis could occur under the experimental conditions(*52, 119, 121*). Thus, it remains to be established whether inoculation of amyloid in these animals initiates amyloidosis thus reflecting amyloid transmissibility, or simply facilitates an ongoing pathogenesis(*122*).

Another mystery in these diseases is the toxic entity. Earlier studies proposed that protein aggregation account for the neurotoxicity in PMD based on the following observations. *First*, protein aggregates have been observed to co-localize with brain lesions in many cases(*29, 123*). *Second*, genes involved in the familial form of these diseases have been found to encode the aggregated proteins(*29*). *Third*, overexpression of the abnormal proteins in animal models induces protein aggregation and causes neurodegeneration(*124-125*). *Fourth*, most pathogenic mutations involved in PMD promote *in vitro* and *in vivo* protein aggregation(*126*).

However, accumulating evidence suggests the possibility that formation of protein aggregates play a neuroprotective, instead of neurotoxic, role in these diseases. As mentioned in the previous section, neuronal death is not always associated with PrP^{Sc} aggregates in prion diseases. In some cases, diseases develop without detectable PrP^{Sc} aggregates(*35-38*). A similar situation has been observed in the animal models of polyglutamine diseases(*127*). Soluble oligomers or diffuse deposits of the misfolded proteins have been shown to correlate with neuronal death in the animal models of AD(*128-131*). In addition, it has been shown that antibodies against soluble Aβ42 oligomers block the neurotoxicity(*132*). Taken together, these studies suggest that precursors of amyloid fibers, such as monomeric or soluble oligomeric forms of misfolded proteins, might account for neuronal death. If it is the case, formation of protein aggregate may protect neurons by sequestering the toxic species.

Table 1.2. A list of protein misfolding diseases. Table was adopted and modified from Caughey, B. et al. (2003) *Annu. Rev. Neurosci.* **26**, 267-298.

Disease	Proteinaceous deposit, abnormal protein	Product of abnormal gene	Phenotype of mutations (including other genes)
Alzheimer's disease	Extracellular amyloid plaques, fibrillar Aβ	Amyloid precursor protein	FAD mutations generally increase production of Aβ42
Parkinson's disease	Lewy body, fibrillar α-synuclein	α-synuclein	FPD mutations seem to cause α-synuclein aggregation or Accumulation
Amyotrophic lateral sclerosis	Intraneuronal inclusions, insoluble SOD1	Superoxide dismutase-1	FALS mutations promote aggregation, but not fibrillization
Transmissible spongiform encephalopathies	Extracellular plaques, protease-resistant PrP (PrP-res)	Prion protein (PrP)	Mutant PrP becomes protease-resistant *in vivo*
Fronto-temporal dementia	Neurofibillary tangles, fibrillar tau	Tau	Mutant variants of tau have altered affinity for microtubules and a tendency to Aggregate
Diffuse Lewy body disease	Cortical Lewy bodies, fibrillar α-synuclein	None (sporadic only)	No mutations have been linked
Huntington's disease	Intranuclear neuronal inclusions, fibrillar Htn	Huntingtin	Expansion of naturally occurring polyglutamine repeat
Spinocerebellar ataxias	Intranuclear neuronal inclusions	Ataxin	Expansion of naturally occurring polyglutamine repeat

Chapter 2. Introduction to Protein Folding

Much of this thesis is focused on kinetic models of protein folding, and their structural interpretation in terms of statistical ensembles of protein conformations (*conformational ensembles*). This chapter is intended as an introduction to such modeling, and protein folding in general.

This chapter will focus on the *in vitro* folding process, which is less complex than *in vivo* folding. *In vitro* folding refers to a process in which protein molecules fold independently of one another and any cellular components. For comparison, in *in vivo* folding, the protein's conformation is shaped by chaperones and other cellular proteins, not to mention the protein's changing cellular environment as it is synthesized and transported to different compartments. By eliminating the cellular contributions, *in vitro* folding studies reveal the interplay between intermolecular and intramolecular interactions that are intrinsic to the polypeptide molecule. Thus, the *in vitro* folding studies pertain to *in vivo* folding; however, they must be integrated with *in vivo* folding studies to understand the physiological processes.

2.1 Equilibrium unfolding.

Most globular proteins have two conformational states, the unfolded state and the folded state (also known as the native state). The folded state is that revealed by X-ray crystallography, in which most atoms of the protein molecule have a stable position, being held in place by a network of many noncovalent interactions, such as hydrogen bonding, steric packing, van der Waals attractions, and hydrophobic interactions. The

relatively stable structure and many interactions give the folded state relatively low entropy and enthalpy. By contrast, the unfolded state describes the high-entropy, high-enthalpy state, in which the protein has no stable structure and is rapidly interconverting between conformations, most of them open conformations with few interactions. In naturally occurring proteins under physiological conditions, both the folded and unfolded states are low in free energy, typically differing only by a few kcal/mol. (For comparison, the thermal agitation energy at room temperature is roughly 0.6 kcal/mol.) Relatively small changes in the solution conditions (such as temperature, pH, salt concentrations, pressure, etc.) can alter whether the folded state or the unfolded state is preferred. The very gradual alteration of solution conditions to cause a folded protein to unfold (e.g., by gradually altering the temperature) is known as **equilibrium unfolding**, because it is carried out under quasi-equilibrium conditions at every step. Such experiments allow us to measure the free-energy difference ΔG_{NU} between the folded and unfolded states.

In addition to the folded and unfolded states, other distinct conformational states may be populated significantly under certain solution conditions. For example, these may be partially folded states, or states where the folded conformation is roughly the same but more labile. Generically, these states are known as intermediate states, because they are often populated at intermediate solution conditions between strongly unfolding and strongly folding solution conditions. These three types of states will be discussed in more detail below; for convenience, I denote the folded (native), unfolded and a generic intermediate states by ***N***, ***U***, and ***I***, respectively.

2.2. Kinetic modeling of protein folding.

The relative concentrations of folded and unfolded conformations under given solution conditions is a function of the relative rates of the underlying basic reactions, folding and unfolding. Since the folded and unfolded states are stable states (free-energy basins), the folding ***U***->***N*** and unfolding reactions ***N***->***U*** are activated processes, meaning that their rate constants vary exponentially with the height of the free-energy barrier, the transition state, between the two states. (This corresponds to Arrhenius' law.) This is true even when there are intermediate states; in general, the rate constants for the transitions among any two conformational states (say, k_{IN} for the transition ***I***->***N***) is governed by an Arrhenius-like equation.

Because protein-folding reactions are unimolecular (e.g., ***I***->***U***), the ensemble of protein conformations will relax to equilibrium as a sum of exponentials with decay constants λ. If there are *p* conformational states (***N***, ***U*** and the various intermediates ***I***) then mathematically, there will be *p-1* decay constants. These observed decay constants are not the same as the fundamental rate constants, but may approach them very closely. For illustration, in two-state folding ***N*** <=> ***U*** where *p*=2, a single exponential phase is observed with the decay constant λ equals $k_{UN} + k_{NU}$. Under strongly folding conditions, $k_{NU} << k_{UN}$ and hence λ is approximately k_{UN}. In the three-state folding model ***N*** <=> ***I*** <=> ***U*** with p=3, two decay rates will be observed, λ_{faster} and λ_{slower}, such that $\lambda_{faster} + \lambda_{slower}$ equals the sum of the four fundamental rate constants, k_{NI}, k_{IN}, k_{IU}, and k_{UI}. In all cases, given the fundamental rate constants under given solution conditions, it is possible

to predict the decay constants λ of protein folding and the corresponding amplitudes of these exponential phases.

Conversely, by carefully observing the decay constants λ under various solution conditions, it is possible to determine the number of intermediate states and estimate the fundamental rate constants of the kinetic model, under the assumption that the Arrhenius law holds. That is the procedure followed in this dissertation. The rate constants and their dependence on solution conditions, in turn, provide structural information about the various states, particularly the intermediates, which are difficult to characterize by other means. Here, I have observed a single intermediate in PrP folding kinetics, and from its deduced properties in variants susceptible to scrapie in different degrees, I argue that it is a plausible precursor for the scrapie isoform PrP^{Sc}. This model suggests new scientific hypotheses and potential treatments by targeting this intermediate.

In the remainder of this chapter, I summarize the current understanding of conformational states and protein folding, as well as the experimental methods used to characterize its kinetics.

2.3. Conformational states.

A simple chemical reaction proceeds from its reactant to its product along a well-defined pathway, i.e. through a sequence of specific structures (Figure 2.1). The point of highest free energy along the reaction coordinate is called the *transition state* (Figure 2.1). After reaching this point, reactant molecules will always go on to form products. A reaction

sometimes involves formation of short-live intermediates on the direct pathway between the reactants and the products (Figure 2.1).

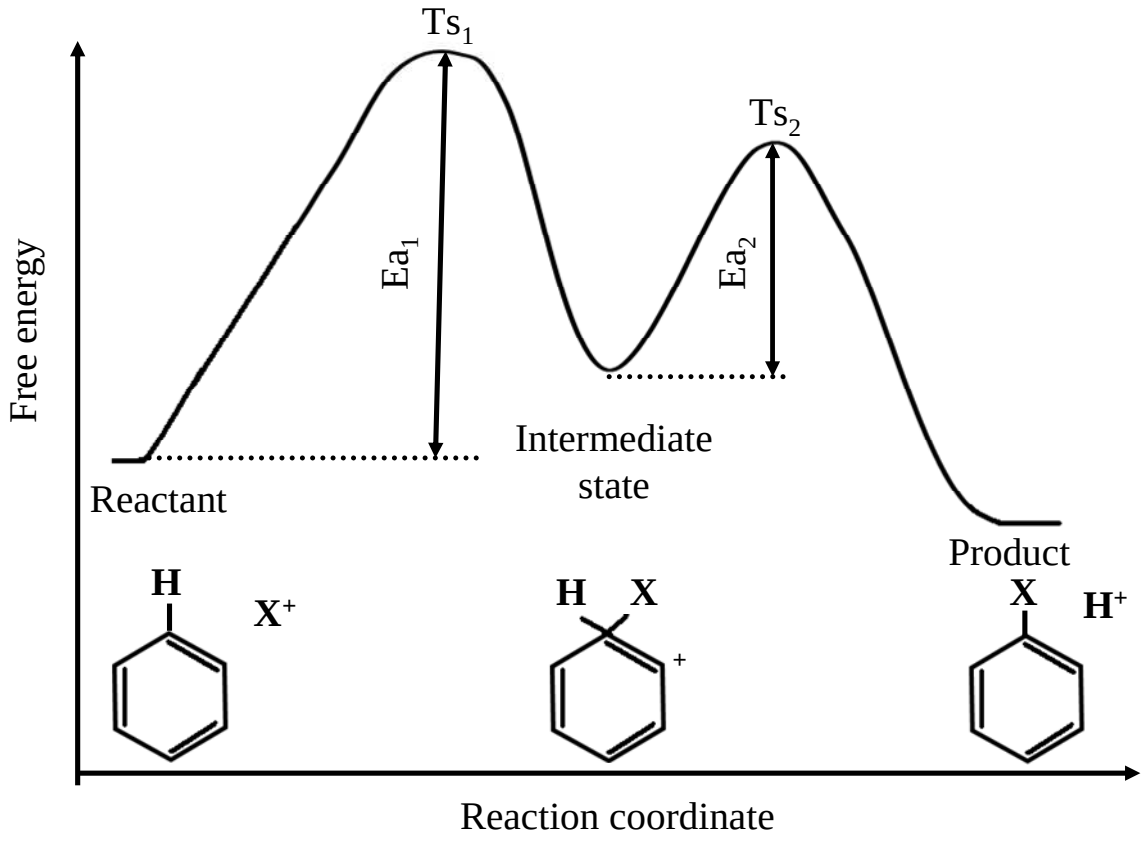

Figure 2.1. An example for a simple chemical reaction involving formation of an intermediate. Ea and Ts are denoted to the activation energy barrier and the transition state, respectively.

Protein folding also involves the conversion of the reactant (an unfolded state) to the product (a native folded state). However, since a polypeptide chain can adopt a larger number of possible conformations (i.e., it possesses a much greater conformational freedom) than small molecules in a simple chemical reaction, the unfolded, intermediate, and transition states in protein folding should be viewed as statistical ensembles of

conformations rather than any particular conformation. These states occurring in protein folding are also called *kinetic species* throughout this dissertation.

2.3.1. The unfolded state. The term *unfolded state* of a polymer has usually been thought to be a random coil with the restriction imposed by steric repulsion between atoms and the excluded volume effect(*133-134*). However, considerable residual structure in unfolded proteins has been observed(*135-137*). Such residual structures are only marginally stable; they form rapidly and dissolve rapidly. Nevertheless, this reduces the accessible conformations of a polypeptide chain.

The conformation of the unfolded state is determined by the balance between interactions of the protein with itself and those of the protein with the surrounding solvent. When interactions within a protein are more energetically favorable than those with the solvent, a protein tends to be more structured. Conversely, when its interactions with solvent are more favorable than those within itself, a protein shows higher degree of randomness(*133-134*). Since the chemical properties of amino acids are diverse, intermolecular interactions with the solvent are not homogeneous along a polypeptide chain(*133-134*). Furthermore, most solvents include more than one component, and a non-uniform distribution of solvent components in a solution has been observed(*138-140*). Thus, the surrounding solvent for each part of a protein may differ from the *mean* solvent composition(*133-134*). Besides the energetic balance between intermolecular and intramolecular interactions, disulfide bonds also play an important role in determining the residual structure of an unfolded protein.

2.3.2. The native state. A *native folded state* of a protein in a conformational ensemble centered on a single well-defined conformation, in which a protein performs its biological function. The three major stabilizing interactions in the native state are hydrogen bonds, van der Waals interactions, and hydrophobic interactions(*134*). Each individual interaction is weak; however, many of them form a '*cooperative system'* to stabilize a protein(*134*). Figure 2.2 represents a simplified cooperative system in protein folding. One interacting pair will bring the other potentially interacting pair into proximity and a more favorable orientation, and decrease the entropic cost for forming the second interacting pair(*134*). As consequence, the contribution of a cooperative system to protein stabilization is much greater than the sum of individual interaction. The interactions involved in cooperativity are primarily long-range(*134*).

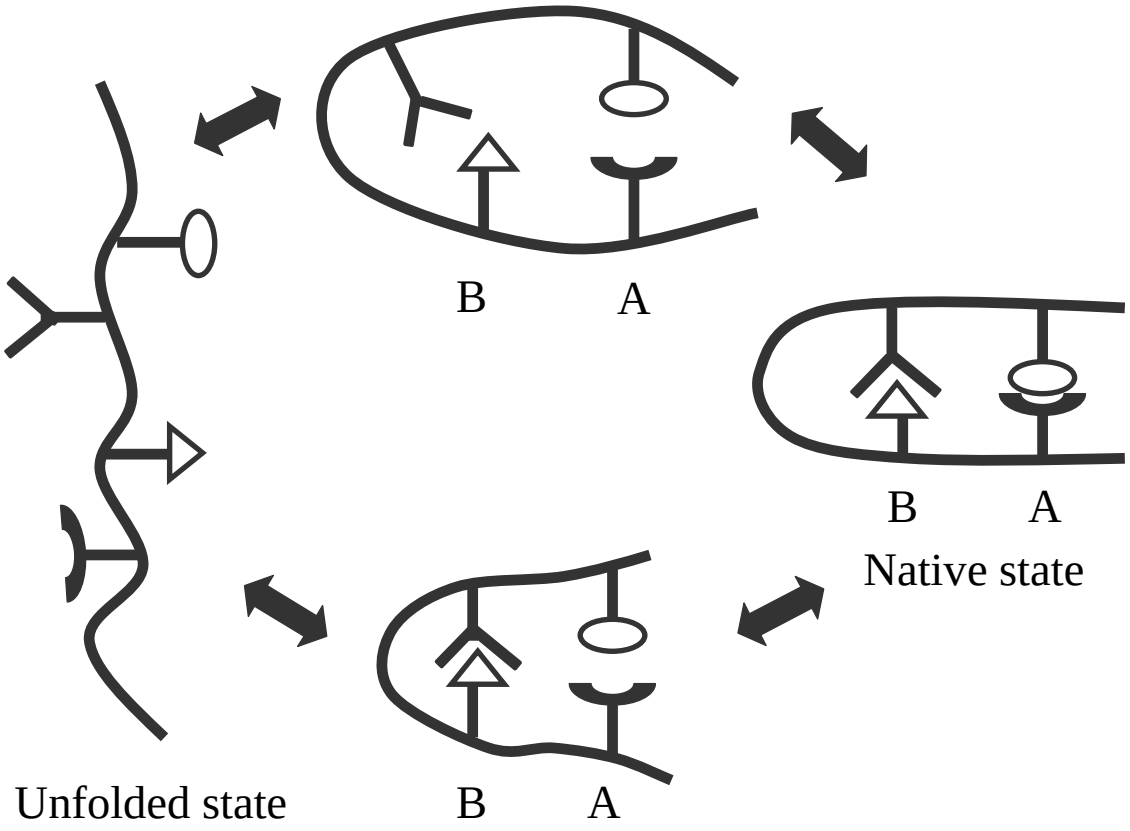

Figure 2.2. Schematic illustration of cooperativity between two interactions in a protein. An oversimplified polypeptide chain with two potential interacting pairs is shown here to explain the formation of a cooperative system. Formation of interacting pair A facilitates and decreases the entropic costs for formation of interacting pair B.

2.3.3. The intermediate states. The driving force for intermediate formation is hydrophobic collapse(*141*). In contrast to random collapsed conformations predicted for a hetropolymer, hydrophobic collapse in a protein shows structural preference and specific interactions(*141*). It has been reported that, on average, about 60% of the surface exposed in the unfolded state is buried in the intermediate state(*141*). In other words, a protein has

exhibited high degree of compactness at this stage. Such compact structure is characterized by approximately correct tertiary folds and native-like but fluctuating secondary structure(*141*).

2.3.4. The transition state. The concept of *folding nucleus* has been introduced (*142-143*) to explain the initiation of protein folding. In the *nonspecific nucleus model*, formation of transition state ensemble (TSE) depends on forming a sufficient number of native interactions without considering which specific contacts are involved(*142*). In the *specific nucleus model(143-147),* folding nucleus represents a specific set of interactions which is shared by all the conformations in TSE. Optional interactions also occur in each conformation; however, their number and location vary from one conformation to another(*142*). Specific and nonspecific nucleus models represent the extreme cases of defining folding nucleus; the real scenario may vary between these two extremes.

2.4. Kinetic models of protein folding.

Initiation of protein folding depends on the diffusion-driven(*148*) contact formations between different regions of an unfolded polypeptide chain. Disulfide bonds impose conformational constraints on unfolded proteins, thus modulating the initiation of folding. By contrast, *cis–trans* isomerism of proline residues usually accounts for the slowest process in protein conformational folding.

2.4.1. Formation of native disulfide bonds. Oxidative folding is defined as a process consisting of disulfide bond formation and forming the native structure of a protein

(conformation folding)(*149-150*). Several characteristics have been observed for such a coupling process. *First,* disulfide bonds bring residues distant in the primary structure into proximity, thus affect interactions between residues by altering the entropic cost(*134, 149*). *Second,* correctly formed disulfide bonds strengthen native local interactions, which evolve concurrently with the formation of native global folds(*149*). *Third,* only the evolution of native tertiary structure has been observed in oxidative folding(*149*). *Fourth,* tertiary structures are stable only when native disulfide bonds are formed(*149*). *Fifth,* native disulfide bonds limit the conformational freedom of their neighboring residues; therefore, folding nucleus are likely to form in the vicinity of disulfide bonds(*149*). Such structures have been found in several studies(*151-154*). In short, disulfide bonds impose bias for conformational folding.

2.4.2. Proline isomerization. Unlike other peptide bonds, which generally favor the trans isomer, those between proline and its preceding amino acid (X-Pro bond) usually exist as an equilibrium mixture in an unfolded ensemble (Figure 2.3)(*155*). However, when an unfolded protein folds into its native structure, X-Pro exists exclusively in either *cis* or *trans* isomer(*155*).

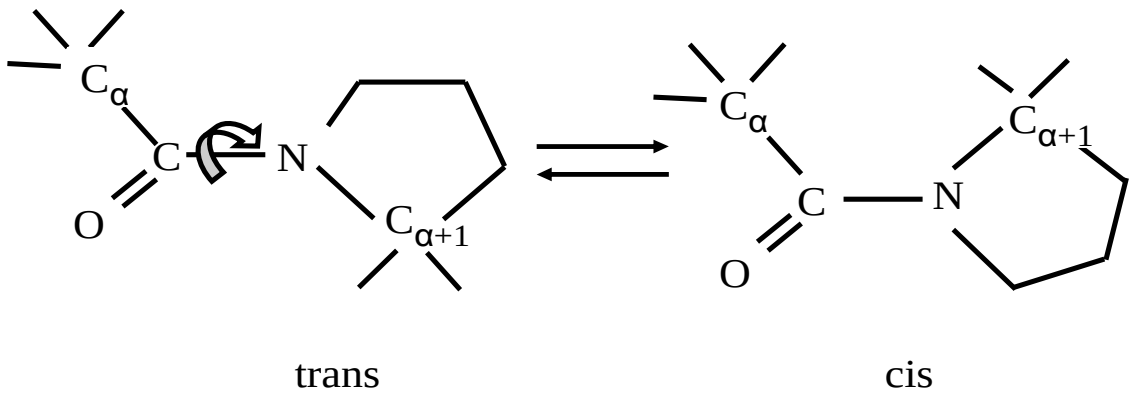

Figure 2.3. Isomeric states of proline peptide bond and its isomerization reaction.

In an unfolded protein ensemble, molecules with native set of X-Pro fold more rapidly than those with at least one non-native X-Pro(*155*). Nevertheless, non-native X-Pro need not block folding progress, and its re-isomerization may not be required for other folding steps(*156*). Re-isomerization of non-native X-Pro is a slow process with a time constant of around 10 to 100 sec at 25^{o}C. This reaction can occur either concurrently with, or after, other faster folding steps. This reaction shows a strong dependence on temperature, but not on denaturant concentrations(*157-158*).

2.4.3. Experimentally observed kinetic models for protein folding. Several small single-domain protein have been found to fold according to a two-state scheme(*159-160*):

$$\boldsymbol{N} \leftrightarrow \boldsymbol{U}$$

where ***N*** and ***U*** represent the native and unfolded states, respectively. In this scheme, only the fully unfolded and the fully folded protein are populated; this all-or-none character is due to the cooperative stabilization. The following factors could account for the apparent two-state folding(*133*): *First*, folding proceeds without passing through an intermediate state. *Second*, the population of the intermediate is too small to be detected.

Third, the spectroscopic property of the intermediate is indistinguishable from that of the unfolded or native folded protein; therefore, $\boldsymbol{U \rightarrow I}$ or $\boldsymbol{I \rightarrow N}$ cannot be detected directly. *Fourth*, the low steady-state concentration of an intermediate required for the sequential folding step is established too rapid to be detected. Because an unfolded ensemble is composed of a highly heterogeneous population, interconversion between each unfolded conformations has to occur very rapidly relative to the main folding step, so that all the molecules can fold into the native state through the same single step(*133*).

In most cases, proteins exhibit more than one folding phase, suggesting that folding involves the formation of intermediates. Nevertheless, such observations are sometimes difficult to be interpreted due to the heterogeneity in unfolded protein ensemble (Figure 2.4). By contrast, unfolding kinetics usually can be described as a single first-order reaction, since the native protein population is highly homogeneous(*133*).

Scheme 1 (on-pathway) $U \leftrightarrow I \leftrightarrow N$

Scheme 2 (off-pathway) $I \leftrightarrow U \leftrightarrow N$

Scheme 3 (parallel pathway)

$$\begin{array}{ccc} & I & \\ & \updownarrow \quad \updownarrow & \\ U & \leftrightarrow & N \end{array}$$

Figure 2.4. Three possible folding schemes account for an experimentally observed folding intermediate. In scheme 1, ***I*** is on the direct pathway between ***U*** and ***N***. In scheme 2, ***I*** is a misfolded state that must unfold before folding to ***N***. In scheme 3, conformational interconversion can occur directly among ***U***, ***N***, and ***I***. ***U***, ***N***, and ***I*** represent the unfolded, native, and intermediate states, respectively.

A long-standing problem in biochemistry and biophysics is the protein-folding problem: How does a protein reach its native folded structure from its unfolded conformational ensemble? This question leads to several sub-questions: Is folding process hierarchical? Does hydrophobic collapse occur concurrently with, or prior to, structure formation? Are there folding nuclei? What is the role of folding intermediates in folding?

2.5. Experimental approaches to study protein folding kinetics.

Protein folding can be initiated using rapid mixing techniques, and followed by optical probes, such as ultraviolet-visible (UV) absorption, circular dichroism, X-ray light

scattering, and fluorescence. The observed exponential responses represent the barrier-crossing events in protein folding; therefore, the number of kinetic species can be deduced from the number of exponential responses. In generally, a kinetic model with *n* kinetic species should produce a signal of *n-1* exponential phases, although not all phases may be detected. A short-lived intermediate state is usually observed only in kinetic studies, although it is sometimes populated to a significant amount that can be detected under certain conditions in equilibrium studies. Some properties of intermediates can be inferred from kinetic data; however, due to the transient nature of intermediates, detailed structural information usually can not be obtained. Detection of the interaction formations along the folding progress can be achieved by applying techniques such as hydrogen/deuterium exchange and mutagenesis combined with kinetic approaches.

2.5.1. Initiation of protein folding.

(1) Protein denaturation. One of the most commonly methods to unfold a protein is using chaotropic agents, such as guanidine hydrochloride (GuHCl) and urea. These two denaturants unfold a protein mainly though disrupting hydrophobic interactions; GuHCl also diminishes ionic interactions(*161*). Although several models suggest that urea and GuHCl increase the solubility of unfolded proteins through hydrogen bonding, a recent report shows that GuHCl does not hydrogen bond to peptide groups(*162*). Other methods, such as pressure, temperature, and pH denaturations, are also routinely used to unfold proteins. High pressure unfolds a protein mainly through changing its packing and hydration properties(*163-164*). Cold denaturation causes reduced hydrophobic interactions thus unfolding a protein(*165*). Heat denaturation disrupts protein structures

through breaking its hydrogen bond and other enthalpically favorable interactions(*165*). The problems associated with this method is that "heat-denatured" proteins are usually partially structured and aggregated, and covalent side reactions sometimes occur as temperature increases. pH denaturation induces protein unfolding by breaking ionic interactions and salt bridges. Similar to heat denaturation, structured proteins are often seen in the denaturing conditions in this method.

(2) Changing external conditions to initiate folding reactions. Protein refolding and unfolding can be initiated by changing external conditions; such process has to be carried out rapidly to be studied kinetically. One way to induce protein folding is to mix a solution containing chemical-denatured proteins with a buffer that favors folding using a stopped- or continuous-flow mixing method. Folding kinetics is then followed by an optical probe, such as UV absorption, circular dichroism, X-ray light scattering, and fluorescence. The time resolution of a mixing device is determined by the dead-time of the instrument, which depends on the time required to complete mixing (mixing time), the flow velocity, and the volume between the mixing area and the point of observation(*166*).

Figure 2.5 represents the principles of flow-kinetics. Solutions containing reactants are delivered into the mixer through two syringes; mixing are completed by either turbulent or laminar flow. The main difference between stopped- and continuous-flow methods is as follows: In the *stopped-flow method*, reactions occurring in an observation cell are monitored after the flow comes to a complete stop(Figure 2.5.A). However, in the

continuous-flow method, mixed solution is allowed to flow continuously without being stopped, and signal is recorded along the flow direction from the downstream of the mixing area (Figure 2.5.B). Since the measurements in a stopped-flow method are made after flow stops completely, its dead-time is limited to ~ 2 ms, and artifacts due to vibration and pressure are sometimes induced(*166*). A much shorter dead-time (10-90 μs) is achieved in a continuous-flow method(*166-167*).

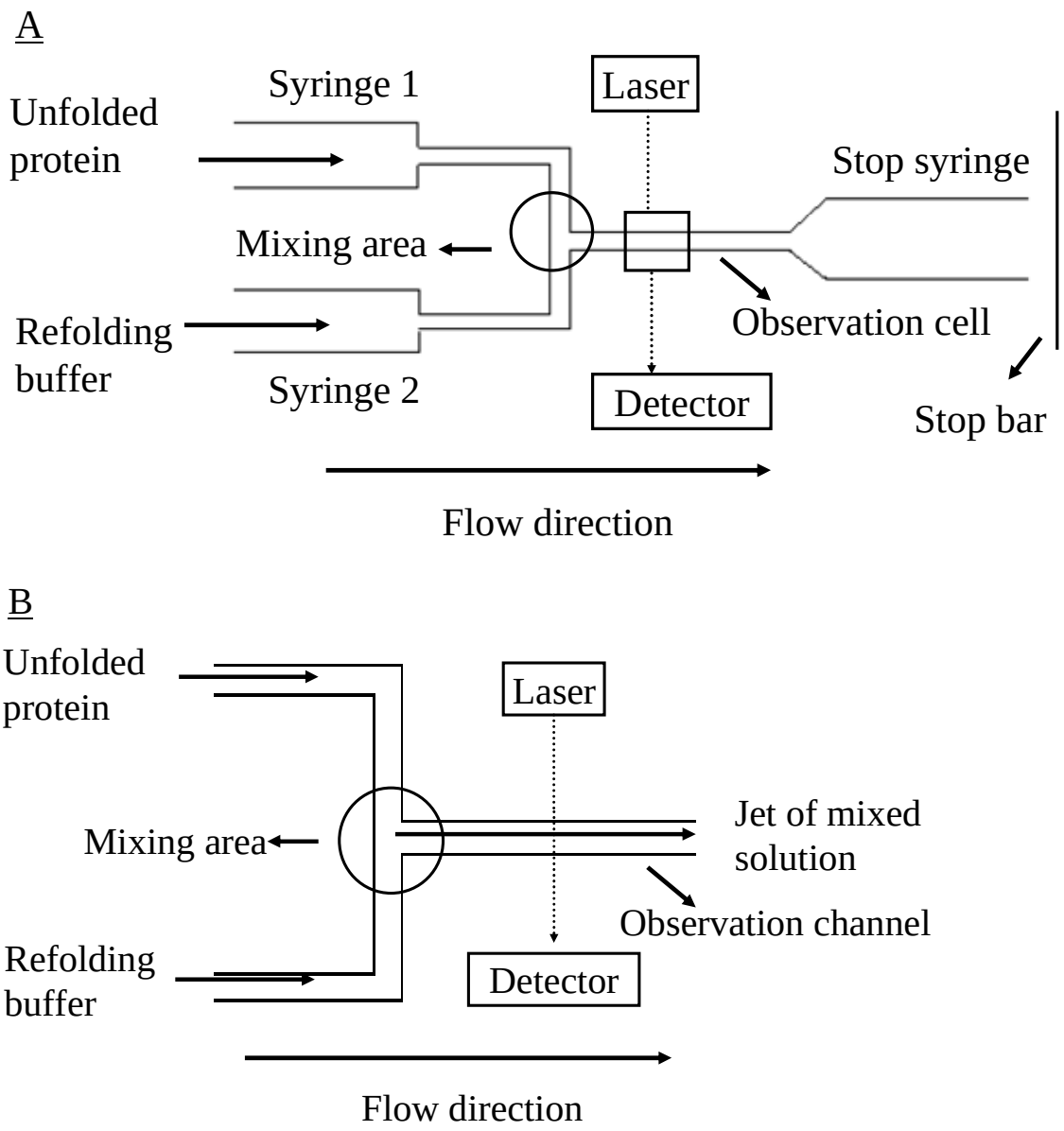

Figure 2.5. Mixing methods for stopped- (A) and continuous-flow (B) experiments. (A) In stopped-flow kinetics, the flow is stopped after a certain volume of solution has passed through the mixer. The detector then starts to record the reaction in the observation cell. (B) In continuous-flow kinetics, optical signal is recorded along the whole observation channel without stopping the flow(*168*).

2.5.2. Optical probes for folding detection.

(1) Protein fluorescence. Absorption of UV radiation by a molecule excites it to an excited singlet state. Fluorescence occurs when this molecule returns to the ground state by emitting a photon. The efficiency of the fluorescence process can be defined as

$$\Phi \text{ (quantum yield)} = \text{(number of photons emitted)/(number of photons absorbed)}$$

Three naturally occurring aromatic residues (Phe, Tyr, and Trp) contribute significantly to protein fluorescence. As compared to Phe and Tyr, Trp has much greater quantum yield and absorbance at the wavelength of excitation. Also, fluorescence emission of Phe and Tyr are easily quenched due to the resonance energy transfer(*133*). Therefore, Trp contributes to most of the observed fluorescence emissions of a protein(*133*).

The three aromatic residues have distinct emission and absorption properties. Although the fluorescence of a protein is a mixture of individual aromatic residues, detection can be made exclusively for Trp by exciting proteins at ~ 295 nm and/or collecting fluorescence above 350 nm(*133*).

Both Trp and Tyr fluorescence are sensitive to their local environment. However, an advantage of Trp over Tyr is that Trp usually occurs rarely in a protein; thus, changes in Trp fluorescence reflects conformational changes in a specific region of a protein. Although the fluorescence intensity can be either stronger or weaker as folding

progresses, the emission maximum of Trp shifts to a shorter wavelength (blue-shift) upon forming native structure(133).

(2) Fluorescence dye. Interaction with fluorescence dye 8-Anilinonaphthalene-1-sulfonic acid (ANS) and its derivative is a commonly used technique to monitor protein folding, since ANS fluorescence emission greatly increases upon binding to a partially unfolded folding intermediate(*169-171*). A high binding affinity of ANS to solvent-accessible hydrophobic regions has been proposed to explain this phenomena(*170*); nevertheless, such binding behavior is not observed in unfolded proteins. Although several alternative theories have been suggested(*170-172*), the exact binding nature remains elusive. In addition, structural perturbation upon binding of ANS to proteins have been reported(*171, 173*). Both factors could complicate data interpretations.

(3) Circular dichroism. Circular dichroism (CD) refers to the differential absorption of left and right circularly polarized light. In the far-UV region (wavelength 240 nm and below), CD signals of a protein arise mainly from its peptide bonds. The characteristic spectra exhibited by different types of secondary structure have been observed(*174*) (Figure 2.6), and routinely used to probe secondary-structure composition of a protein.

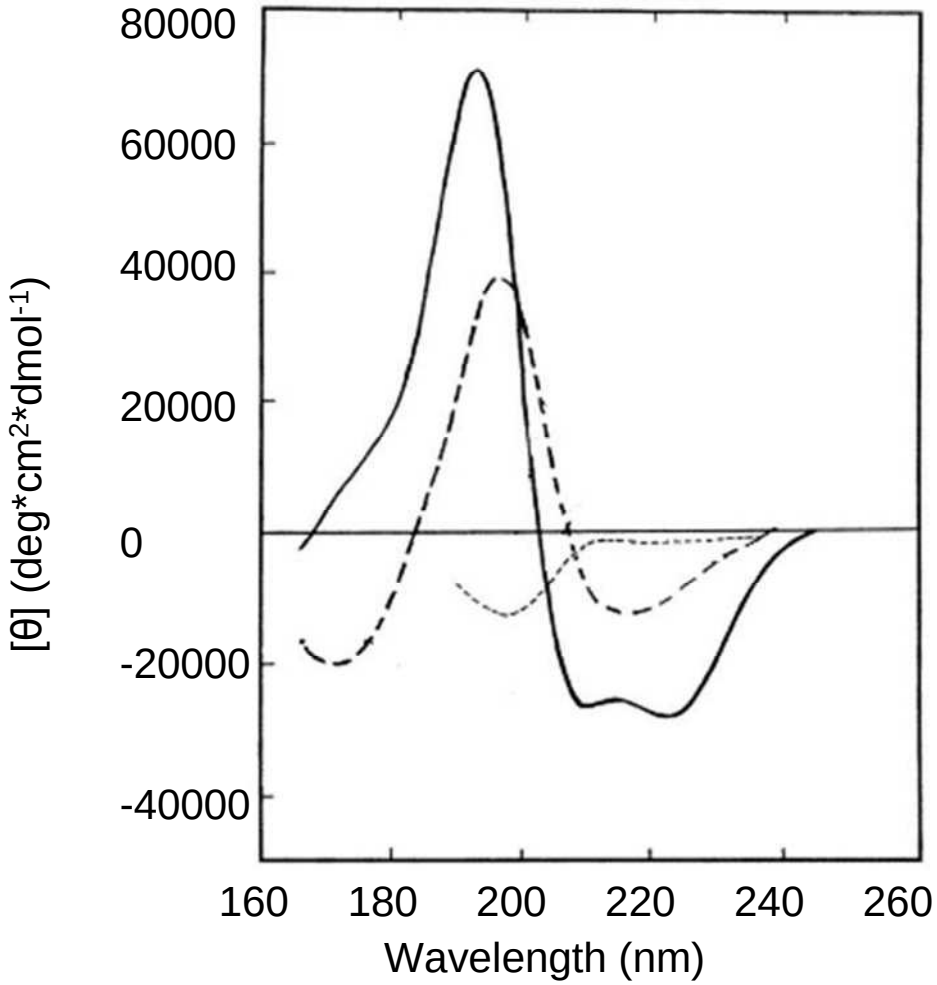

Figure 2.6. Far-UV CD spectra associated with various types of secondary structure. Solid line, α-helix; long dashed line, anti-parallel β-sheet; short dashed line, irregular structure. Figure was adopted with modification from Kelly, S. M. et al. (2005) *Biochim. Biophys. Acta.* **1751**, 119-139.

2.5.3. Probe interactions formation along the folding pathway. Interactions formation in protein folding can be assessed at single residue level by applying techniques such as hydrogen/deuterium exchange and mutagenesis combined with the kinetic approaches mentioned above.

(1) Hydrogen/deuterium exchange. Exchange of protons between proteins and surrounding solvent occurs spontaneously. Such reaction barely happens on the hydrogen attached to the backbone carbon atom, and proceeds too fast to be measured for protons located on protein side chains (-OH, -SH, -NH_2, and –COOH)(*175*). Only the exchange reactions occur on amide protons can be measured easily(*175*).

Hydrogen bonding and solvent accessibility determine the exchange reactions. Amide protons involved in hydrogen-bonded structure exhibit slow exchange; nevertheless, those free from hydrogen bonding exchange more rapidly, even when they are not exposed to solvent(*134, 176*). In other words, hydrogen bonding is more important than solvent accessibility in determining exchange reactions(*134*). In an unfolded protein or polypeptide chain, hydrogen exchange is a fast process; however, exchange for amide protons in a native form is much slower. Since the exchange rate for an individual amide proton depends on its involvement in hydrogen bonding and its solvent accessibility, isotopic exchange of amide proton is an excellent probe for structure formation.

Hydrogen exchange labeling has been coupled with flow-kinetics to obtain detailed structural information for early folding events occurring on millisecond time-scale. As shown in Figure 2.6, unfolded proteins are first equilibrated with D_2O in denaturing solution, so that all the liable backbone and side-chain amide protons are exchanged with deuterium (Figure 2.6.A)(*134*). The well-equilibrated solution (in Syringe 1) is then mixed with refolding solution in D_2O (in syringe 2) to initiate refolding reaction (Figure 2.6.B). Proteins are allowed to refold for a chosen time interval (T_1-T_0) until being mixed

with a *pulse buffer* containing H_2O buffer solution at high pH (Syringe 3)(*134*). Refolding at this time point (T_0) is stopped. Amides that already form a stable hydrogen bond at this time point remain deuterated (ND), while those exposed amides become fully protonated (NH) (Figure 2.6.C)(*134*). After a pulse time (T_2-T_1), the solution is mixed with H_2O at low pH to quench deuterium to hydrogen exchange, and refolding is allowed to complete (Figure 2.6.D). The fully folded protein is then collected and analyzed using NMR. By choosing different time interval (T_1-T_0) to cover the refolding reaction, the time course of hydrogen bond formation during protein folding can be monitored.

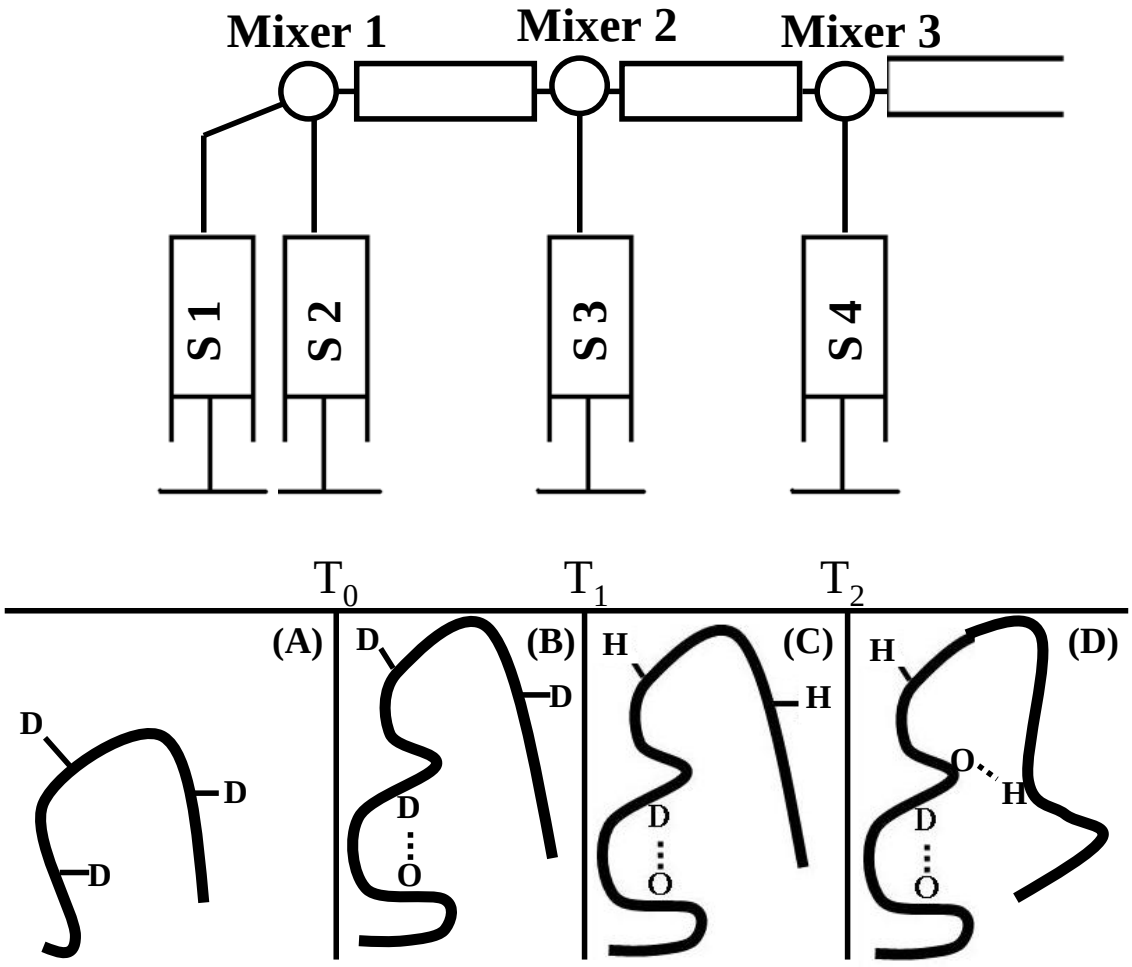

Figure 2.7. Schematic illustration for pulsed hydrogen exchange method. Instrumental setting (quenched-flow technique) is on the top. Sequence of reactions (bottom) is illustrated using an oversimplified polypeptide chain. S is denoted to syringe.

(2) Transition-state analysis. A comprehensive mapping of protein folding process can be achieved by protein engineering. To assess the contribution of individual amino acid to folding progress, side chains of a protein are modified by site-directed mutagenesis to delete or alter existing weak interactions without perturbing the overall structure(*134*). A pairwise interaction can be identified by removing the amino acids involving in the

interaction separately and together(*177*). Folding kinetics and equilibrium properties are measured for the wild-type and mutant proteins. The free energies of the native, intermediate, and transition states can be calculated from equilibrium and rate constants. After the energy profile is established, the free energy difference between the wild-type and the mutant protein in each state is compared. Φ_{Ts} and Φ_I are introduced to analyze interaction formation at each residue involved in the transition and intermediate states (Figure 2.7):

$$\Phi_{Ts} = \Delta\Delta G_{U\text{-}Ts}/\Delta\Delta G_{UN}$$

$$\Phi_I = \Delta\Delta G_{UI}/\Delta\Delta G_{UN}$$

where $\Delta\Delta G_{U\text{-}Ts}$, $\Delta\Delta G_{UI}$, and $\Delta\Delta G_{UN}$ are the apparent energy differences between the wild-type and mutant proteins in the transition, intermediate, and native states relative to the unfolded state, respectively. A Φ value of 1 indicates that the interaction affected by the mutation is formed as completely as in the native protein, whereas a Φ of 0 suggests that the interaction at this site is not formed, as in the unfolded state(*134, 177-179*).

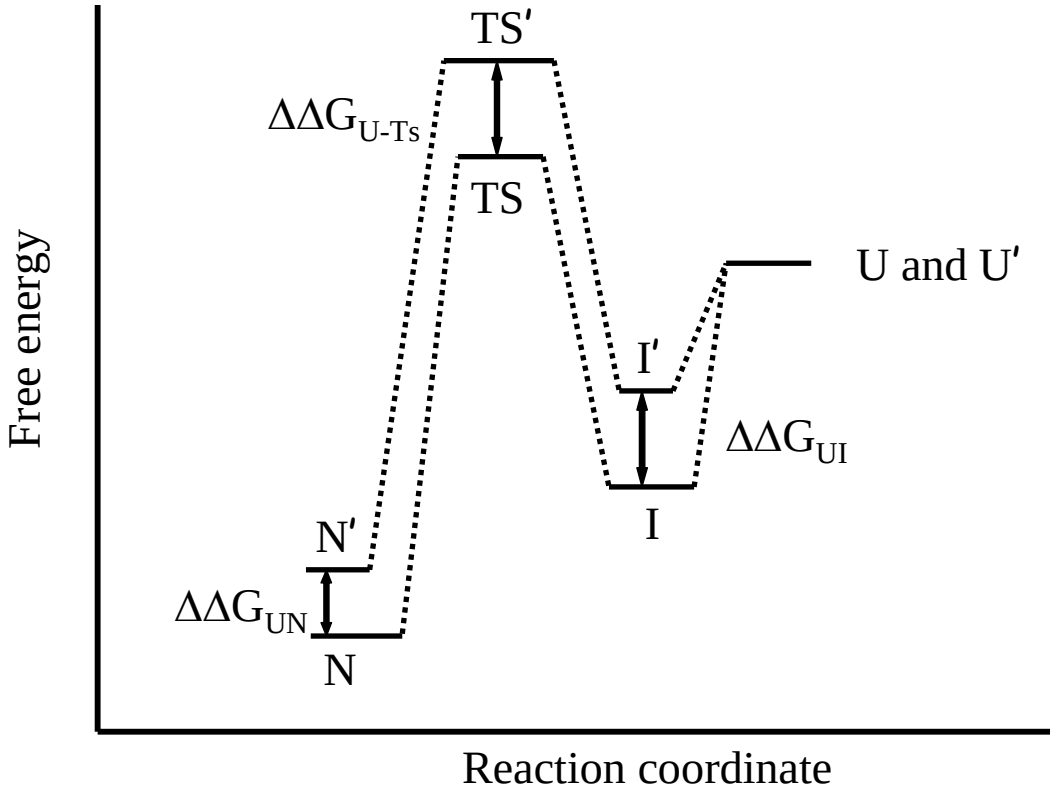

Figure 2.8. Free energy diagram for Φ-value analysis of transition and intermediate states. *N*, *TS*, and *I* represent the native, transition, and intermediate states, respectively. Prime is denoted to mutant.

2.6. Theoretical aspects of protein folding.

2.6.1. Initiation of protein folding. Contact order of a protein provides a measure of the average sequence separation of the contacting residues in the folded state(*180*). The first step for protein folding is to form contacts between different regions of an unfolded protein. As in a simple chemical reaction, the free energy landscape of protein folding is determined by the trade-off between the loss of entropy and the gain of favorable native interactions. Entropy cost increases with an increasing distance between the contacting residues in the primary structure, since a larger portion of a polypeptide chain has to be

restricted in order to form native contacts. Conceivably, proteins with lower contact order fold faster than those with higher contact order(*180*). Such simple correlation has been observed for several proteins(*181*). However, recent evidence indicate that primary structure is also important in determining folding speed by affecting the relative free energies of ordering different part of a polypeptide chain(*180-185*). When there are several routes along the free energy surface, which involve forming interactions between residues equally distant in the primary structure, folding reactions will favor those with the lowest local free energy of ordering(*180-181*).

2.6.2. Roles of intermediates in protein folding. The role of intermediates in protein folding is still under debate. Fersht(*186*) suggested that a stable unfolded state may increase the free energy barrier for conversion to the native folded state under certain conditions, thus is unbeneficial for folding reactions. Consistent with this idea, a *gap theory* has been proposed. In this model, folding rates show positive correlation with the energy difference between the native state and the state closest to it(*142, 187*). Statistic evidence has shown that hydrophobic residues in a naturally occurring protein sequence tends to be further apart from each other than expected for a random distribution(*188*), suggesting that nature selection tends to weaken local contacts in order to destabilize the unfolded state. The same idea has been applied to intermediate formation. Shakhnovich *et al.* and Fersht *et al.* proposed that folding is generally faster without passing through an intermediate state(*186, 189-190*), since the free energy of an intermediate usually lays between the unfolded and the native states. Taken together, these studies suggested that accumulation of an intermediate is a kinetic trap, instead of a facilitator, in protein

folding. On the other hand, formation of an intermediates does decrease the *entropic* costs for structural rearrangements in the sequential folding step, and thus is advantageous for efficient folding(*142*). Contrary to the studies mentioned above, conditions stabilizing intermediates have been observed to accelerate folding reactions(*141, 191-195*), suggesting that intermediates play a productive role in protein folding.

2.6.3. Theoretical models for protein folding. Since the 1950s, three classical models have been put forward to visualize protein folding. In the *framework model* (also called the *hierarchical model*) (Figure 2.8.A)(*134, 196-197*), secondary structure forms first, followed by packing these pre-existing structural elements into the native tertiary structure. This model predicts that secondary structure elements themselves are stable in an unfolded protein; the most difficult step in folding is docking these structural elements. However, experiments have shown that the isolated secondary structure is rarely stable in solution(*198*). Although different amino acids confer different secondary structure propensities to polypeptide chains(*199-200*), most isolated peptides that form regular secondary structure in a protein are disordered in solution(*198*). Hydrophobic interactions and long-range contacts within a protein are required to stabilize secondary structure elements(*145*). In the *nucleation-growth model* (Figure 2.8.B)(*201*), small nucleus encompassing localized secondary-structure elements occur randomly all over the unfolded protein(*134, 202*). These nuclei are not stable, but serve as templates for rapid propagation of tertiary structure. The nuclei involved in the folding process are not specific(*134*). This model predicts the absence of folding intermediates, thus became

unfavorable after intermediate states were observed experimentally(*202*). In the *hydrophobic collapse model(203)*, hydrophobic interactions collapse a protein first, then folding occurs in a confined volume(*134*). Conformational search is thus facilitated by decreasing the conformational freedom of a polypeptide chain(*134*). The problem in this model is that the excess non-specific hydrophobic interactions may interfere subsequent structural rearrangements(*204*); it also contradicts to experimental evidence where secondary structure is formed concurrently with collapsing(*205*).

In 1995, Fersht and his colleagues proposed the *nucleation-condensation model* based on their studies on chymotrypsin inhibitor 2 (CI2) protein(*145*). This model states that tertiary interactions, including hydrophobic and other long-range interactions, form in concert with secondary interactions in the transition state. As the tertiary interactions stabilize otherwise unstable secondary structures, folding becomes more hierarchical and eventually follows the framework model(*204, 206*). Although this model is in good agreement with several experimental studies(*204, 206-209*), it remains to be determined whether protein folding follows such a mechanism.

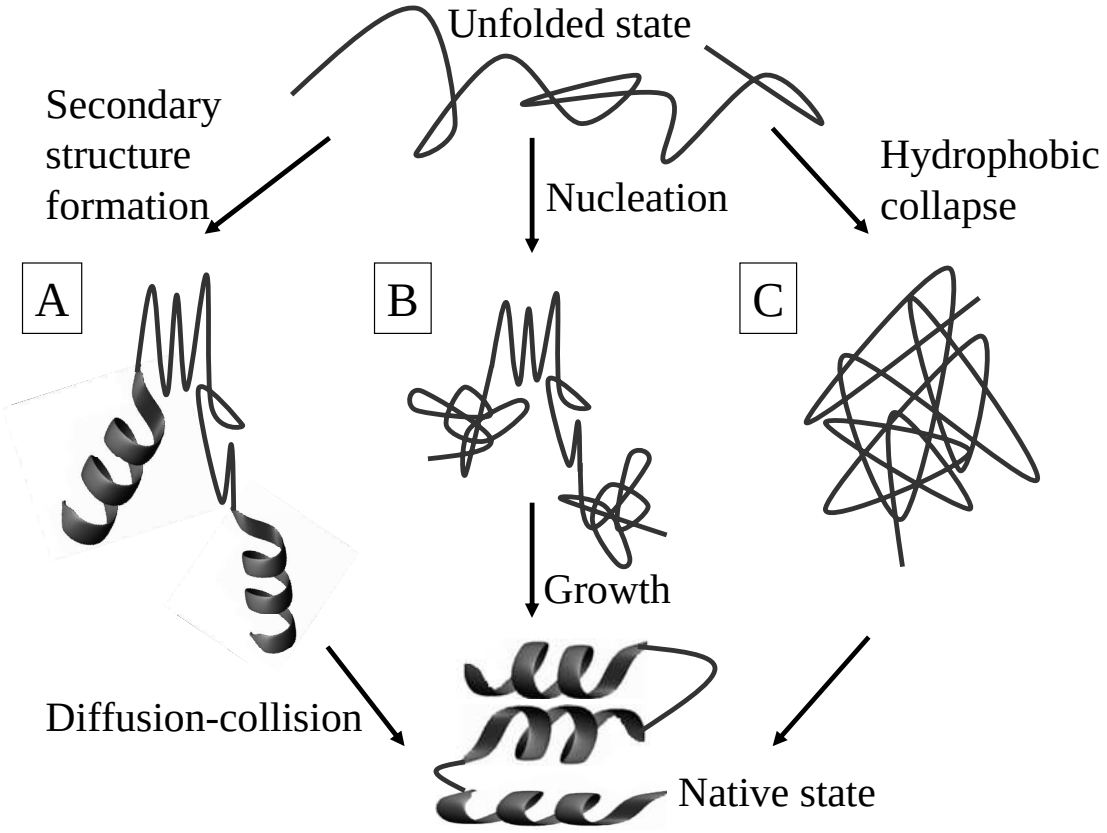

Figure 2.9. Illustration of three classical folding mechanisms. (A) Framework model. (B) Nucleation-growth model. (C) Hydrophobic-collapse model.

2.6.4. Visualization of protein folding. In 1973, Christian Anfinsen proposed the famous *thermodynamics hypothesis*, stating that the native structure of a protein corresponds to the global minima of free energy. In other words, formation of the native folded structure does not depend on the kinetic routes(210-211). However, Cyrus Levinthal noticed that most folding reactions complete on the millisecond time-scale. By the given large conformational space of a polypeptide chain, random searching of the native state seems implausible for an unfolded protein to find its native structure within such a short time(*212*). Hence, the search is not fully random, but determined by a trade-off in entropy

and enthalpy. This is also evident experimentally, in the small free-energy barriers between the native and unfolded states.

To help in visualizing this trade-off, the concept of a *free energy landscape* for protein folding was introduced(*213*). Free-energy landscapes have a funnel-like shape(*213-214*), represents the conformational space as a function of intramolecular-plus-solvation free energy of a given protein (Figure 2.9)(*212, 215*). The key component in this model is the number of possible conformations at each energy level(*212*). A protein molecule does not need to follow a specific folding route; instead, a number of paths are available. The conformational space decreases as folding progresses; a series of local optimization occurs during this process. It finally leads to the bottom of the funnel, which corresponds to the global energy minima, i.e. the native structure.

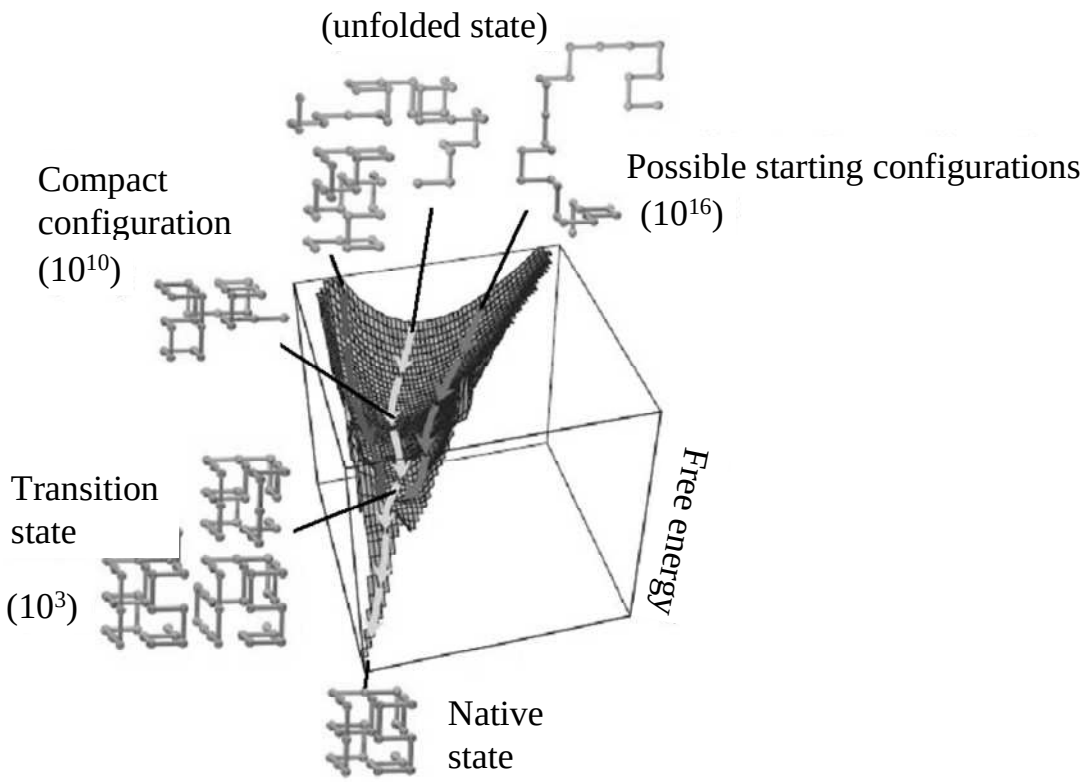

Figure 2.10. Schematic representation of the free energy surface calculated for the folding of a 27-mer. This free-energy surface was constructed using Monte Carlo simulation. The possible configuration decreases as the folding progresses down to the bottom of the funnel. Figure was adopted and modified from Dinner, A. R. et al. (2000) *Trends. Biochem. Sci.* **25**, 331-339.

Several local energy minima may exist and form shallow valleys on the free energy surface (Figure 2.10.A). Energetic variations within the same energy level are due to fluctuations of local structures, such as rotation of an individual side-chain. The local energy minima correspond to the most stable conformations at each energy level(*214*).

Interconversion between these low-energy species in the local minima usually occurs rapidly(*212, 214*).

Protein folding is determined by the smoothness of its free energy landscape. Levinthal's argument does not hold because it assumes the same possibility for a protein to travel through each configuration without considering the variations in the free energy of each path(*214*). It leads to a free energy landscape with a shape of a flat golf course (Figure 2.10.B): There is only one minimum on the free energy surface, which corresponds to the global energy minima. In other words, local energy minima does not exist(*214*). In the real situation, however, the paths have different likelihood, based on their free energies. The probability for a protein molecule passing through conformations with lower free energies is higher than through those with higher free energies(*214*).

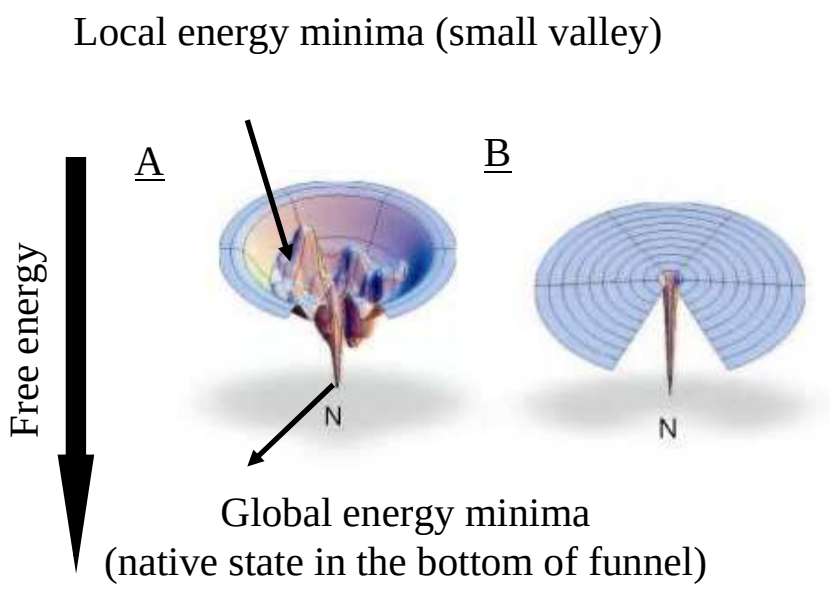

Figure 2.11. Simplified schematic diagram for illustrating different types of free energy surface. Each point on the free energy surface represents each possible conformation. (A) shows a free energy surface with several small valleys, which correspond to local energy minima. (B) shows a free energy surface with equally likely conformations without considering the energy differences in each configuration (golf course-like landscape). In this model, folding is through random searching. Figure was adopted with modification from Dill, K. A. et al. (2008) *Annu. Rev. Biophys.* **37**, 289-316.

Both thermodynamics and kinetics play important roles in determining folding paths. If the structure with global energy minima is not kinetically accessible for other local energy minima within a reasonable time (i.e., the energy barrier between the small valleys to the bottom of the funnel is too high), proteins will not fold to the structure corresponding to the lowest free energy(*214*). To satisfy both energetic elements, Gō proposed that kinetic pathway of folding is consistent with, and leads to, the state of

minima free energy(*216*). Such situation can be archived by evolutionarily ordered folding pathway, in which accessible conformational space decreases rapidly to reach the lowest energy state when folding proceeds through defined transition and intermediate states(*133*).

From the view of free energy landscape, the transition state (TS) in protein folding should represent the lowest energy barrier on the way to form the native structure(*142*). To avoid TS conformational ensemble (TSE) falling back to the unfolded state, it should resemble the native state but be distinct from the unfolded state(*142*). Since folding reactions descent rapidly to the native state after passing through TS, TSE should contain native interactions(*142*). In an unfolded polypeptide chain, local interactions are the dominate force, some of which are present in TSE and the native state(*142*). To be dissimilar to the unfolded state, some native non-local interactions should form in TSE(*142*). Therefore, formation of TSE is a process where the local interactions fluctuate until proteins form certain native non-local interactions; such conformational ensemble can be viewed as a distorted form of the native structure(*142*).

Chapter 3. Experimental Designs

The current development of methods for preventing, detecting, and treating prion diseases is limited by our knowledge of its pathogenesis. Although the role of PrP^{Sc} aggregates in prion diseases is unclear, all the proposed pathogenic models involve a structural conversion from PrP^{C} to PrP^{Sc}(*52, 217*); for this dissertation, I denote this conversion as 'misfolding'. To understand the initiation of PrP misfolding, the *normal* folding pathway has to be characterized.

Sheep susceptibility to classical scrapie is governed by the polymorphisms at positions 136, 154, and 171 in ovine PrPs (ovPrPs)(*88, 94-96*). Since the key event in prion diseases is the PrP^{C}-to-PrP^{Sc} conversion, I hypothesized that polymorphisms exert their effects on PrP^{Sc} precursors, i.e., they affect the disease susceptibility by modulating the structural conversion. I aim to examine whether folding and unfolding of ovPrPs proceed through an intermediate. If such an intermediate exists, I aim to study its role in PrP misfolding by examining whether its population and/or structure correlate with scrapie susceptibilities of ovPrP variants, and to elucidate the role of the sole disulfide bond in its formation. Thus, three specific aims have been proposed:

3.1. Specific aim one: Assay for an ovPrP folding intermediate.

3.1.1. The major gap in knowledge.

Previously observed kinetic intermediates in normal PrP folding. An early study suggested that murine PrP (muPrP) folds with a half-life of ~ 170 μs without populating an intermediate(*218*). However, since these measurements were taken with 2000 μs time resolution, they do not seem reliable(*219-220*). A later study of human PrP (huPrP) was undertaken with 100 μs time resolution, and observed the accumulation of an early intermediate with a time constant of ~ 50 μs, followed by a rate-limiting folding step with a time constant of ~ 700 μs(*219*). It is unclear whether such an intermediate exists in other PrP species, and if so, whether the properties of this intermediate are consistent across species.

3.1.2. Hypothesis.

In Specific Aim One, I hypothesize that folding and unfolding of ovPrPs proceed through one or more intermediate state(s). This would be consistent with huPrP, which has a very similar primary sequence to ovPrP.

3.1.3. Methods.

This project is in collaboration with Dr. Heinrich Roder at Fox Chase Cancer Center in Philadelphia. Folding and unfolding kinetics were followed by tryptophan fluorescence using a continuous-flow capillary mixing method. This method offers two advantages: *First*, tryptophan fluorescence is an excellent probe of the folding process because of its high sensitivity to environmental changes. In contrast to commonly used fluorescent dyes, such as 8-anilino-1-naphthalenesulfonate (ANS), the intrinsic fluorescence probe Y221W perturbs the protein conformation minimally. *Second*, the high time resolution (90 μs) of

the continuous-flow system(*166*) allows folding and unfolding events occurring on microsecond time-scale to be detected directly. Continuous-flow systems are at present the most reliable method for recording such events. Such a high time resolution is *necessary* for following the folding kinetics of PrPs, since this reaction has been reported to occur on the microsecond time-scale(*218-221*). *Third*, such high time resolution is required for direct observation of the folding intermediates of many proteins. On the other hand, two disadvantages are associated with this mixing technique. *First*, this method requires large amounts of protein sample. *Second*, the maximum observation time of this method is limited to ~ 1000 to 2000 μs. In other words, reactions occurring more slowly than 1000 μs cannot be observed with this technique.

3.2. Specific aim two: Establish the relationship between (un)folding kinetics and susceptibility of ovPrP variants to classical scrapie.

3.2.1. Major gap in knowledge.

(1) PrP^{Sc} precursor occurring on the normal folding pathway. An important step in designing therapeutic targets for prion diseases is to identify the PrP^{Sc} precursor. The precursor of PrP^{Sc} occurring under physiological cellular conditions, denoted here as ***PrP^{*}_{Cell}***, has not yet been identified, although a precursor occurring under non-physiological oligomer-forming and fibrillization conditions (denoted here as PrP^{*}_{Fib}) has been observed(*222-227*). Presumably, the structure of PrP^{*}_{Cell} should be ready for conversion to PrP^{*}_{Fib} or PrP^{Sc}. In other words, the conformation of PrP^{*}_{Cell} should either be (1) similar to PrP^{*}_{Fib} or PrP^{Sc}, or (2) flexible enough to undergo structural conversion.

If the PrP^{*}_{Cell} of both resistant and susceptible variants are poised to form PrP^{*}_{Fib} or PrP^{Sc} (i.e., if the structures of the precursor in these allelic variants do not differ significantly), the genetic modulation should be reflected in the *population* of the precursor.

(2) Previously proposed mechanisms for genetic modulation in classical sheep scrapie. Several mechanisms have been proposed to explain the genetic modulation observed in classical scrapie. Glycosylation patterns have been suggested to differentiate scrapie susceptibilities by modulating the accessibility to residue A/V171(*228*). Increased susceptibility to classical scrapie displayed by homozygous VLRQ sheep correlates with higher level of plasma PrP^{C}(*229*). OvPrP variants susceptible to classical scrapie appear to have longer cellular half-lives, when compared to the resistant ones(*230*). The propensities of ovPrPs for structural conversion, both *in vitro* and *in vivo*, correlate with their susceptibilities to classical scrapie(*231-235*).

In Kelly's model, any mutation destabilizing the native state is predicted to enhance amyloid formation(*236*). However, this model is in apparent contradiction with previous observations. In classical scrapie, susceptible variants are *more* stable than the resistant ones, as measured by the free energy difference between the native and unfolded states, ΔG_{NU}(*233, 237-238*). Different *in vivo* clearance has been proposed to explain this paradox(*230, 233, 237-238*); nevertheless, it cannot account for the increased *in vitro* propensities to misfolding observed in susceptible variants.

Native PrP^{C} has been suggested to be PrP^{Sc} precursor. Zhang *et al.* found that Syrian hamster PrP^{C} possesses a relatively open conformation based on circular dichroism and NMR measurements, and proposed that the flexible region of native PrP^{C} is susceptible to structural conversion(*46*). Welker *et al.* suggested a domain swapping model, where oligomerization proceeds through a thiol/disulfide exchange reaction between two native PrPs(*239*) (Figure 3.1). Such dimeric structure has been observed by Knaus and his colleagues(*43*). Nevertheless, a later report on *in vitro* conversion study seems to contradict to this model(*240*).

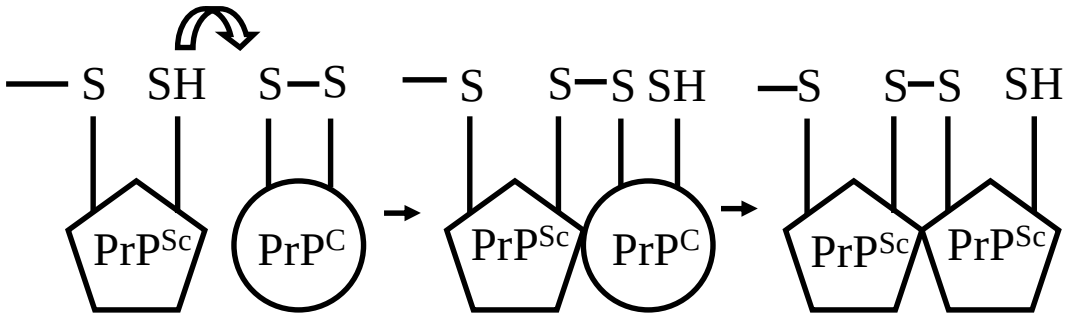

Figure 3.1. Conversion from PrP^{C} to PrP^{Sc} through disulfide polymerization in the domain swapping model. Attack of the terminal thiolate of PrP^{Sc} on the disulfide bond of PrP^{C} initiates the PrP^{C}-to-PrP^{Sc} conversion. Association with PrP^{Sc} weakens the tertiary structure protection of the disulfide bond in PrP^{C}, thus facilitating polymerization reactions(*239*).

Several studies have been carried out to assess the relationship between the native state and the susceptibility to prion diseases. Many of the mutations corresponding to human inherited prion diseases do not alter the thermodynamic stability in the native state

relative to the wild-type huPrP(*241-242*). In the case of classical scrapie, susceptible alleles confer even *higher* structure stability in their native forms, as compared to the resistant ones(*233, 237-238*). Moreover, a recent study shows that muPrPs carrying pathogenic or protective mutations in human or sheep prion diseases exhibit structures and backbone dynamics similar to their wild-type counterpart in the native state(*243*). Taken together, these studies suggest that genetic modulations associated with prion diseases do not exert their effects on the native form. Therefore, if they are associated with folding whatsoever, they must exert their effects on a folding intermediate. If so, a folding intermediate seems to be a potential PrP^{Sc} precursor.

Kuwata *et al.* have identified the intermediate states of human and hamster PrPs by high pressure NMR(*244-246*), but their correlation with the disease occurrence has not been established. As mentioned earlier, Apetri *et al.* observed a kinetic intermediate in huPrP refolding(*219-221*). The mutations linked to familial prion diseases result in a pronounced increase in the population and the hydrophobicity of this intermediate(*219, 221*). However, such an intermediate was not observed for murine PrP(*218*). It remains to be established whether genetic variations in different mammalian species modulate disease susceptibility in the same way as observed in human inherited prion disease.

3.2.2. Hypothesis.

To explain the paradox mentioned above, I hypothesize that the folding intermediate observed in *Specific Aim One* is the PrP^{Sc} precursor, and genetic modulation in classical scrapie exerts its effects on this kinetic species, and not on the native form. In other

words, I hypothesize that the structure and population of this intermediate are critical in determining the susceptibility of ovPrP allelic variants.

3.2.3. Methods.

This hypothesis will be tested by comparing the folding and unfolding kinetics of four ovPrP variants using the method described in *Specific Aim One*. The relationship between the susceptibilities and the intermediates associated with four allelic variants will be established, then the plausible role of the intermediate in classical scrapie will be inferred.

3.3.Role of the disulfide bond in stabilizing the folding intermediate.

3.3.1. Major gap in knowledge.

The role of the sole disulfide bond (Figure 3.2) of PrPs in prion diseases remains controversial. Some studies suggest that an intact native disulfide bond is required for the PrP^{C}-to-PrP^{Sc} conversion (*247-249*); however, others indicate that this disulfide bond has to be reduced to initiate misfolding(*239, 250-253*). Welker *et al*. suggest that an intermolecular disulfide bond does not bridge monomeric PrP^{Sc}, and, in contradiction to the previous studies, temporary reduction of the intramolecular disulfide bond is not necessary for converting to PrP^{Sc}(*240*). A very recent report has shown that the disulfide bond restricts the motion of the putative transmembrane domain (residues 111-135) of Syrian hamster PrP, thus affecting the initiation of misfolding by regulating membrane binding(*254*).

3.3.2. Hypothesis.

I hypothesize that the disulfide bond in PrP suffices to stabilize the formation of the previously observed folding intermediate (see *Chapter Four*). Although the role of the disulfide bond in prion diseases has not been well established, the importance of disulfide bonds in protein conformational folding(*149*) suggests that the disulfide bond may be involved in the PrP misfolding. A native disulfide bond imposes conformational constraints on its neighboring residues, stabilizing its native local structure; this property permits the formation of folding intermediates in some proteins(*149, 151-154*). Therefore, the disulfide bond in PrPs may exert its effects by stabilizing a folding nucleus for the intermediate. (*Folding nucleus* is defined here as a specific subset of native interactions required for stabilizing an intermediate state.) If so, and if PrP misfolding proceeds through a folding intermediate, the local structure around the disulfide bond may serve as a folding nucleus for directing structural conversion to both PrP^{C} and PrP^{Sc}.

Figure 3.2. Positions of the sole disulfide bond and model peptides in ovPrP. (A) Ribbon representation of the structure of ovPrP (PDB entry: 1UW3). The disulfide bond is shown in gold. P1 and P2 are shown in blue and red, respectively. (B) Sequence alignment of homologous PrP. α and β are denoted to α-helix and β-sheet in PrPs.

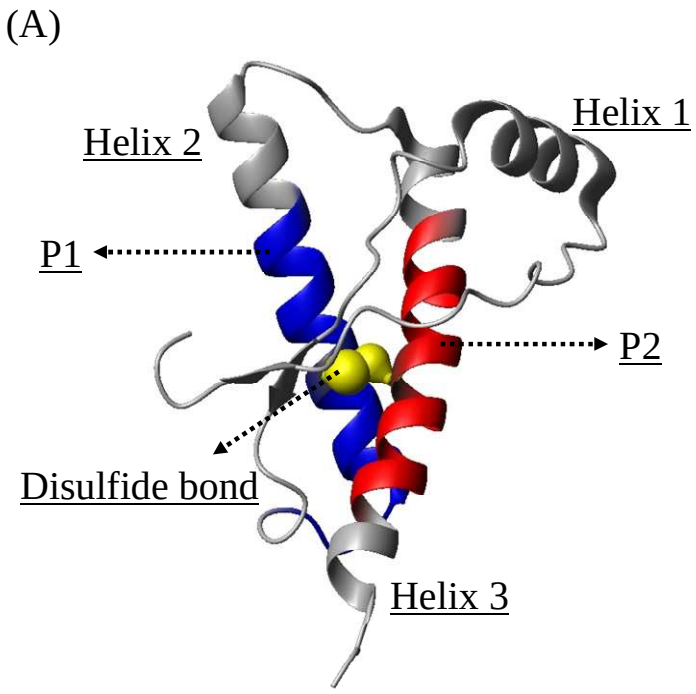

Figure 3.2. (cont'd)

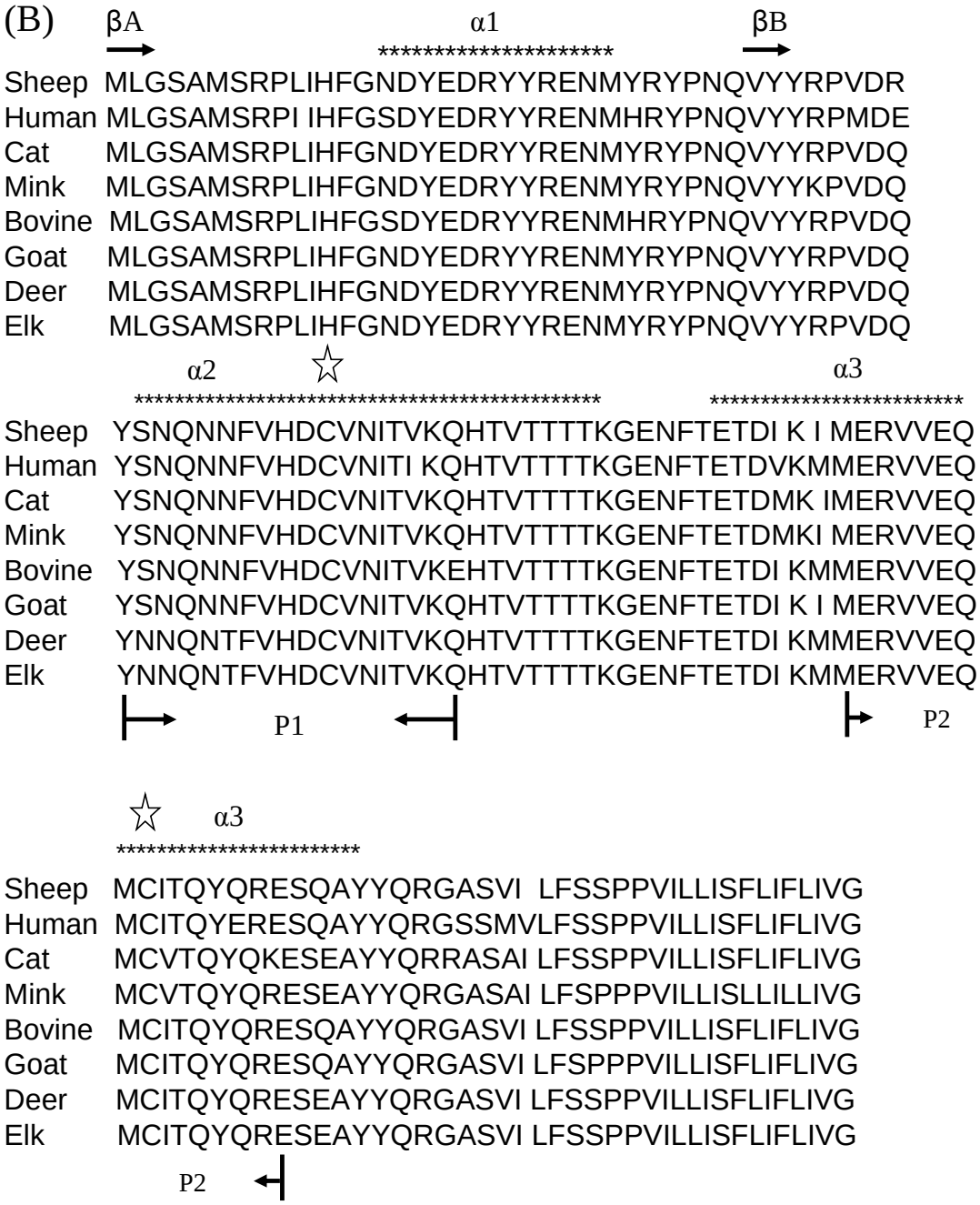

3.3.3. Methods.

To examine this hypothesis, a peptide model flanking the sole disulfide bond will be used to measure the local folding of PrP through circular dichroism (CD) and hydrogen/deuterium exchange (HDX).

(1) Selection of peptide models. I chose to use a peptide model, instead of the full-length protein, because it allows me to sort out the contributions of local and global interactions in forming the folding intermediate. The peptides are selected based on the conservation of the residues around the disulfide bond without considering their involvement in the secondary-structure elements. This allows me to assess the role of the disulfide bond, instead of the intrinsic secondary-structure propensity of the peptides, in the local structure formation. Two peptides are selected: (P1)YSNQNNFVHDCVNITVKQH (residues 169-187), and (P2) MERVVEQMCITQ YQRE (residues 206-221). P1 involves the N-terminus of helix 2 (residues 175-197), whereas P2 involves the central region of helix 3 (residues 202-230). Both peptides do not cover the whole of their helices (Figure 3.2).

(2) Hydrogen/deuterium exchange and circular dichroism measurements. The hydrogen/deuterium exchange (HDX) method allows me to probe the hydrogen bonding and solvent accessibility of individual residues in the peptides. If interactions around the intramolecular disulfide bond suffice to form the PrP folding intermediate, the P1P2 model peptide should adopt its native structure (α-helix) in solution. Therefore, its HDX rate will be significantly decreased compared to its monomeric components (P1 and P2). HDX is able to probe individual amides that are involved in stable secondary structure and stable hydrogen bonding, and also gives insight into the formation of tertiary structure. However, marginally stable secondary structure and other interactions that are not involved in stable hydrogen bonding are not detectable by this method(*134*). This limitation can be overcome by monitoring the folding reaction with far-UV circular

dichroism (CD). This technique measures the average secondary-structure content, including the structure elements that are only marginally stable(*134*). Mass spectrometry, instead of NMR, is chosen to monitor HDX reactions in this study because of its low sample requirements.

Chapter 4. Effects of Polymorphisms Associated with Scrapie Susceptibility on the Folding Kinetics of Ovine Prion Proteins

4.1. Introduction.

Prion diseases are a class of neurodegenerative diseases that includes scrapie in sheep and goats, bovine spongiform encephalopathy in cattle (mad cow disease), as well as fatal familial insomnia, Gerstmann-Straussler-Scheinker syndrome, and Creutzfeldt-Jacob disease in humans. According to the prevailing hypothesis(*255*), prion diseases result from the misfolding of a naturally occurring prion protein (PrP) from its normal cellular form (PrP^{C}) to a virulent scrapie form (PrP^{Sc}). This abnormal isoform PrP^{Sc} is able to catalyze the conversion of PrP^{C} to itself(*255*), and its aggregation has been proposed to explain the neuronal death in prion diseases(*30-31, 255*). Although some studies suggest that PrP^{Sc} aggregates are not neurotoxic(*20, 34, 256*), all models of pathogenesis involve the structural conversion of PrP(*52, 217*). PrP^{C} is a copper-binding cell-surface glycoprotein composed of an unstructured N-terminal domain and a globular C-terminal domain (residues ~120-233) of known structure, comprising three α-helices, a short two-stranded antiparallel β-sheet, and a disulfide bond (Cys182-Cys217) linking helices 2 and 3 (Figure 4.1)(*42-45, 257-258*). Relatively little is known about the structure of PrP^{Sc},

except that it appears to have significantly more β-sheet and slightly less α-helix (17-30% α-helix; 43-54% β-sheet) compared to PrP^C (47% α-helix; 3% β-sheet)(*13-15*).

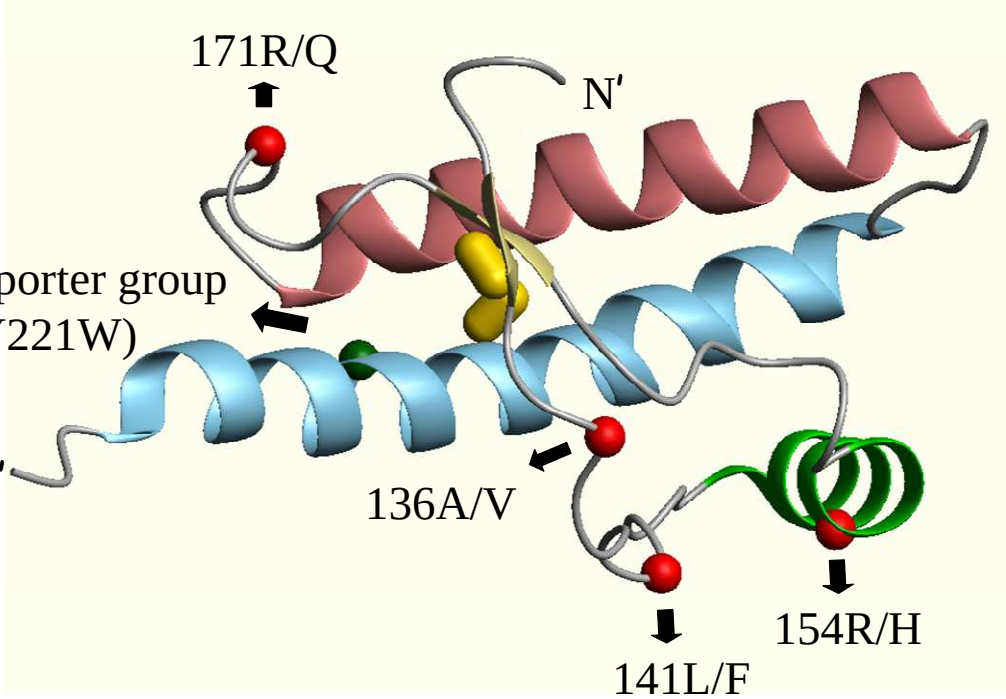

Figure 4.1. Ribbon representation of the structure of ovPrP (residue 126-233). Helix 1 is shown in green; helix 2 is shown in mauve; helix 3 is shown in blue. The antiparallel β-sheet is shown in yellow; the disulfide bridge is shown in gold. The residues involved in genetic modulation in sheep scrapie are shown in red; the introduced fluorescence reporter is shown in green. Figure was drawn with MOLMOL(*47*).

Polymorphisms of ovine PrPs (ovPrPs) have been associated with differing susceptibility to classical and atypical scrapie, particularly at positions 136 (A/V), 141 (L/F), 154 (H/R), and 171 (Q/R) (Figure 4.1)(*88*). In classical scrapie, the $A_{136}L_{141}R_{154}R_{171}$ (ALRR) and $A_{136}L_{141}H_{154}Q_{171}$ (ALHQ) alleles confer resistance, whereas the $V_{136}L_{141}R_{154}Q_{171}$ (VLRQ) and $A_{136}L_{141}R_{154}Q_{171}$ (ALRQ) genotypes are correlated with susceptibility(*88,*

94-96). Several factors, alone or in combination, might account for this genetic modulation(*228-229, 231, 233-235, 237-238, 259*). Variations in glycosylation patterns between allelic variants have been suggested to modulate scrapie susceptibilities by altering solvent accessibility(*228, 259*). PrP^{C} variants susceptible to classical scrapie appear to have longer cellular half-lives and higher plasma concentrations, when compared to resistant variants, giving them more opportunities to convert and oligomerize(*49, 229, 233, 238, 260*). Finally, the propensity for PrP^{C}-to-PrP^{Sc} conversion, both *in vitro* and *in vivo*, also correlates with susceptibility to classical scrapie(*231, 234-235, 237*).

Since this structural conversion requires at least partial unfolding, it is plausible to hypothesize that more susceptible variants are less stable structurally(*236*). However, exactly the opposite is observed for classical scrapie: variants with lower structural stability (as measured by the free energy difference ΔG_{NU} between the folded and unfolded states) are *less* prone to the disease than those with higher structural stability(*233, 237-238*). Different *in vivo* clearance has been proposed to explain this inverse correlation; nevertheless, it cannot explain the higher *in vitro* conversion propensities displayed by susceptible variants(*231, 234*). To account for this apparent paradox, I made the working assumption that polymorphisms affect the susceptibility by modulating the population and/or structure of the PrP^{Sc} precursor, which I took to be a folding intermediate. This hypothesis led me to examine two questions: *First*, do the folding and unfolding of ovPrPs proceed through an intermediate? *Second*, if so, is this folding intermediate the PrP^{Sc} precursor?

To study these questions and the folding of PrP^C in general, I measured the microsecond folding and unfolding kinetics of these four allelic variants under various solution conditions, including two temperatures (5 and 15 °C), two pH values (5 and 7), and two denaturants [guanidine hydrochloride (GuHCl) and urea]. The unfolding kinetics of ALRQ, ALRR, and VLRQ variants exhibited two exponentials at pH 7: an initial lag phase followed by a slower exponential decay. The double exponential indicates the presence of at least one intermediate species besides the native (***N***) and unfolded (***U***) species. Biophysically, the most plausible kinetic model is $\boldsymbol{N \rightarrow I_\alpha \rightarrow U}$, in which the native species ***N*** unfolds quickly to a native-like intermediate $\boldsymbol{I_\alpha}$ before unfolding completely to ***U***. This intermediate is denoted as $\boldsymbol{I_\alpha}$ because, being similar to the native species ***N***, its secondary structure seems likely to be largely α-helical. Such α-helix-rich species have been observed on oligomerization pathways(*222-225, 261*). Adopting this kinetic model, I find that the population and structural stability of $\boldsymbol{I_\alpha}$ in the variants correlate with their differing propensities towards classical scrapie. Variants with higher classical scrapie propensity are characterized by higher populations and more stable tertiary structure in $\boldsymbol{I_\alpha}$. Hence, I conjecture that the formation of this partially unfolded, native-like intermediate $\boldsymbol{I_\alpha}$ is an early step in the formation of PrP^{Sc}.

4.2. Experimental procedure.

4.2.1. Protein preparation and purification. The plasmid encoding ovPrP94-233, ALRQ allele with an N-terminal $(His)_6$ tag was a generous gift from Dr. P. M. Bayley. Based on

this parental plasmid, ALRR, ALHQ, VLRQ, and AFRQ plasmids were constructed by site-directed mutagenesis using QuikChange kit (Stratagene) and the following primers:

For A134 → V134 mutation: 5'-GGC TAC ATG CTG GGA AGT GTG ATG AGC AGG CCT CTT ATA C-3' and 5'-GTA TAA GAG GCC TGC TCA TCA CAC TTC CCA GCA TGT AGC C-3'

For L141 → F141 mutation: 5'-GGA AGT GCC ATG AGC AGG CCT TTT ATA CAT TTT GGC AAT GAC-3' and 5'-GTC ATT GCC AAA ATG TAT AAA AGG CCT GCT CAT GGC ACT TCC-3'

For R154 → H154 mutation: 5'-GAG GAC CGT TAC TAT CAT GAA AAC ATG TAC CGT TAC CCC-3' and 5'-GGG GTA ACG GTA CAT GTT TTC ATG ATA GTA ACG GTC CTC-3'

For Q171 → R171 mutation: 5'-CTA CAG ACC AGT GGA TCG CTA TAG TAA CCA GAA C-3' and 5'-TTC TGG TTA CTA TAG CGA TCC ACT GGT CTG TAG-3'

All sequences were confirmed by DNA sequencing.

These plasmids were transformed into competent *E. coli* BL21 (DE3) cells. To express recombinant proteins, *E. coli* cells containing the desired plasmid were grown in LB medium containing 100 μg/ml ampicillin with shaking at 250 rpm at 37 ^{o}C. Based on

induction studies, once the optical density reaches 0.6 - 1.0, expression is induced by adding isopropyl β-D-1-thiogalactopyranoside (IPTG) to a final concentration of 1 mM. The culture was then incubated overnight. After the cells were harvested, sonication was used to disrupt the cells. Soluble proteins and inclusion bodies in the cell lysate were separated by centrifugation at 12,000 rpm. Since the expressed ovPrPs accumulate in inclusion bodies (Figure 4.2), inclusion bodies were collected and incubated in 8 M urea with gentle stirring at 4^{o}C for a few hours to solubilize the proteins.

Purification was carried out by metal-affinity chromatography using nickel-nitrilotriacetic acid (Ni-NTA) resin (Qiagen). OvPrPs were eluted in a elution buffer containing 50 mM NaH_2PO_4, 300 mM NaCl, 0.5 M imidazole, and 5 mM β-mercaptoethanol, pH 8.0. The purified proteins were then immediately dialyzed into a buffer containing either 50 mM sodium acetate (pH 5) or 50 mM imidazole (pH 7) using Millipore protein concentrator. This step has to be completed in half an hour; otherwise, extensive aggregation occurs. The yield of pure protein is about 1 mg/L of culture.

Protein concentration was determined by the optical density at 280 nm using an extinction coefficient of 22015 $M^{-1}cm^{-1}$ predicted from the amino-acid composition. The identity of the purified protein was confirmed by SDS-PAGE, Western blotting (Figure 4.3), and mass spectrometry (Figure 4.4).

Sedimentation equilibrium experiments were carried out on a Beckman XLI analytical ultracentrifuge at 15000 rpm, 25 ^{o}C. After 6 days, the traces converged to a classic

Boltzmann distribution with an estimated molecular weight of ~17 kDa, in close agreement with molecular weight of ovPrP94-233 (16.9 kDa), suggesting that the purified ovPrP is monomeric (Figure 4.5).

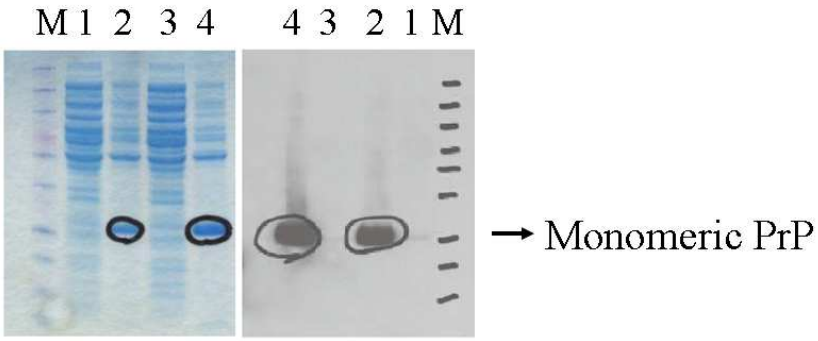

Figure 4.2. SDS-PAGE and Western blotting show the expression of ovPrP in *E. coli*. Left panel, SDS-PAGE (12%) analysis. Right panel, Western blotting analysis using anti-poly(histidine) as the primary antibody. Lanes 1 & 3: Cytosolic fraction of cell lysate corresponding to 25 °C and 30 °C growth temperatures, respectively. Lanes 2 & 4: Inclusion body of cell lysate corresponding to 25 °C and 30 °C growth temperatures, respectively. M: Invitrogen protein ladder.

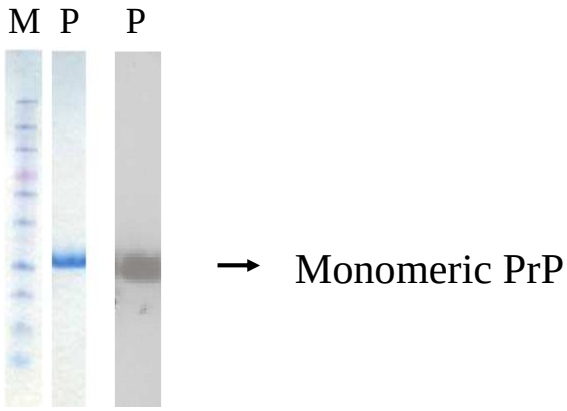

Figure 4.3. Monomeric ovPrP(ALRQ) eluted from Ni-NTA column. Left panel, SDS-PAGE (12%) analysis. Right panel, Western blotting analysis using anti-poly(histidine) as the primary antibody. P: ovPrP. M: Invitrogen protein ladder.

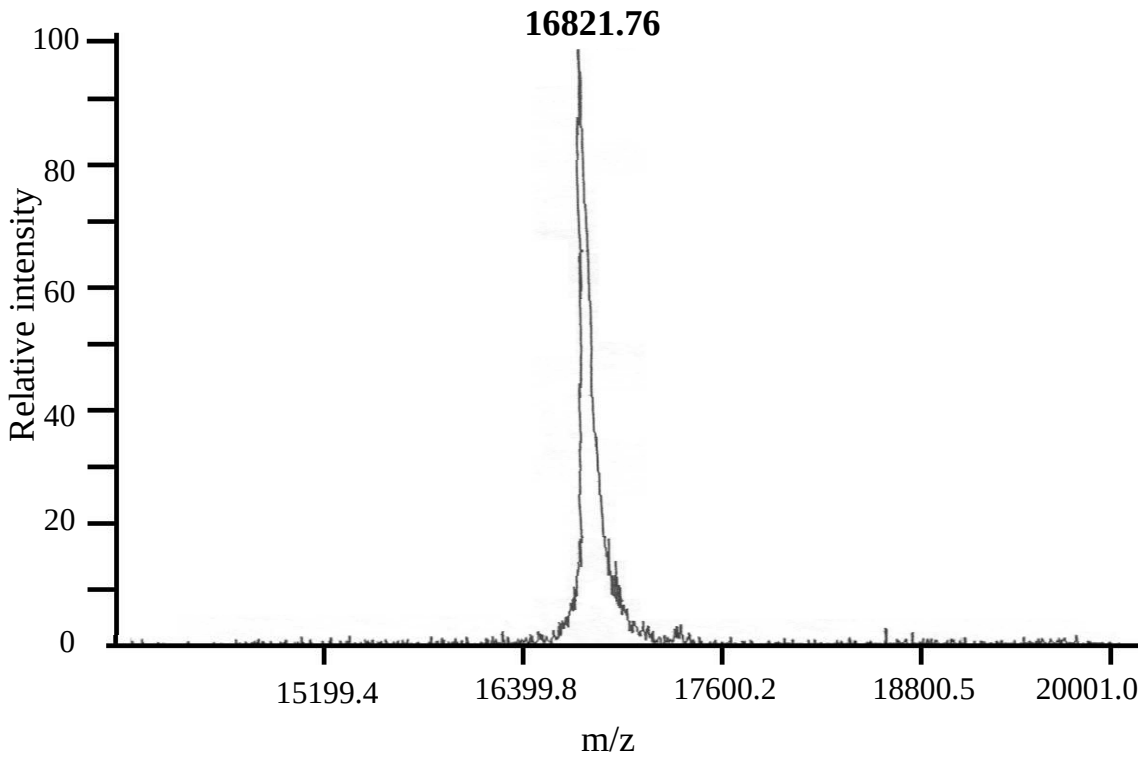

Figure 4.4. MALDI mass spectrum of the ALRQ variant.

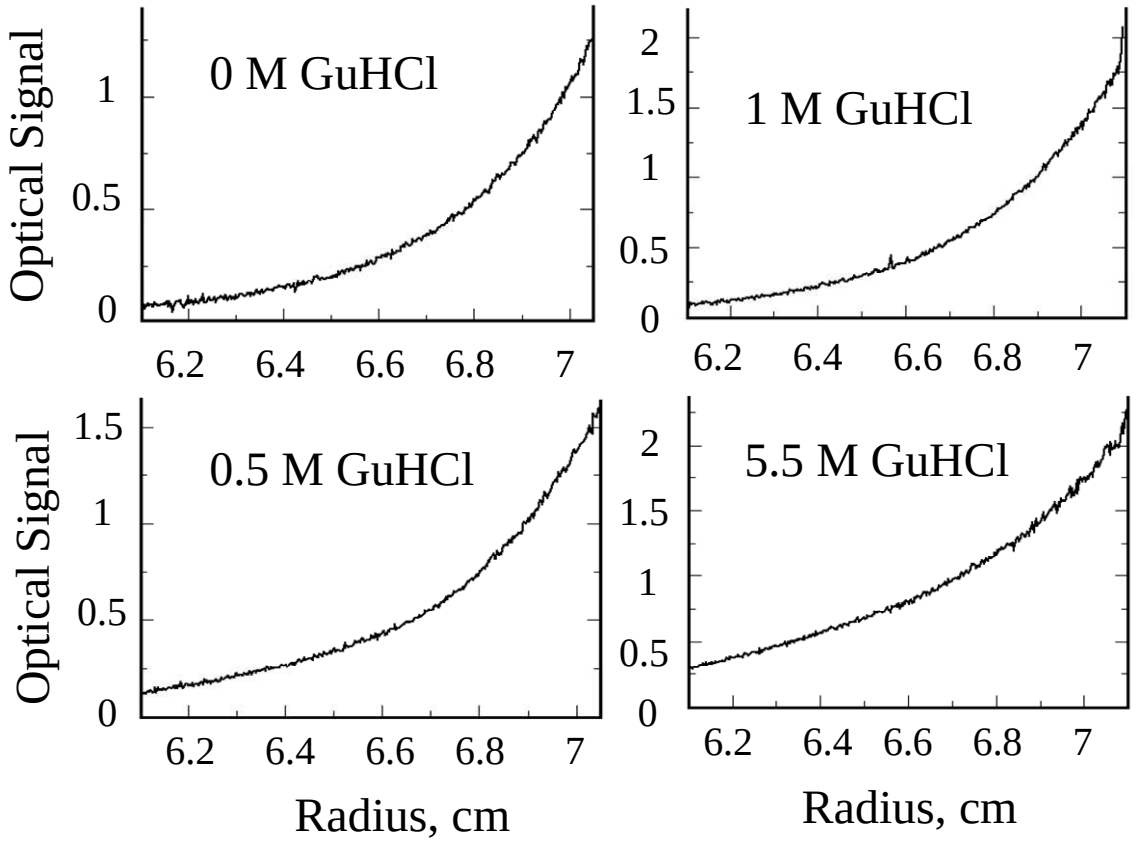

Figure 4.5. Concentration profiles of sedimentation equilibrium. As shown in the figure, the concentration profiles assume a Boltzmann distribution, indicating that ovPrP was monomeric under these four different solution conditions. Measurements were carried out in 50 mM sodium acetate with various concentrations of GuHCl, pH 5.

4.2.2. Tryptophan fluorescence reporter. The local environment of a tryptophan changes as a protein undergoes conformational changes. Since tryptophan fluorescence is sensitive to environmental changes, it was used to probe folding process in this study. The only tryptophan (Trp102) in wild-type ovPrP94-233 is located in the unstructured N-terminal segment and thus is a poor probe of conformational folding (Figure 4.6). The mutation W102F was made to eliminate the signal from the native tryptophan, and the

mutation Y221W was made to introduce a fluorescent reporter (Figure 4.1). A corresponding mutation was made in an earlier kinetic study of human PrP(*219-221*). Site-directed mutagenesis was carried out for all the variants as described above using the following primers:

For W102 → F102 mutation: 5'-GGT AGC CAC AGT CAG TTC AAC AAG CCC AGT AAG CC-3' and 5'-GGC TTA CTG GGC TTG TTG AAC TGA CTG TGG CTA CC-3'

For Y221 → W221 mutation: 5'-GCA AAT GTG CAT CAC CCA GTG GCA GAG AGA ATC CCA GGC-3' and 5'-GCC TGG GAT TCT CTC TGC CAC ATT TGC-3'

The secondary structure of native ovPrP and its double mutant W102F/Y221W was assessed by circular dichroism (CD); both spectra exhibit a double minimum at around 208 and 222 nm, which is typical for an α-helical protein (Figure 4.7). Equilibrium unfolding experiments monitored by far-UV CD and fluorescence indicate that the double mutant has native-like stability (Figure 4.8), and that its fluorescence shows a significant increase in the quantum yield (approximately 4- to 6-fold) upon unfolding (Figure 4.9).

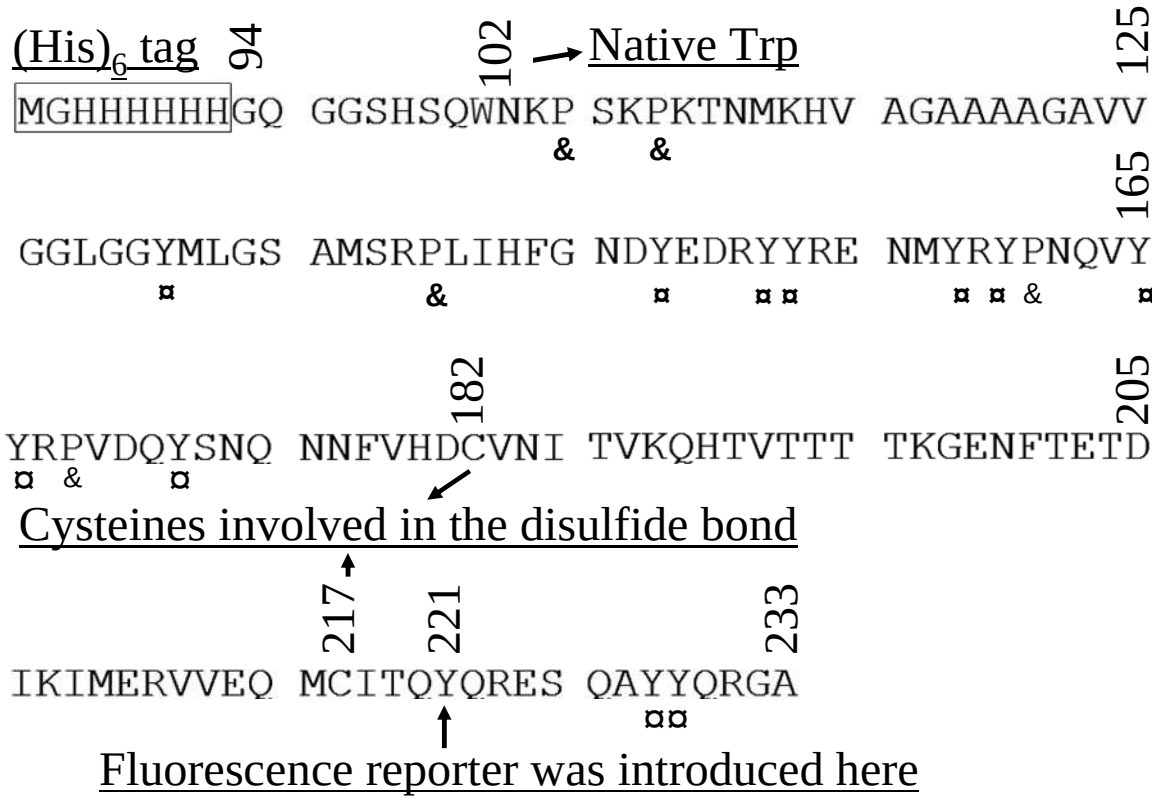

Figure 4.6. Primary structure of the wild-type ALRQ variant. Positions of the native tryptophan, fluorescence reporter, and cysteines involved in the sole disulfide bond are indicated. The native prolines and tyrosines are labeled with the symbols & and ¤, respectively.

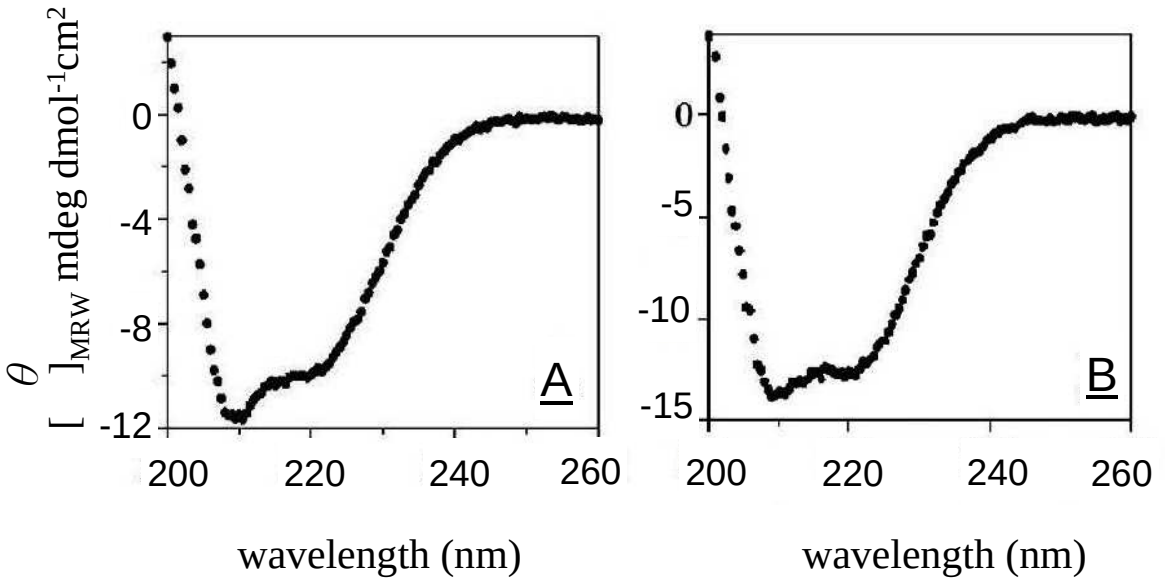

Figure 4.7. Far-UV circular dichroism spectra of the wild-type ovPrP and the ovPrP(W102F/Y221W). The spectrum of ovPrP(W102F/Y221W) (A) exhibits similar secondary structure as observed in wild-type ovPrP (B). Experiments were carried out in 50 mM sodium acetate, pH 5. The unit of Y-axis is in mean residue molar ellipticity (x 10^3).

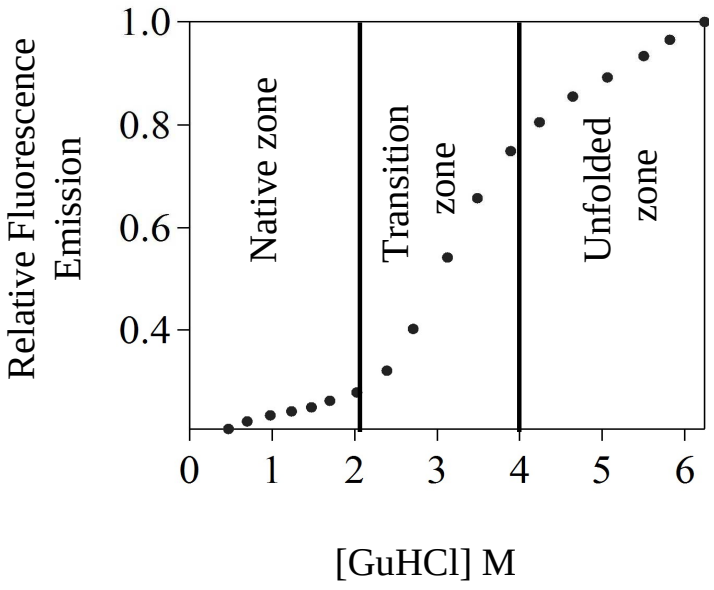

Figure 4.8. Representative equilibrium transition curve of ovPrP(W102F/Y221W) monitored by tryptophan fluorescence. Excitation wavelength was 290 nm; fluorescence emission between 300 to 400 nm was collected. All the signal was normalized by the signal of unfolded protein (taken at 6.2 M GuHCl). Only the transition curve monitored at 360 nm is shown here.

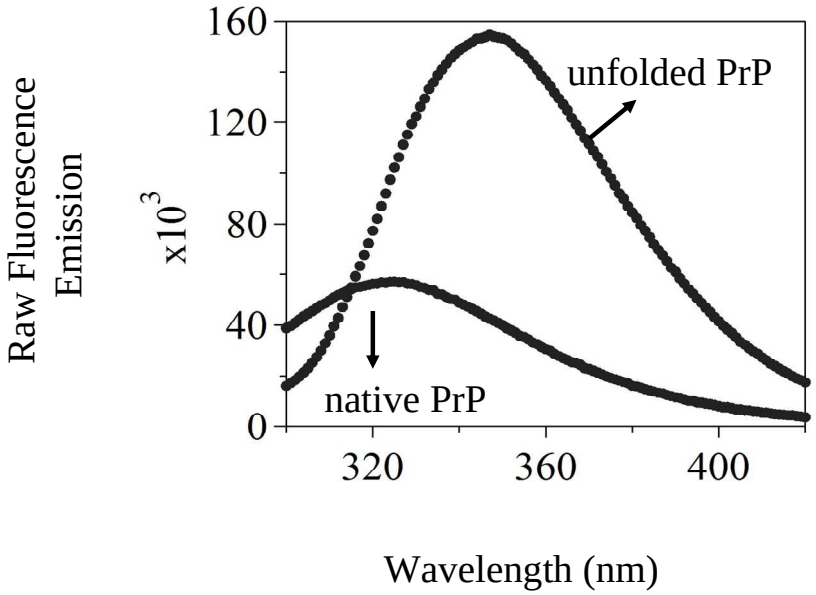

Figure 4.9. Fluorescence emission of native and unfolded ovPrP(W102F/Y221W).

4.2.3. Continuous-flow measurements.

(1) Instrumentation.

Figure 4.10 illustrates the continuous-flow capillary mixing apparatus. Reactants are delivered into the mixing region by the driven syringes through the two coaxial capillaries. Both solutions were forced through the narrow gaps between the platinum sphere and the outer capillary, where mixing occurs rapidly under extremely turbulent flow. The completely mixed solutions then enter the observation channel, still under highly turbulent flow. Reactions are followed by recording the fluorescence emission along the observation channel; distance along the channel is converted into time axis according to the flow rate in use.

(2) Experimental procedure.

The folding and unfolding kinetics of ovPrPs were followed by tryptophan fluorescence of Trp221 using a continuous-flow capillary mixing method described previously(*166*). The excitation wavelength was 296.7 nm. Only fluorescence above 324 nm was collected to minimize the signals from the tyrosines in the protein. For most experiments, mixing was carried out at 15 ^{o}C at a flow rate of 1.8 ml/s, with a final protein concentration of ~11 μM. The refolding (resp. unfolding) reactions were initiated by diluting the unfolded (resp. native) protein at 1:5 ratio into the same buffer containing various denaturant concentrations. The buffer consisted of either GuHCl or urea in either 50 mM sodium acetate, pH 5 or 50 mM imidazole, pH 7. The concentration of denaturants was determined from their refractive index.

Figure 4.10. Sample delivery and detection in the continuous-flow method. (A) Schematic diagram of the capillary mixing apparatus. Figure was adopted and modified from Roder, H. et al. (2006) *Chem. Rev.* **106**, 1836-1861. (B) Illustration of mixing reaction. (C) Folding events occurring in the mixing apparatus.

(A)

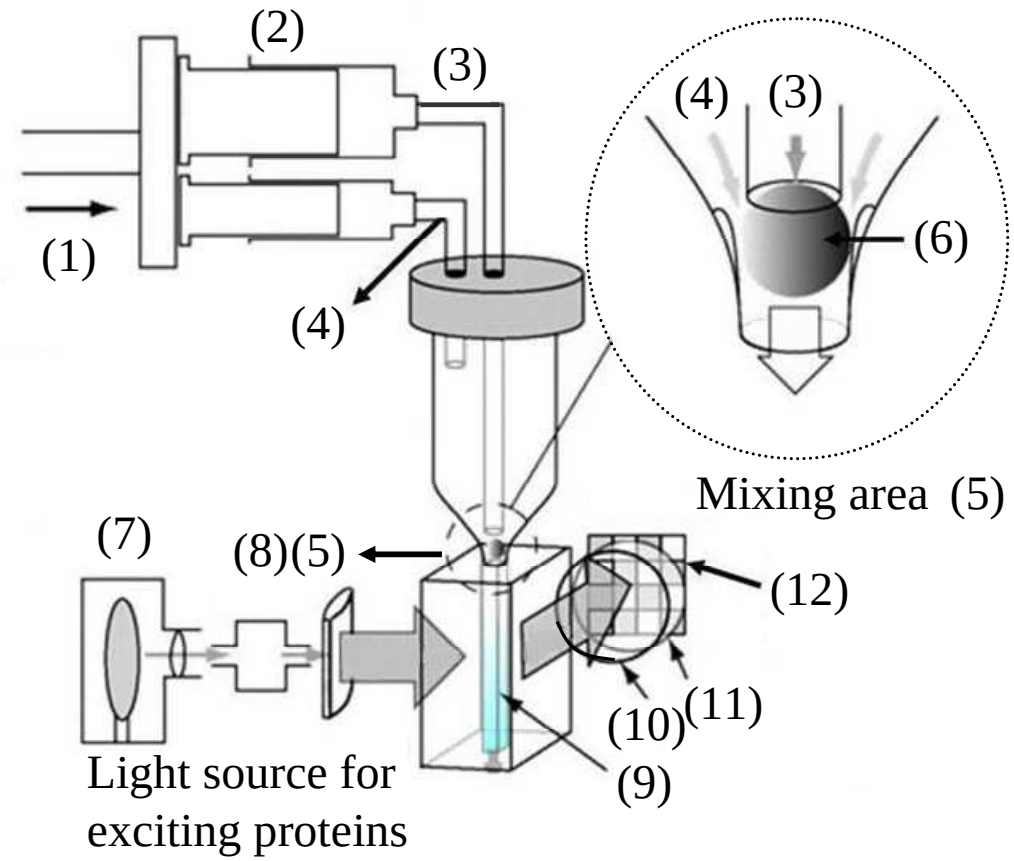

(1): Syringe drive. (2): Syringes. (3): Inner capillary. (4): Outer capillary. (5): Mixer. (6): Pt sphere (200 μm). (7): Arc lamp. (8): Monochromator. (9): Observation channel. (10): Filter (250 μm)^2. (11): Lens. (12): CCD detector for recording fluorescence emission.

Figure 4.10 (cont'd)

(B)

Syringes (1) and (2) are filled with refolding buffer and unfolded PrP, respectively.

↓

Refolding buffer and unfolded PrP are delivered to the mixing area through inner and outer capillaries, respectively.

↓

The completely mixed solution enters the observation channel.

↓

Protein fluorophore is excited by the light source set at 296.7 nm.

↓

Protein fluorescence passes through a 324 nm high-pass filter (i.e. only fluorescence above 324 nm can pass through the filter and be collected), and is recorded using the CCD camera.

Figure 4.10 (cont'd)

(C)

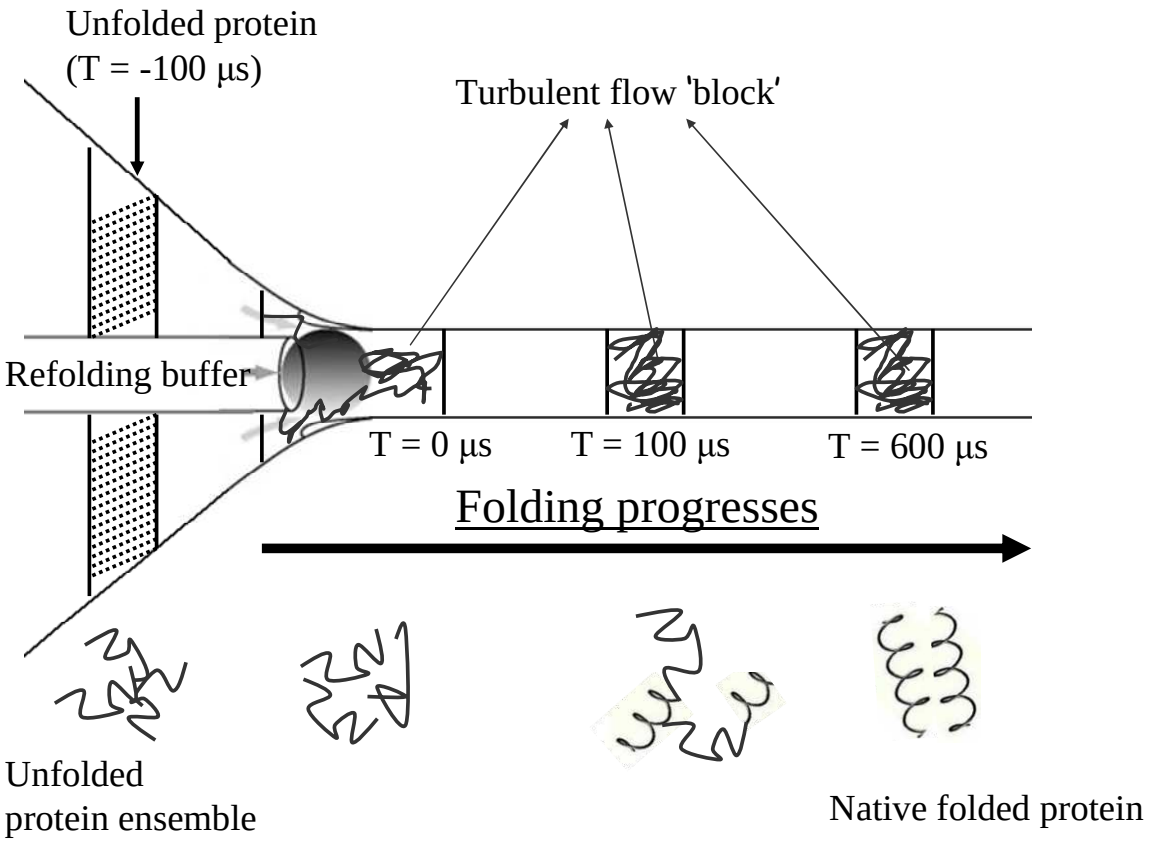

T = -100 μs: Refolding buffer and unfolded protein are in the inner and outer capillaries, respectively. T = 0 μs: The two solutions are mixed by extremely turbulent flow to establish the final solution conditions and thus initiate the folding reaction. T = 100 μs: The protein is on the way to forming its native state. T = 600 μs: The folding protein reaches its native state.

(3) Control experiments.

To determine the mixing efficiency and assess possible artifacts, a series of control experiments was carried out as follows:

Dead-time calibration. Dead-time of the continuous-flow instrument was determined as described previously(*262*). Briefly, quenching reactions between *N*-acetyl tryptophan amide (NATA) and *N*-bromo-succinamide (NBS) were carried out at several quencher concentrations. The kinetic traces are extrapolated to the time before the first observable point and intersect at one point, which we define as the absolute time zero. The fluorescence signal at this point is equal to one sixth of the signal produced by NATA before it passes through the mixing channel. The time interval between the intersection and the first observable point is the instrument dead-time (Figure 4.11).

The dead-time of the capillary mixer was determined to be ~90 μs at 1.8 ml/s. Viscosity was taken into account by including appropriate amount of glycerol to match the viscosity caused by denaturants in the mixing experiments. The formulae for calculating B-viscosity coefficients are as follows(*263*):

For urea: $y = 0.0633x + 0.9679$ (4.1)

For GuHCl: $y = 0.0643x + 0.9756$ (4.2)

For glycerol: $y = 0.3047x + 0.9479$ (4.3)

where x and y represent the concentration of cosolutes and the relative viscosity, respectively.

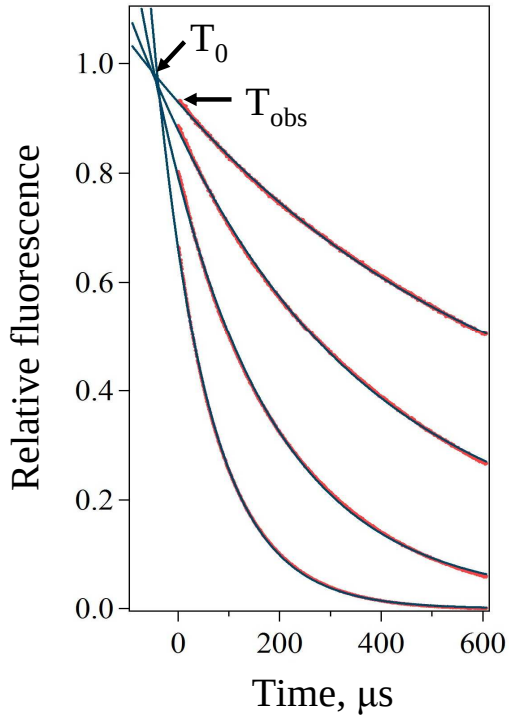

Figure 4.11. Time course of the quenching reactions between NATA and NBS of various concentrations. All the traces were normalized by the signal of NATA in the absence of NBS. The concentrations of NATA was kept constant at 37.5 μM (after mixing). The solid line represents the best fit of the kinetic traces to one exponential. T_0 and T_{obs} represent the absolute time zero (the intersection of traces) and the first observable time point. The dead-time of the instrument is defined as (T_{obs} - T_0).

Mixing artifacts.

(i) Control experiments taken under the same initial and final conditions. These two experiments were designed to probe mixing artifacts that occur even when the solution

conditions are not changed upon mixing. In the *unfolded* control (resp. *native* control) experiments, proteins in either 5 M (resp. 1.8 M) GuHCl or 8 M (resp. 3 M) urea were diluted at 1:5 ratio into the same buffer with the *same* concentration of denaturant. Since the solution conditions remain constant, the protein conformational ensemble should not change; in particular, the protein fluorescence should remain constant over the whole experiment. NATA spectra were also taken under the same *unfolded* and *native* conditions. Since the fluorophore of NATA is fully exposed under every solution condition, the observed NATA fluorescence should not exhibit time-dependent changes. If changes in NATA fluorescence are observed, these changes should be attributed to artifacts resulting from the instrument and/or solution conditions, and are expected to occur in PrP control experiments as well. Another potential artifact is that proteins might undergo mechanical stretch (shear stress) when passing through the extremely turbulent region of the mixer. If such an artifact exists, protein conformational ensembles might be pulled out of equilibrium and may relax in the observation channel. Since NATA is a small molecule, it is immune to shear stress. Therefore, by comparing PrP and NATA spectra, one can assess the contribution of such mechanical artifacts for proteins.

(ii) Control experiments taken under refolding and unfolding conditions. These experiments were designed to probe mixing artifacts that result from changing solution conditions. Except that NATA was used instead of PrPs, these conditions were the same as those used for our main PrP kinetic studies. In the *refolding* control (resp. *unfolding* control) experiments, NATA in either 5 M (resp. 1.8 M) GuHCl or 8 M (resp. 3 M) urea were diluted at 1:5 ratio into the same buffer with *differing* concentrations of denaturant.

Again, since the fluorophore of NATA is fully exposed under every solution condition, NATA fluorescence should remain constant over the whole experiment. By comparing spectra of NATA taken in such control experiments with those taken in the first pair of control experiments (i), one can probe artifacts resulting from mixing two solutions that contain different concentrations of denaturant.

Estimate the effects from protein association. To determine whether the observed ovPrP (un)folding kinetics was affected by protein association, refolding measurements for the ALRR variant were carried out at six different concentrations (ranging from 3.2 μM to 13.5 μM for the final GuHCl concentration), pH 7. A systematical concentration dependence within this range was not found, suggesting that the observations mainly reflect the folding of monomeric ovPrP. Nevertheless, it cannot exclude the possibility that the concentration required for multimeric ovPrP dissociation is lower than 3.2 μM.

Baseline for kinetic traces. Most experiments were taken at a flow rate of 1.8 ml/s, corresponding to a time window of ~0.6 ms. To get a better baseline for kinetic traces, the fluorescence emission of the flow-through from each refolding measurement was recorded. However, extensive protein aggregation in the flow-through was observed within half an hour; thus, the signal from the flow-through was not able to correct the baseline of kinetic traces.

As an alternative method, traces were taken at a flow rate of 0.9 ml/s, which doubles the coverage of the time frame, to estimate the baseline correction. The traces taken at both

flow rates were combined; the combined traces exhibit exponential phases similar to those observed in the measurements taken at 1.8 ml/s flow rate (Figure 4.12), suggesting that the baseline in the former measurements is well-defined.

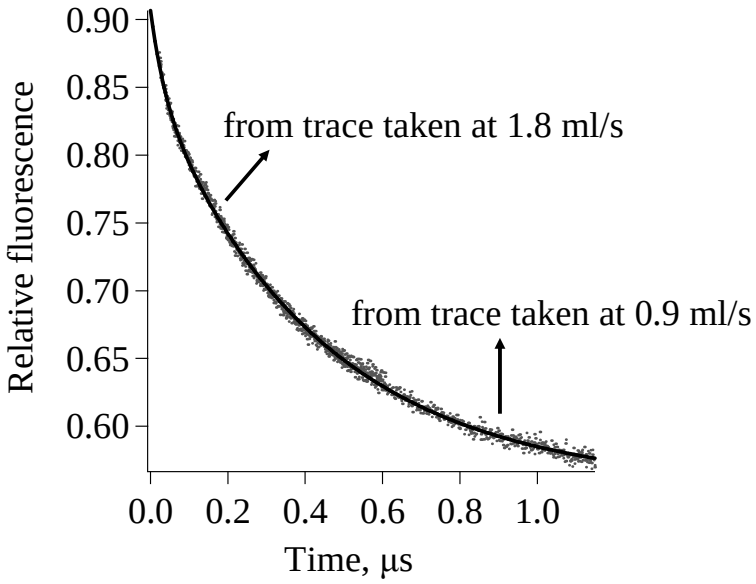

Figure 4.12. Combination of ALRQ refolding kinetic traces taken at flow rates of 0.9 and 1.8 ml/s. Traces were taken in 2 M GuHCl at pH 5 and 15 ^{o}C. The solid line represents the best fit to the combined trace.

4.2.4. Exponential fitting.

The fluorescence signal was fit to a sum of exponentials using the Levenberg-Marquardt algorithm as implemented in IGOR Pro software (Wavemetrics Inc.). In every case, the residuals were examined to confirm the absence of systematic errors. At most two exponentials were required to fit the kinetic traces.

4.2.5. Data analysis.

(1) Chevron plot analysis. The natural logarithm of an elementary refolding or unfolding reaction rate generally has a linear dependence on denaturant concentration(*264*):

$$\ln k_{ij} = \ln k_{ij}^{o} + (m^{\ddagger}_{ij}/RT)[\text{denaturant}] \quad (4.4)$$

where k_{ij}^{o} is the rate constant from species *i* to *j* in the absence of denaturant, T is the temperature in Kelvin, and R is the universal gas constant. The slope $m^{\ddagger}_{ij}$, which describes the free-energy dependence on denaturant concentration, is approximately proportional to the change in the buried surface area that occurs between the reactant and the transition state(*265*).

In a two-state (un)folding reaction (N ↔ U), where no intermediates are involved, the observed rate constant is

$$\lambda = k_{NU} + k_{UN}, \quad (4.5)$$

where λ is the measured rate constant, k_{NU} and k_{NU} are the unfolding and refolding rate constants, respectively. Under refolding conditions, the folding rate constants k_{UN} are significantly larger than their reverse unfolding rate constants k_{NU}, and therefore $\lambda \approx k_{UN}$. By contrast, under unfolding conditions, the unfolding rate constants k_{NU} are significantly larger than their reverse folding rate constants k_{UN}, and therefore $\lambda \approx k_{NU}$. Thus, the plots of ln λ as a function of denaturant concentration (chevron plot) for a two-state (un)folding protein adopt a V-shape with a minimum at which ln k_{NU} = ln k_{UN}, i.e., the number of molecules in the native state is equal to that in the unfolded state (Figure 4.13).

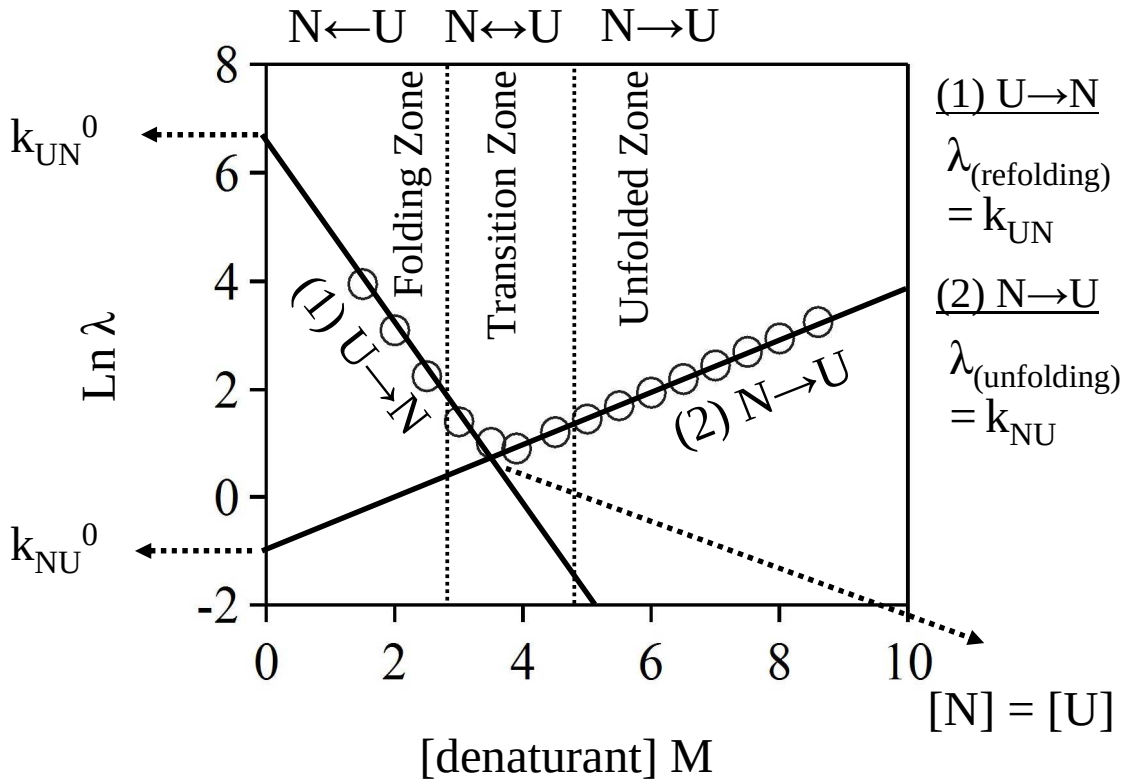

Figure 4.13. Denaturant dependence of the folding and unfolding rates for a two-state (un)folding protein. λ is denoted to the *observed* decay constant; k is denoted to the *microscopic* rate constant. By assuming (un)folding mechanisms are conserved in different denaturant concentrations, k_{UN}^{o} and k_{NU}^{o} can be derived from linear extrapolation.

However, if a protein folds according to a three-state regime with an intermediate on the direct pathway between native and unfolded states, i.e. ***N*** ↔ ***I*** ↔ ***U***, a deviation from the V shape is expected (Figure 4.14).

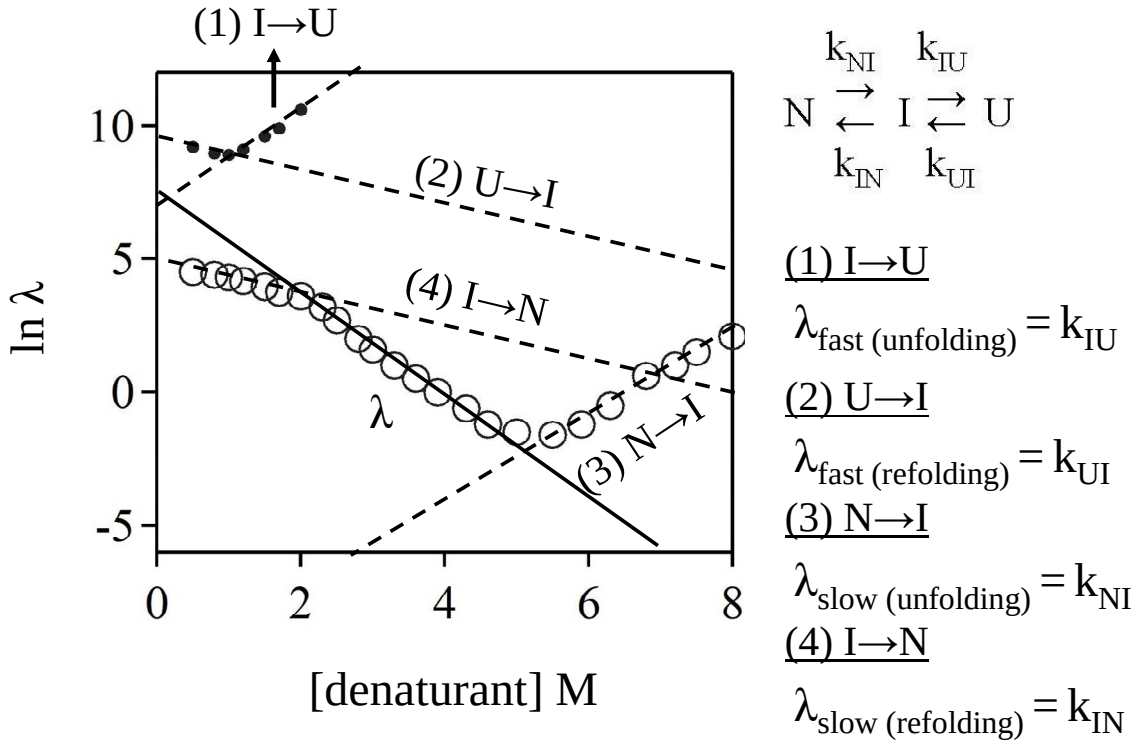

Figure 4.14. Denaturant-dependence of the folding and unfolding rates for a three-state (un)folding protein. λ is denoted to the *observed* decay constant; k is denoted to the *microscopic* rate constant. The points represent the observed decay constant (λ). The solid and dash lines represent the fitted dependence of decay constants.

Figure 4.14 represents the chevron plot for a three-state (un)folding protein. Under strongly refolding conditions ([denaturant] ≤ 2 M in this case), the refolding intermediate is well-populated. Both k_{UI} and k_{IN} can be resolved from the kinetic data in this region. Under mildly refolding conditions (2 M ≤ [denaturant] ≤ 4 M in this case), the equilibrium between U and I (U ↔ I) shifts to U, and the intermediate is no longer populated(*141*). Although the reaction approaches a two-state mechanism, the small population of the intermediate still contributes to the observed rate constant (λ); therefore,

the microscopic rate constant k_{IN} cannot be obtained from the decay constant λ in this region.

(2) Quantitative analysis for the compactness of folding intermediates.

Chemical denaturation exerts its effect on partially unfolded intermediates or fully unfolded states through changing their solvent-exposed surface area(*141*). Such effects are reflected in the $m^{\ddagger}_{ij}$ value in **Equation 4.4**. A $m^{\ddagger}_{ij}$ value represents the change in the solvation free energy induced by denaturant(*266*), thus provides a quantitative measure of the average compactness. In a three-state folding regime, the compactness of the intermediate state relative to the unfolded state can be represented by an α value:

$$\alpha_{UI} = m^{\ddagger}_{UI} - m^{\ddagger}_{IU} / (m^{\ddagger}_{UI} + m^{\ddagger}_{IN} - m^{\ddagger}_{NI} - m^{\ddagger}_{IU}) \qquad (4.6)$$

where $\alpha_{UI} = 0$ represents an intermediate state with the same surface-burial as the unfolded state, whereas a $\alpha_{UI} = 1$ represents an intermediate state which is as compact as the native state.

(3) Kinetic modeling.

The exponential responses correspond to transitions between protein conformational states in which a free-energy barrier is crossed; therefore, the number of kinetic species can be deduced from the number of exponential responses. In general, a kinetic model with *n* kinetic species should produce a signal of *n-1* exponential phases, although not all phases may be detected; conversely, the detection of *p* exponential phases implies at least

p+1 kinetic states. By assuming the persistence of kinetic mechanisms in different denaturant concentrations, kinetics that exhibits two exponentials under unfolding conditions indicates at least three states exist in ovPrP unfolding and refolding: the native state ***N***, the unfolded state ***U,*** and an intermediate state denoted as ***I***.

The most general three-species kinetic model has the form

$$\mathbf{N \leftrightarrow I \leftrightarrow U \leftrightarrow N}$$

in which each species can interconvert with the other two. If the protein is initially entirely in the native state ***N*** (as in the unfolding experiments), the initial time derivative of this fluorescence signal is given by

$$-dF/dt = A_{fast}\,\lambda_{fast} + A_{slow}\,\lambda_{slow} = k_{NI}\,(Q_N - Q_I) + k_{NU}\,(Q_N - Q_U)$$

where Q_N, Q_I and Q_U represent the quantum yields of the native, intermediate and unfolded species, respectively. Experimentally, *-dF/dt* is approximately zero under unfolding conditions. Since the fluorescence signal of ovPrP shows 4- to 6-fold increase upon unfolding, $(Q_N - Q_U)$ is non-zero. Therefore, the zero initial slope implies that k_{NU} is negligibly small and $Q_I \approx Q_N$. Since the quantum yield is highly sensitive to conformational changes, the rough equality of Q_I and Q_N suggest that the tertiary structure of $\boldsymbol{I_\alpha}$ is native-like, particularly in the vicinity of the reporting tryptophan (the third α-helix). More generally, $\boldsymbol{I_\alpha}$ should be structurally closer to the native state ***N*** than

to the unfolded state ***U***. By the given similarity of ***N*** and $\boldsymbol{I_\alpha}$ in their conformations, and the negligible conversion rate between ***N*** and ***U***, I argue that the most plausible model for this observation is $\boldsymbol{N \leftrightarrow I \leftrightarrow U}$.

4.3. Results.

4.3.1. Unfolding of ovPrPs. The unfolding kinetics of variants ALRQ, VLRQ, ALHQ, and ALRR were measured in GuHCl at pH 7, 15^{o}C (Figure 4.15). Figure 4.16 shows the representative kinetic trace of ALRQ variant taken in the presence of 5.6 M GuHCl, along with the best fit to one or two exponentials. As shown in the figure, the second exponential improves the quality of the fit significantly. Since the unfolding of ALRQ, ALRR, and VLRQ variants exhibits two exponential phases under strongly unfolding conditions, ***the kinetic model must have at least one intermediate***. The two decay constants, $\lambda_{slow\ (unfolding)}$ and $\lambda_{fast\ (unfolding)}$, increase monotonically with increasing GuHCl concentration, and can be fit to straight lines on a semilogarithmic plot (Figure 4.21; Table 4.1). The amplitude of the slower decay is larger and negative, as expected from the increase in the quantum yield of ovPrPs observed in equilibrium unfolding. By contrast, the amplitude of the faster exponential is positive; the mutual cancellation of these amplitudes produces a lag phase. At lower denaturant concentrations (but still above the unfolding threshold), one exponential term suffices to fit the unfolding kinetic traces satisfactorily. Unfolding experiments were also carried out in urea; however, no useful information can be obtained due to the narrow unfolded zone of ovPrP under this condition.

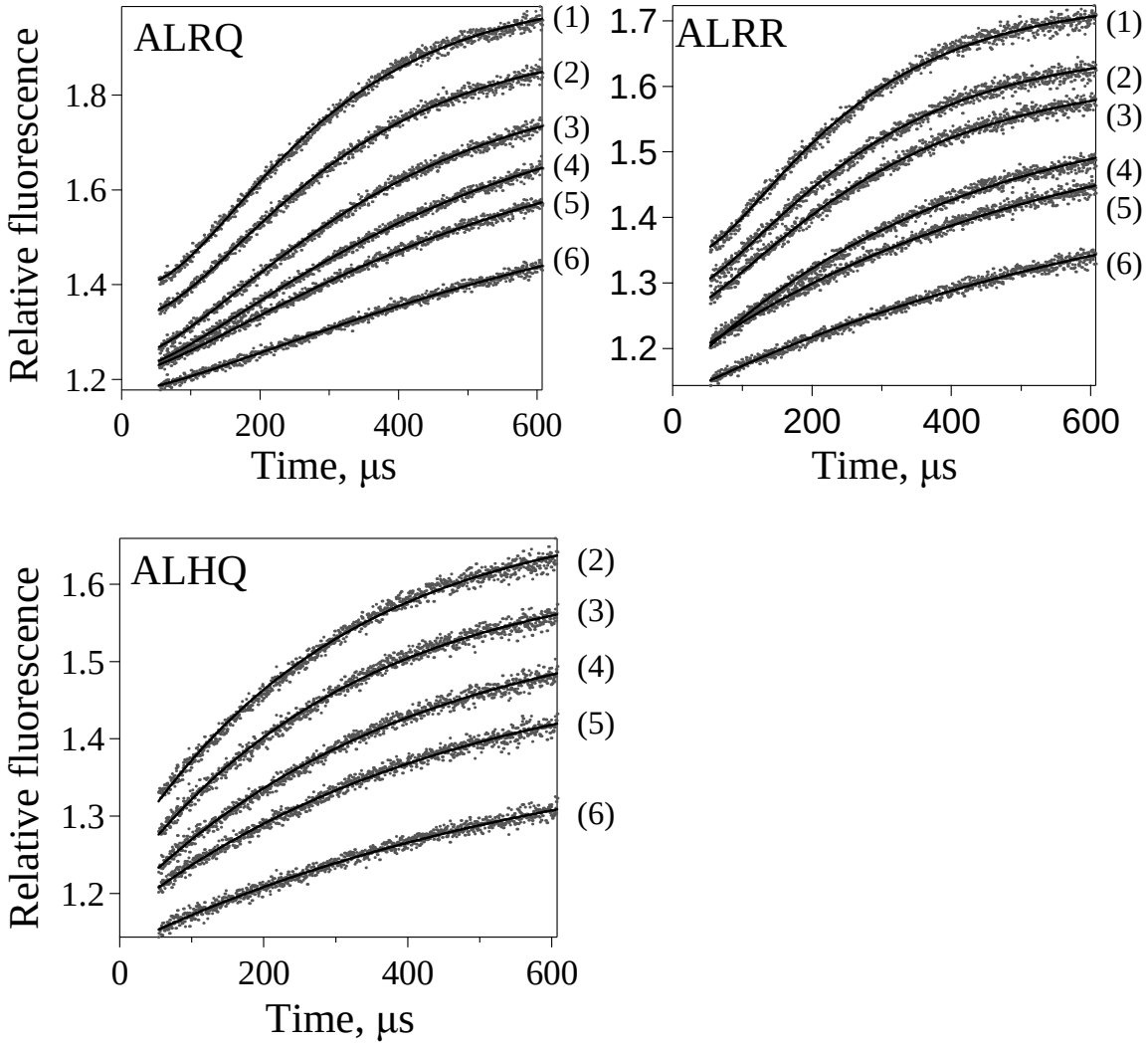

Figure 4.15. Unfolding kinetic traces taken for ovPrPs in the presence of various concentrations of GuHCl at pH 7, 15°C with the best fit to one or two exponentials. (1): 6 M GuHCl; (2): 5.6 M GuHCl; (3): 5.2 M GuHCl; (4): 4.8 M GuHCl; (5): 4.4 M GuHCl; and (6): 4 M GuHCl. Solid lines represent one- or two-exponential fit to the kinetic traces. Fluorescence signal was normalized by the fluorescence of native ovPrPs.

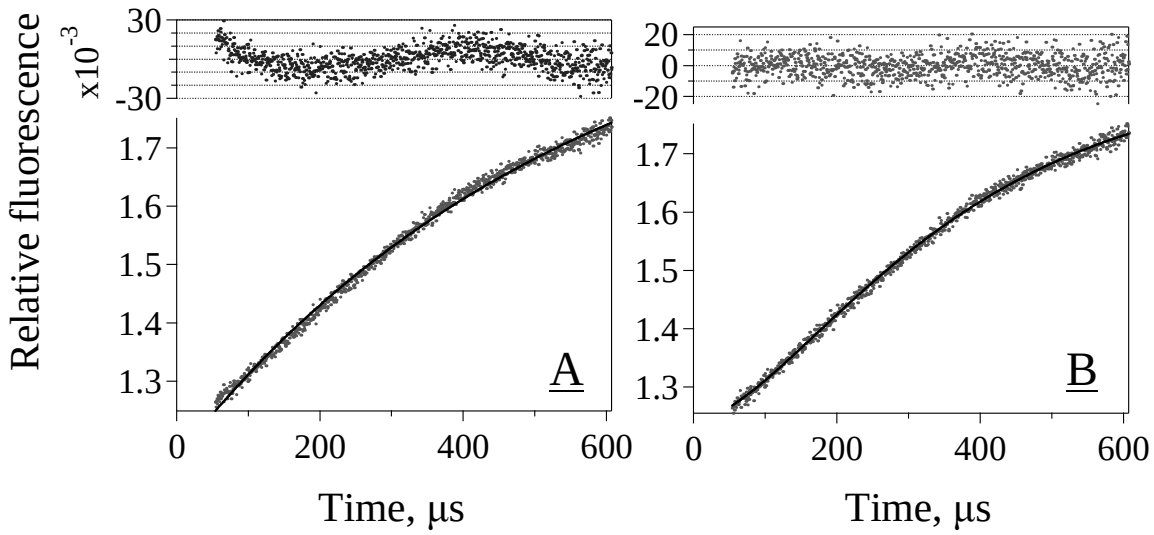

Figure 4.16. Kinetic trace taken for ALRQ variant in the presence of 5.2 M GuHCl at pH 7 and 15°C with the best fit to one (A) or two (B) exponentials. Solid lines represent one- or two-exponential fit to the kinetic trace. Residuals of the fits are shown above the kinetic trace. Fluorescence signal was normalized by the fluorescence of native ovPrPs.

4.3.2. Refolding of ovPrPs. Refolding measurements were carried out in GuHCl at pH 5 or 7 at 15°C. Figure 4.17 shows the representative kinetic trace taken for ALRQ variant in the presence of 1.45 M GuHCl at pH 5 with the best fit to one and two exponentials. As shown in the figure, two exponential terms are required to fit the data completely. A similar fitting situation was encountered for refolding traces of all the allelic variants taken at different GuHCl concentrations and at different pH values (Figure 4.18 and 4.19). Based on the control experiments (see Methods), the first phase with a time constant of ~10 μs is attributed to the artifacts caused by initial changes in the refractive index; only the slower decay represents ovPrP refolding. These refolding rate constants are plotted in

Figure 4.21 on a semilogarithmic plot; the deduced kinetic parameters are listed in Table 4.1. Other fitting parameters are plotted in Figure S1 (see Supplemental Materials).

Refolding experiments were repeated under several alternative conditions: (1) urea at pH 7, 5^{o}C (for ALRQ), (2) urea at pH 5, 15^{o}C (for ALRR), and (3) GuHCl at pH 7, 5^{o}C (for ALRR) to determine if the folding behavior of ovPrP changes with solution conditions. Since ovPrPs exhibit only one refolding phase under these conditions (Figure 4.20 and Figure S2), I conclude that ovPrP variants refold without a detectable intermediate under refolding conditions. Several factors might account for this observation, including (1) the intermediate is poorly populated under refolding conditions; (2) the second refolding phase (I $\rightarrow$ N) occurs too fast to be discerned; and (3) the second refolding phase has a negligible amplitude.

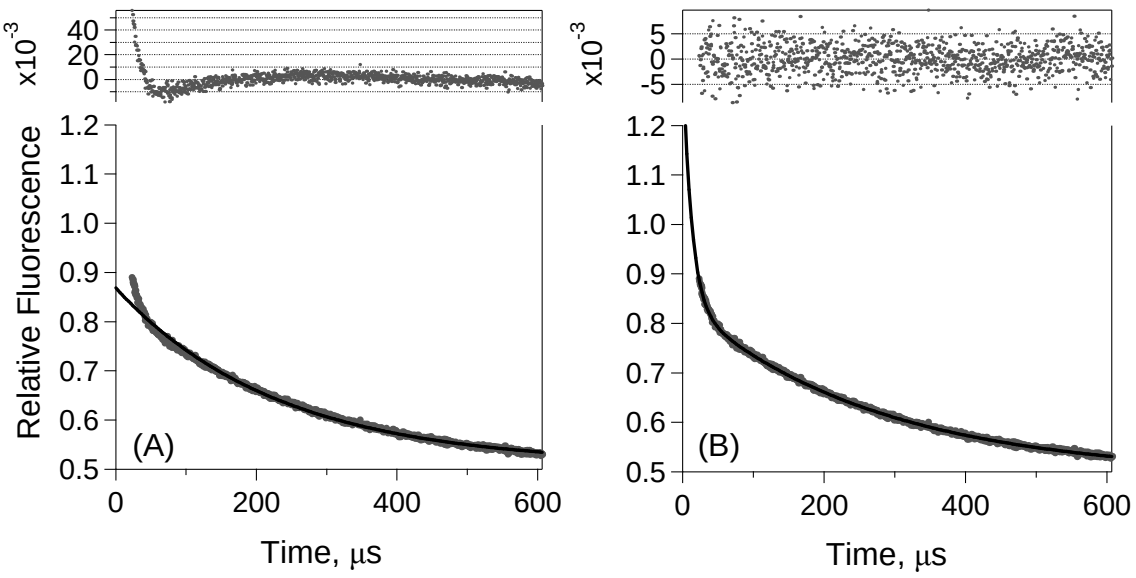

Figure 4.17. Refolding kinetic trace taken for ALRQ variant in the presence of 1.45 M GuHCl at pH 5 and 15^{o}C with the best fit to one (A) or two (B) exponentials. Residuals of the fits are shown above the kinetic traces. Solid lines represent one- or two-exponential fit to the kinetic traces. Kinetic traces were normalized by fluorescence signal of unfolded ovPrPs.

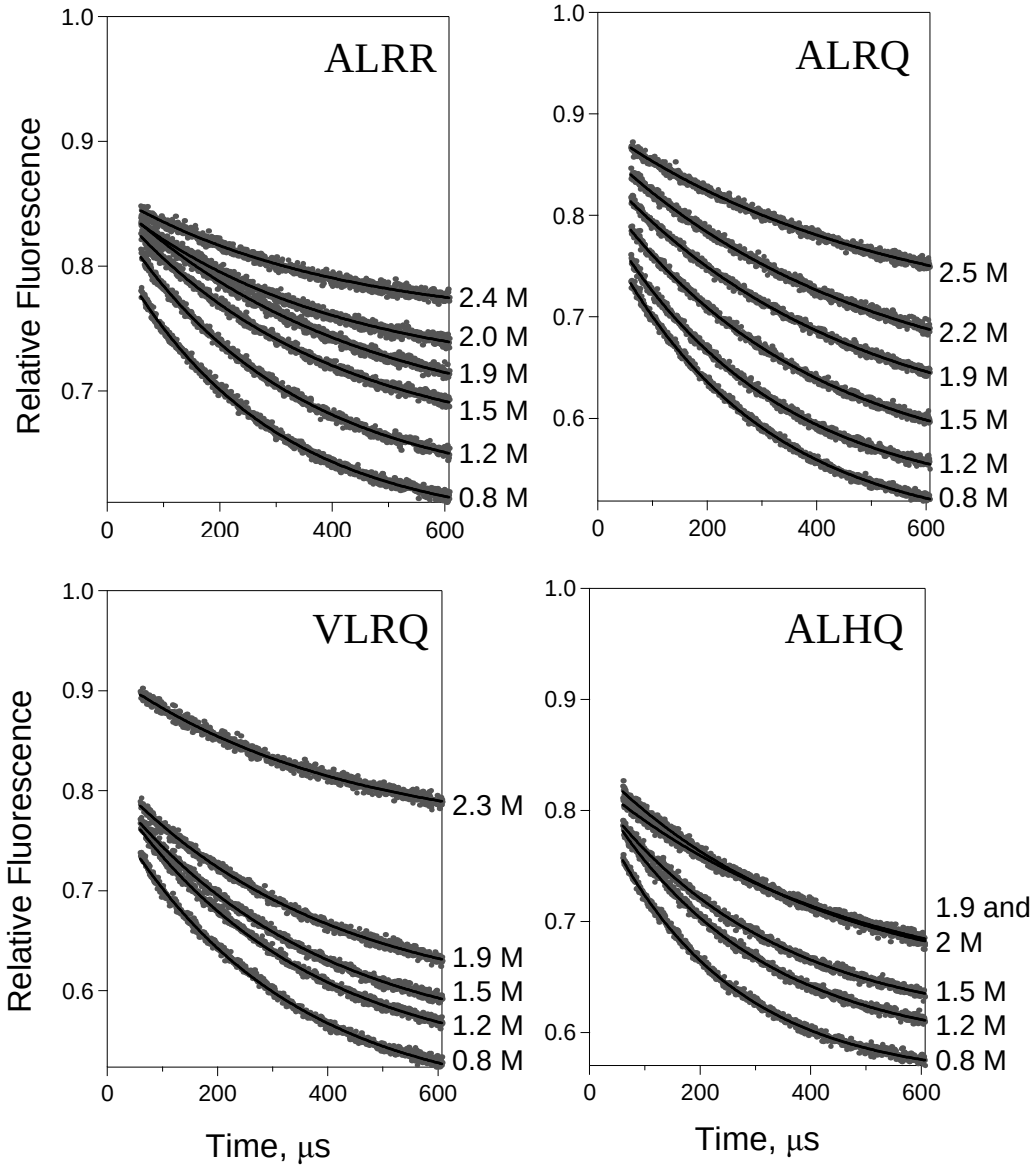

Figure 4.18. Refolding kinetic traces taken for ovPrPs in the presence of various concentrations of GuHCl at pH 7, 15°C with the best fit to two exponentials. Data were taken in 50 mM imidazole, pH 7. The fluorescence signal was normalized by the fluorescence of unfolded ovPrPs. Solid lines represent two-exponential fits to the kinetic traces. Corresponding GuHCl concentrations are indicated next to the traces. For the accuracy of data analysis, I included the artifact phase in the exponential fitting; however, for clarity, I show here only the signal from ovPrP refolding.

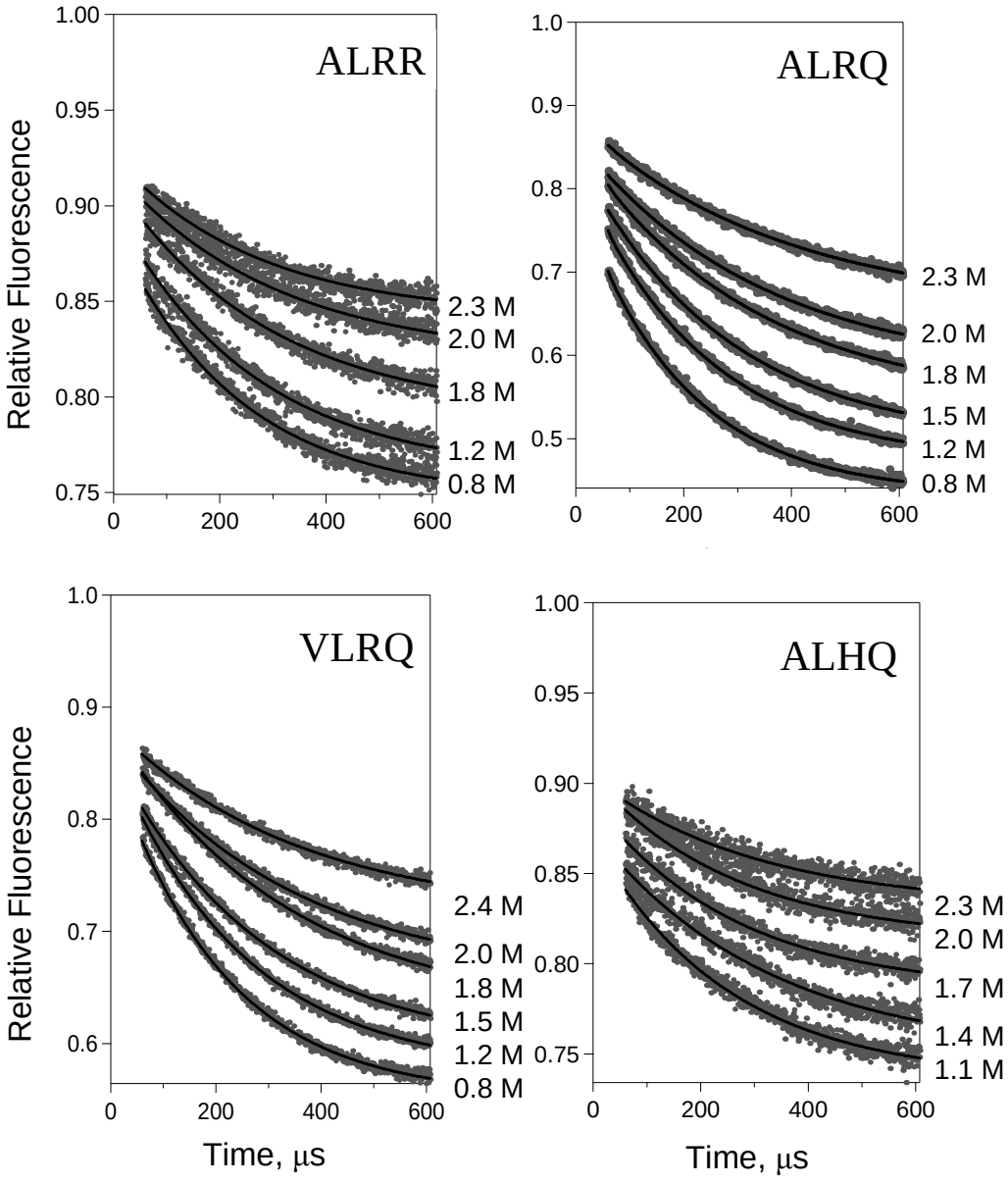

Figure 4.19. Refolding kinetic traces taken for ovPrPs in the presence of various concentrations of GuHCl at pH 5, 15°C with the best fit to two exponentials. Data were taken in 50 mM sodium acetate, pH 5. Fluorescence signal was normalized by the fluorescence of unfolded ovPrPs. Solid lines represent two-exponential fits to the kinetic traces. Corresponding GuHCl concentrations are indicated next to the traces. Similar refolding behavior was observed for AFRQ variant, which is involved only in atypical scrapie (Figure S2). For the accuracy of data analysis, I included the artifact phase in the

Figure 4.19 (cont'd)

exponential fitting; however, for clarity, I show here only the signal from ovPrP refolding.

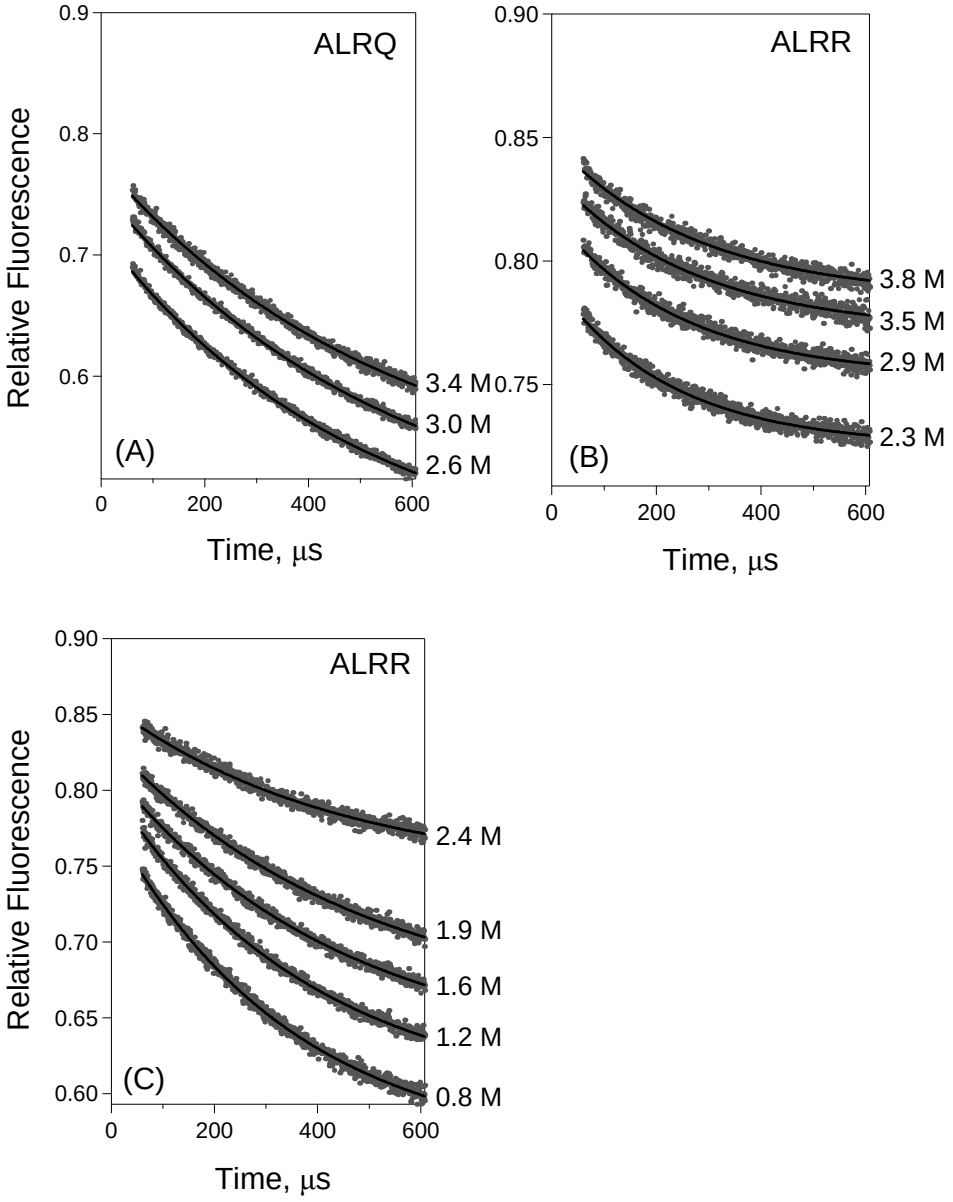

Figure 4.20. Refolding kinetic traces taken for ovPrPs in the presence of various concentrations of urea or GuHCl with the best fit to two exponentials. (A): urea at pH 7, 5^{o}C. (B): urea at pH 5, 15^{o}C. (C): GuHCl at pH 7, 5^{o}C. Fluorescence signal was normalized by the fluorescence of unfolded ovPrPs. Solid lines represent two-exponential fits to the kinetic traces. Corresponding denaturant concentrations are indicated next to the traces. For the accuracy of data analysis, I included the artifact phase in the exponential fitting; however, for clarity, I show here only the signal from ovPrP refolding.

Figure 4.21. Chevron plots of ALRQ (A), ALHQ (B), ALRR (C), and VLRQ (D) variants at pH 7, 15 °C. λ is denoted to the *observed* decay constant; *k* is denoted to the *microscopic* rate constant (see *Methods* for detail explanation). The points represent the observed decay constant (λ), The solid and dash lines represent the fitted dependence of decay constants of the slow and fast phases, respectively.

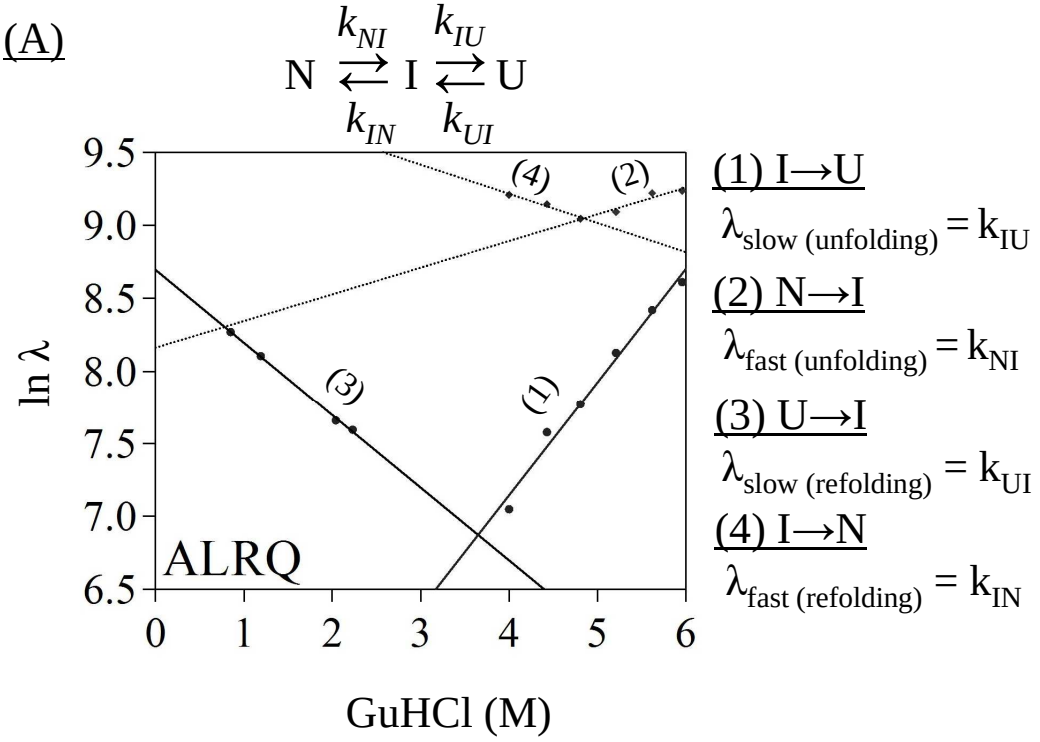

Figure 4.21 (cont'd)

(B)

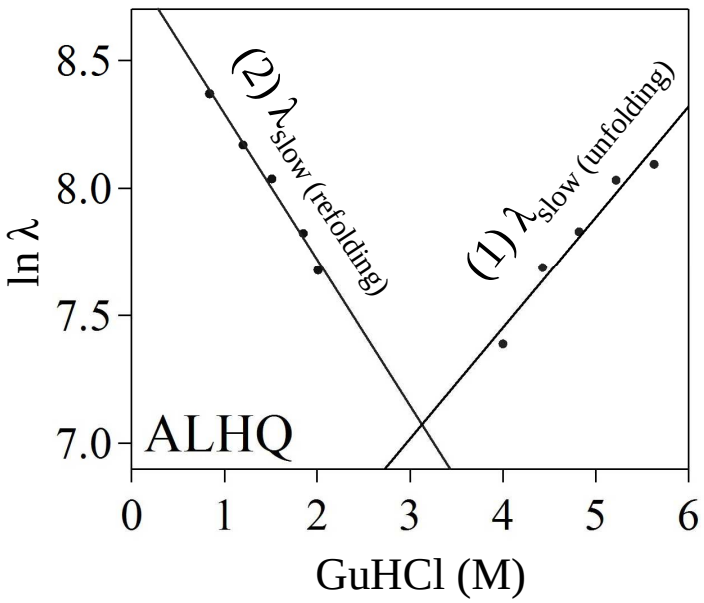

(1)
Observed rate for N → U
$\lambda_{(unfolding)}$

(2)
Observed rate for U → N
$\lambda_{(refolding)}$

(C)

$$N \underset{k_{IN}}{\overset{k_{NI}}{\rightleftarrows}} I \underset{k_{UI}}{\overset{k_{IU}}{\rightleftarrows}} U$$

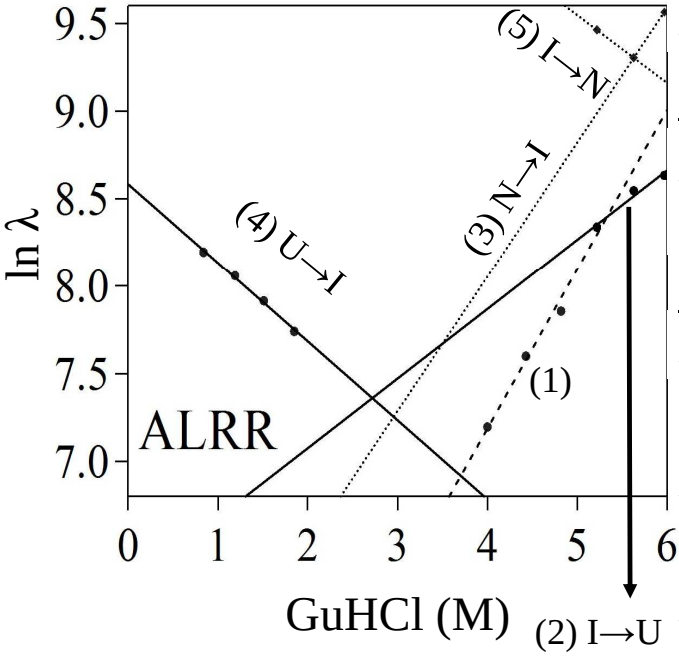

(1)
Observed rate for N → U
$\lambda_{slow\ (unfolding,\ [GuHCl]<5.2M)}$

(2) I→U
$\lambda_{slow\ (unfolding,\ [GuHCl]\geq 5.2M)} = k_{IU}$

(3) N→I
$\lambda_{fast\ (unfolding)} = k_{NI}$

(4) U→I
$\lambda_{slow\ (refolding)} = k_{UI}$

(5) I→N
$\lambda_{fast\ (refolding)} = k_{IN}$

Figure 4.21 (cont'd)

(D)

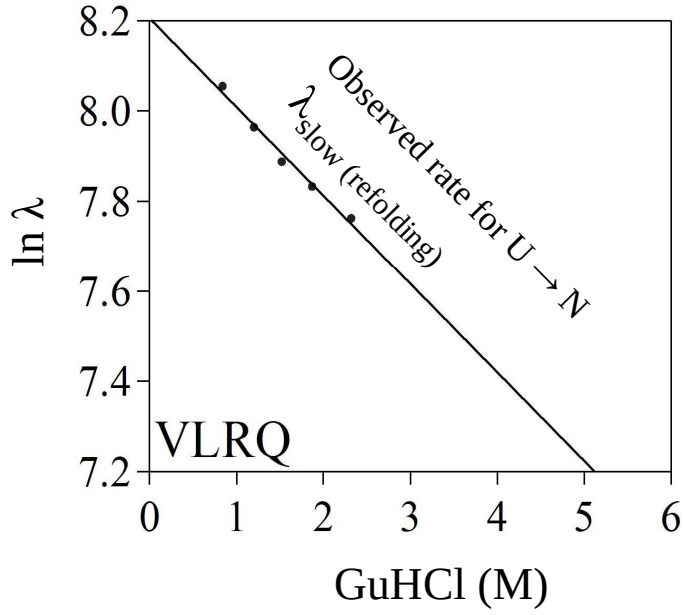

Table 4.1. Kinetic parameters for the folding of ovPrPs. k and λ are in s^{-1}, τ is in μs, m_{ij} is in $kJ \cdot mol^{-1} \cdot M^{-1}$, and ΔG is in $kJ \cdot mol^{-1}$.

(1) at pH 7: *U↔I↔N (k: microscopic rate constant)*

	k_{UI}^0	τ_{UI}	k_{IU}^0	τ_{IU}	k_{IN}^0	τ_{IN}	k_{NI}^0	τ_{NI}	T (^oC)	denaturant
ALRQ	5973.6	167.40	56.3	17761.99	22314.7	44.81	3506.6	285.18	15	GuHCl
ALRR	5341.7	187.21	534.1	1872.31	96954.8	10.31	146.4	6830.60	15	GuHCl

	$m_{UI}^{\ddagger}$	$m_{IU}^{\ddagger}$	$m_{IN}^{\ddagger}$	$m_{NI}^{\ddagger}$	T (^oC)	denaturant
ALRQ	-1.194	1.862	-0.477	0.437	15	GuHCl
ALRR	-1.077	0.949	-0.925	1.834	15	GuHCl

	K_{UI}	ΔG_{UI}	K_{IN}	ΔG_{IN}	ΔG_{UN}	[U]:[I]:[N]	α_{UI}	T (^oC)	denaturant
ALRQ	106.1	-11.16	6.36	-4.42	-15.58	1:106:675	0.77	15	GuHCl
ALRR	10	-5.51	662.26	-15.54	-21.05	1:10:6623	0.42	15	GuHCl

(2) at pH 7: *U↔(I)↔N (λ: observed rate constant)*

	λ_{UN}^0	τ_{UN}	λ_{NU}^0	τ_{NU}	$m_{UN}^{\ddagger}$	$m_{NU}^{\ddagger}$	T (^oC)	denaturant
ALHQ[§]	7064.9	141.54	303.9	3290.56	-1.368	1.038	15	GuHCl
VLRQ[‡]	3754.1	266.38			-0.521		15	GuHCl
ALRR	3597.5	277.97			-0.296		5	GuHCl
ALRQ	4336.8	230.58			-0.634		5	urea

§: An intermediate state was not observed for ALHQ variant. However, the absence of *I* is not conclusive.

‡: An intermediate state was observed for VLRQ variant. However, the present data do not allow the kinetic parameters to be deduced.

Table 4.1. (cont'd)

(3) at pH 5: *U↔(I)↔N (λ: observed decay constant)*

	λ_{UN}^{0}	τ_{UN}	$m_{UN}^{\ddagger}$	T (^{o}C)	denaturant
ALRQ	7321.7	136.58	-1.129	15	GuHCl
VLRQ	7084.0	141.16	-1.137	15	GuHCl
ALHQ	5322.5	187.88	-0.590	15	GuHCl
ALRR	4902.0	204.00	-0.498	15	GuHCl
AFRQ	9008.3	111.01	-1.404	15	GuHCl
ALRR	6537.4	152.97	-0.438	15	urea

4.4. Discussion.

4.4.1. Kinetic intermediate is a plausible PrP^{Sc} precursor. Under unfolding conditions, the kinetic traces exhibit a lag phase, meaning that the initial rate of change of fluorescence is roughly zero. Thus, the quantum yields of the intermediate and native states are similar. The tertiary structure of this intermediate is native-like, particularly in the vicinity of the reporting tryptophan (the third α-helix), since quantum yield is highly sensitive to conformational changes. In other words, this intermediate is largely α-helical. Hence, this intermediate is denoted as $\boldsymbol{I_\alpha}$.

The relative populations of $\boldsymbol{I_\alpha}$ in the susceptible variant (ALRQ) is about 10 times higher than that in the resistant variant (ALRR). The surface exposure of this intermediate also differs these two variants: the ALRQ variant shows ~77% of surface-burial in its intermediate relative to its native state, in contrast with ~42% for the ALRR variant. By assuming $\boldsymbol{I_\alpha}$ is on the direct pathway between native and unfolded states (see arguments in *Methods*), the differences in the surface exposure suggests that $\boldsymbol{I_\alpha}$ in the susceptible variant (ALRQ) is structurally closer to its native state, as compared to the resistant variant (ALRR). This correlation indicates that the more stable native-like structure of $\boldsymbol{I_\alpha}$ in the susceptible variants correlates with the propensity to convert to PrP^{Sc}. Consistent with this idea, structural conversion to PrP^{Sc} has been suggested to proceed through an α-helix-rich species under oligomer-forming conditions(*222-225*, *261*).

Based on these correlations, I argue that $\boldsymbol{I_\alpha}$ is the PrP^{Sc} precursor, and that the genetic modulation found in classical scrapie exerts its effect on the population and structure of this kinetic species. Similar situations have been observed in human familial prion disease, where the pathogenic mutations result in a pronounced increase in the population and the hydrophobicity of the kinetic intermediate of human PrP (huPrP)(*219, 221*), although the structural properties of this kinetic species were not able to be discerned.

Herein, a model is proposed to explain amyloid formation in classical scrapie:

$$\textit{Conformational folding of } PrP^{C}\text{: } N \leftrightarrow I_\alpha \leftrightarrow U$$

$$\textit{Assembly of } PrP^{Sc} \textit{ oligomers: } (PrP^{Sc})_n + I_\alpha \rightarrow (PrP^{Sc})_{n+1}$$

In the susceptible variants, the higher population of $\boldsymbol{I_\alpha}$ gives them more opportunities for oligomerization, and its more stable structure makes the conversion to PrP^{Sc} more feasible. Exogenous PrP^{Sc} is required for misfolding in this model, since naturally occurring allelic variants of ovPrP, including those confer high susceptibility to classical scrapie, cannot induce the disease spontaneously(*267-269*).

Native PrP^{C} has been suggested to be the PrP^{Sc} precursor that occurs in *normal* PrP folding. Zhang *et al.* proposed that Syrian hamster PrP^{C} possesses a relatively open conformation, which is ready for the PrP^{C}-to-PrP^{Sc} conversion(*46*). Welker *et al.* suggested that oligomerization proceeds through a thiol/disulfide exchange reaction

between two native PrPs(*239*). Although such dimeric structure has been observed(*43*), a later report on *in vitro* conversion study seems to contradict to this model(*240*).

Several studies have been carried out to determine the role of the native PrPs in prion diseases. Many of the mutants linked to human prion diseases do not differ from the wild-type huPrP in the thermodynamic stability in their native state(*241-242, 270*). In the case of classical scrapie, susceptible alleles even exhibit higher structure stability in their native forms as compared to the resistant ones(*233, 237-238*). Moreover, pathogenic or protective mutations associated with human or sheep prion diseases do not alter structures and backbone dynamics in the native state of PrPs(*243, 270*). Taken together, these studies suggest that polymorphisms modulate prion diseases by exerting their effects on an intermediate species, instead of the native form. Thus, a folding intermediate seems to be a more plausible PrP^{Sc} precursor.

4.4.2. Intermediates observed under refolding conditions. The current study shows that ovPrPs refold with a time constant of ~100-300 μs without a resolvable kinetic intermediate under various refolding conditions, including two temperatures (5 and 15 °C), two pH values (5 and 7) and two denaturants (GuHCl and urea). Although an intermediate state was not observed directly, ovPrP refolding should proceed through an intermediate state, assuming the conservation of kinetic mechanism in different concentrations of denaturant(*177, 207, 271*). Such conserved folding and unfolding pathways are standard in proteins(*177*).

The present experiments contrast with previous studies. A kinetic study of huPrP was undertaken with 100 μs time resolution(*219*). Accumulation of an early intermediate with a time constant of ~50 μs and a rate-determining folding step with a time constant of ~700 μs was observed in urea at 5^{o}C, pH 4.8 and 7(*219*). Since I could not resolve such an intermediate under refolding conditions, the folding kinetics of ovPrPs differ from human PrPs, possibly reflecting structural differences in their respective intermediates. Such species differences have been observed for the intermediate state in human and Syrian hamster PrPs(*244*). Instrumentation should not be a concern when comparing the present data with the previous huPrP study, since the same capillary mixing system was used for both experiments, with improved detector sensitivity in the current study.

Supplemental materials.

Figure S1. Amplitudes and rate constants from the best fit to refolding kinetic traces. Rate constants were plotted on semilogarithmic scale. Traces were taken in (A) - (E): 50 mM sodium acetate with various concentrations of GuHCl , at pH 5 and 15^{o}C; (F) - (I): 50 mM imidazole with various concentrations of GuHCl, at pH 7 and 15^{o}C.

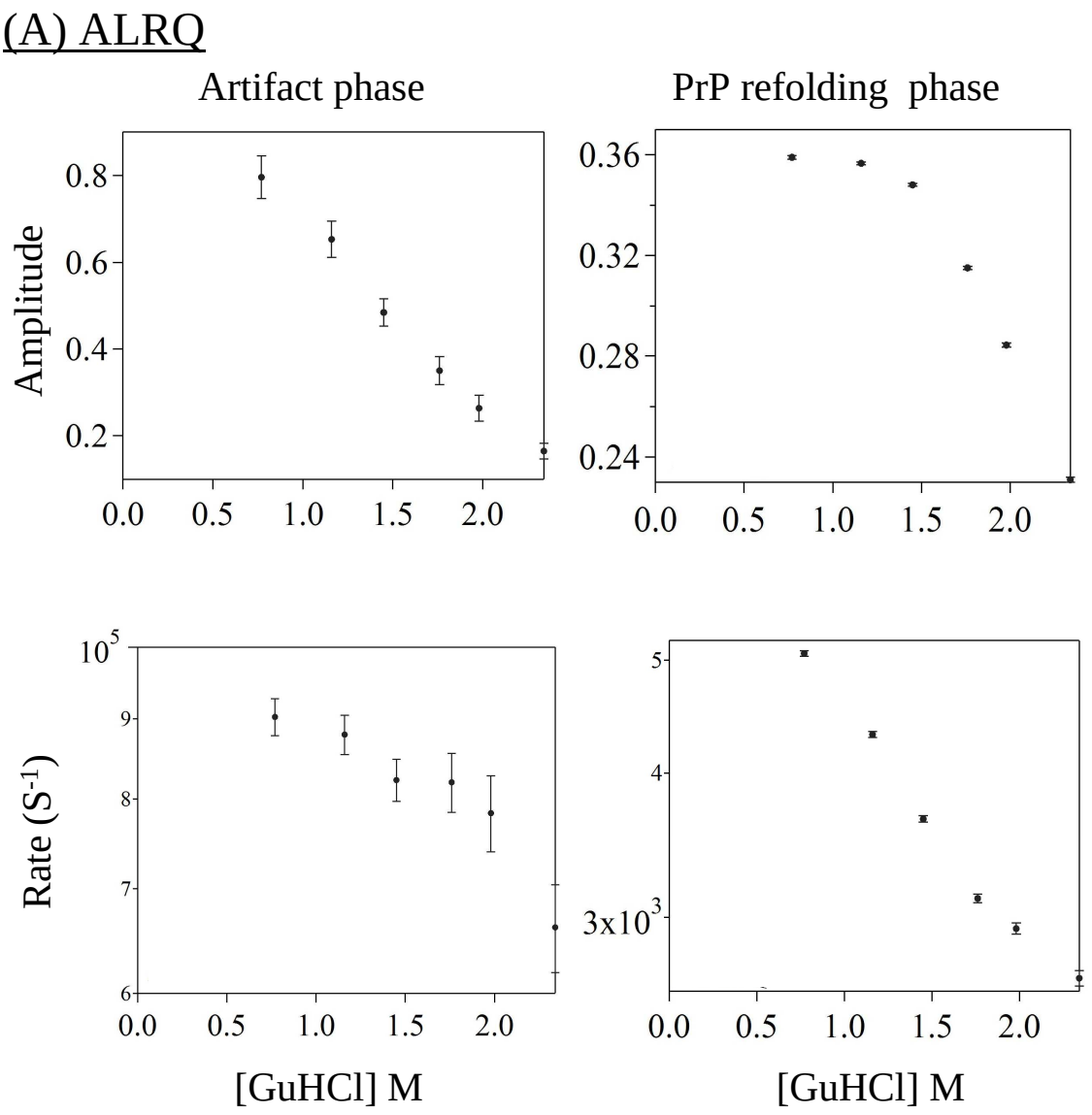

Figure S1. (cont'd)

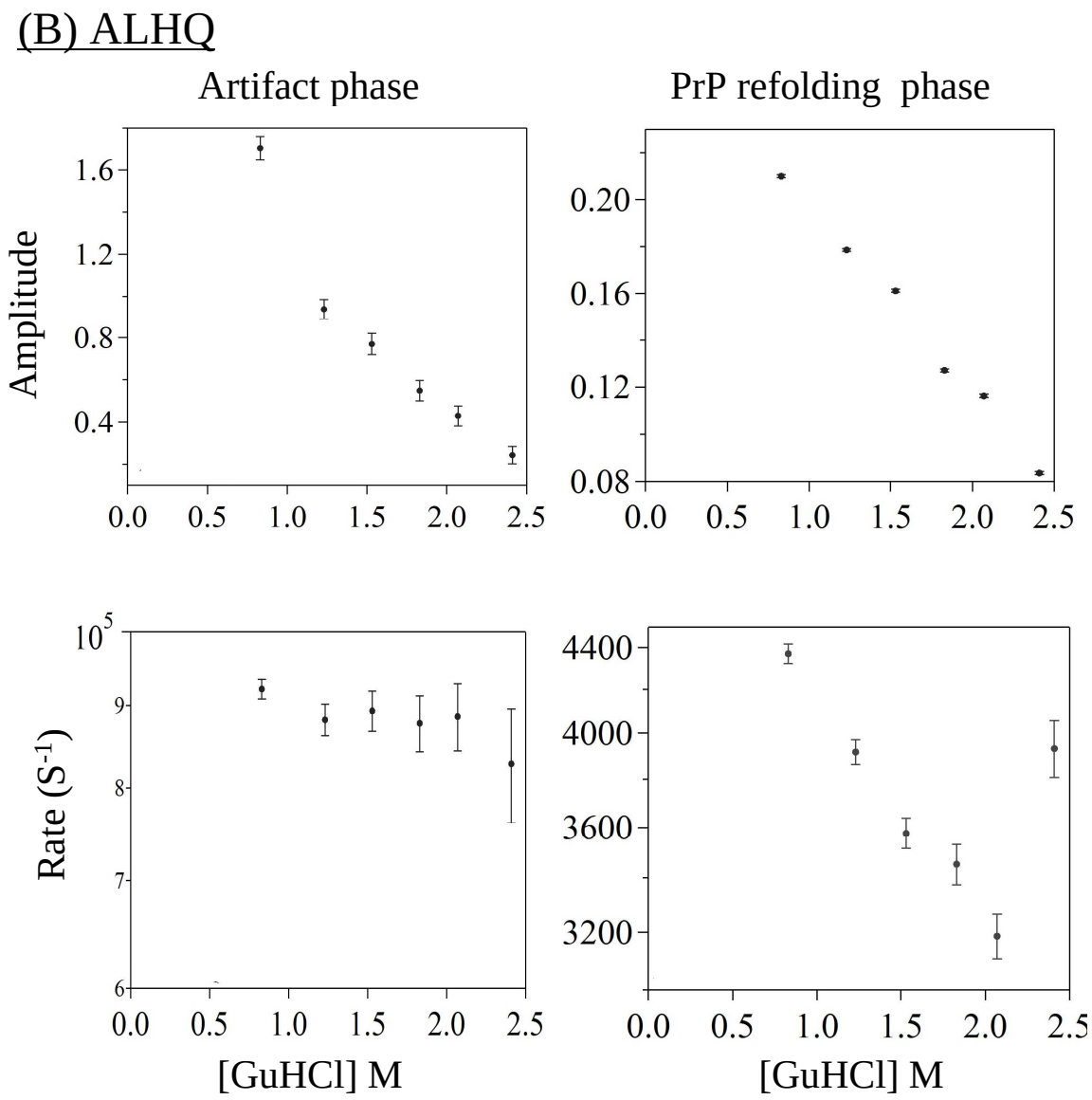

Figure S1. (cont'd)

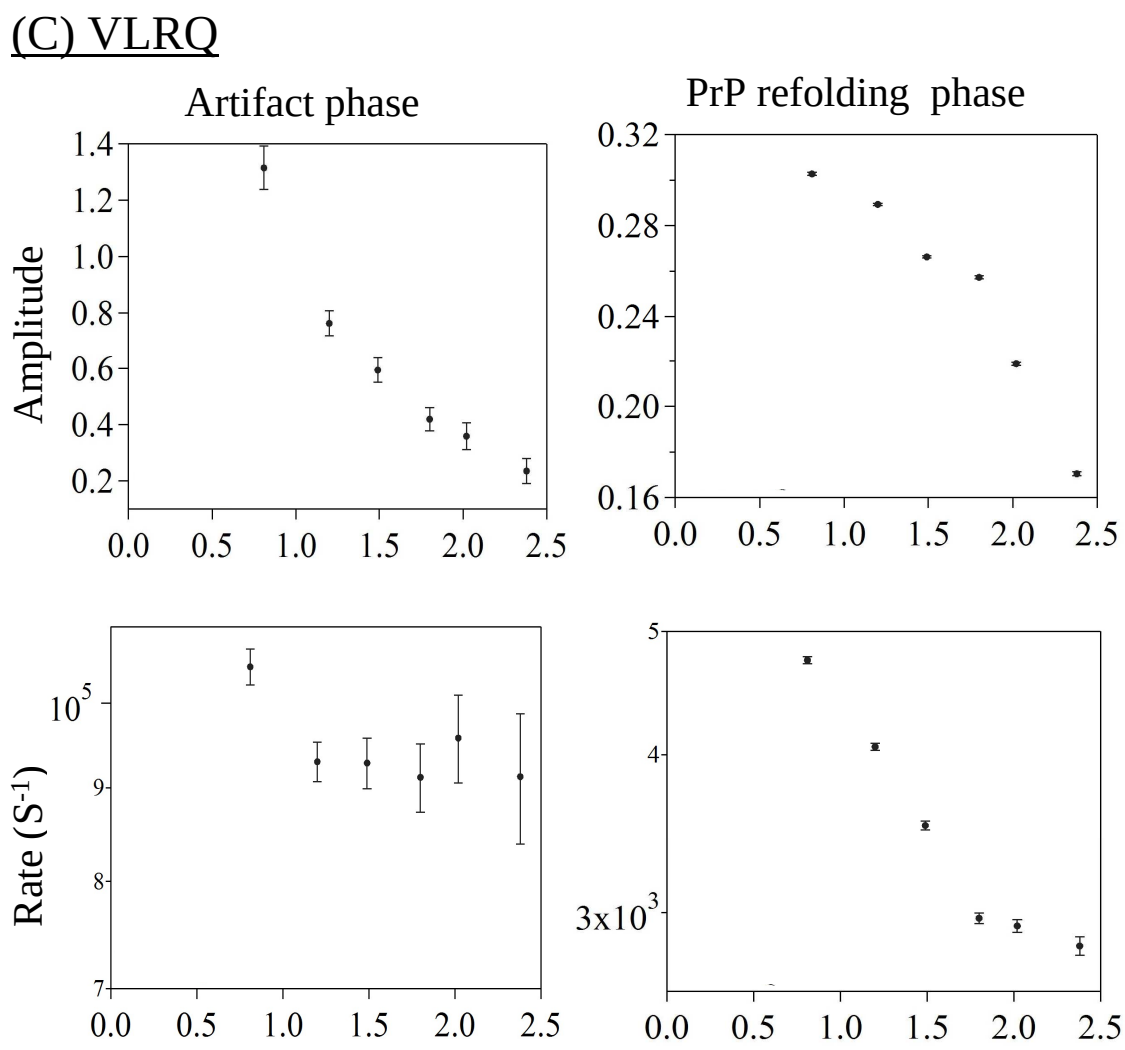

Figure S1. (cont'd)

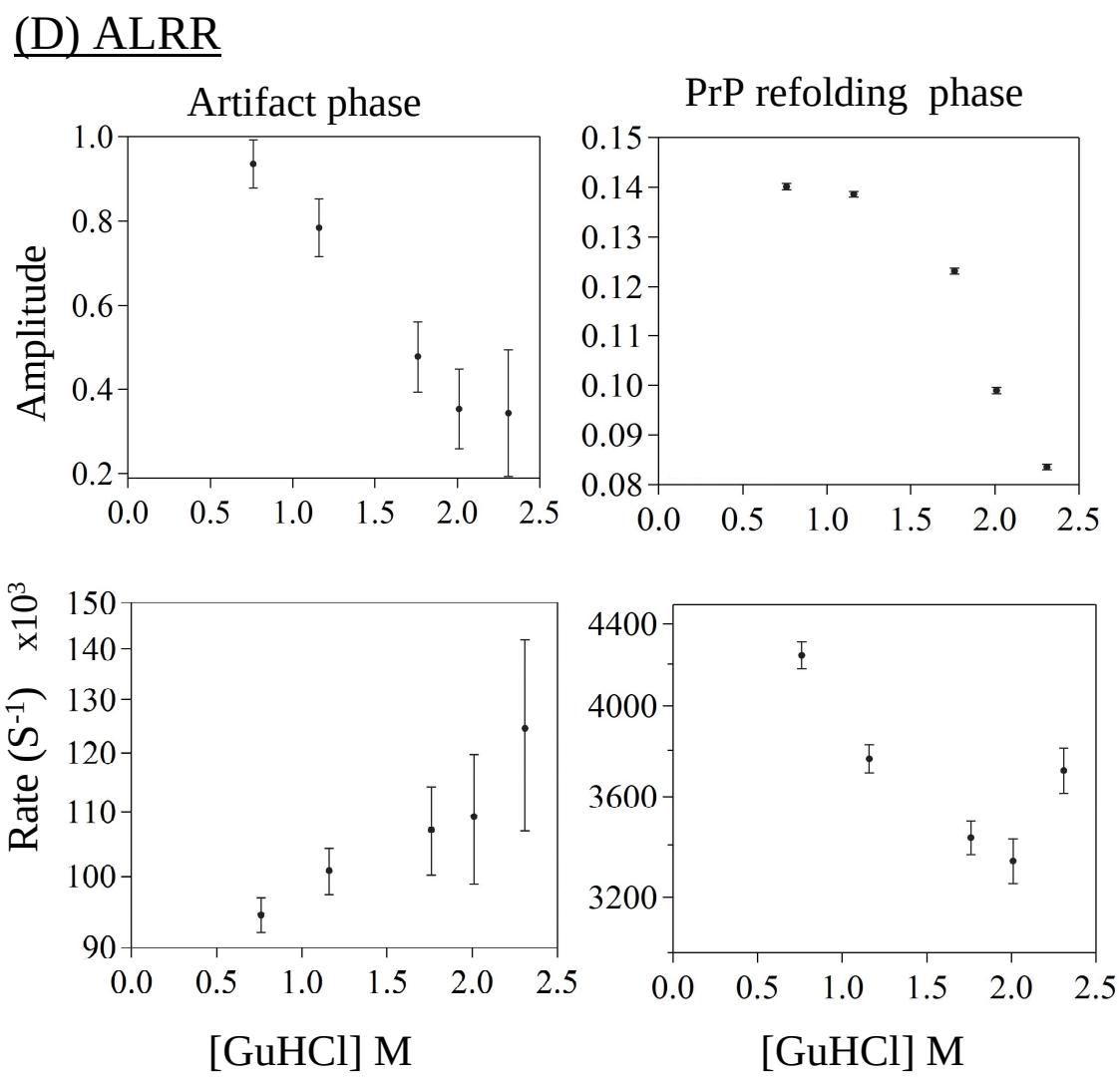

Figure S1. (cont'd)

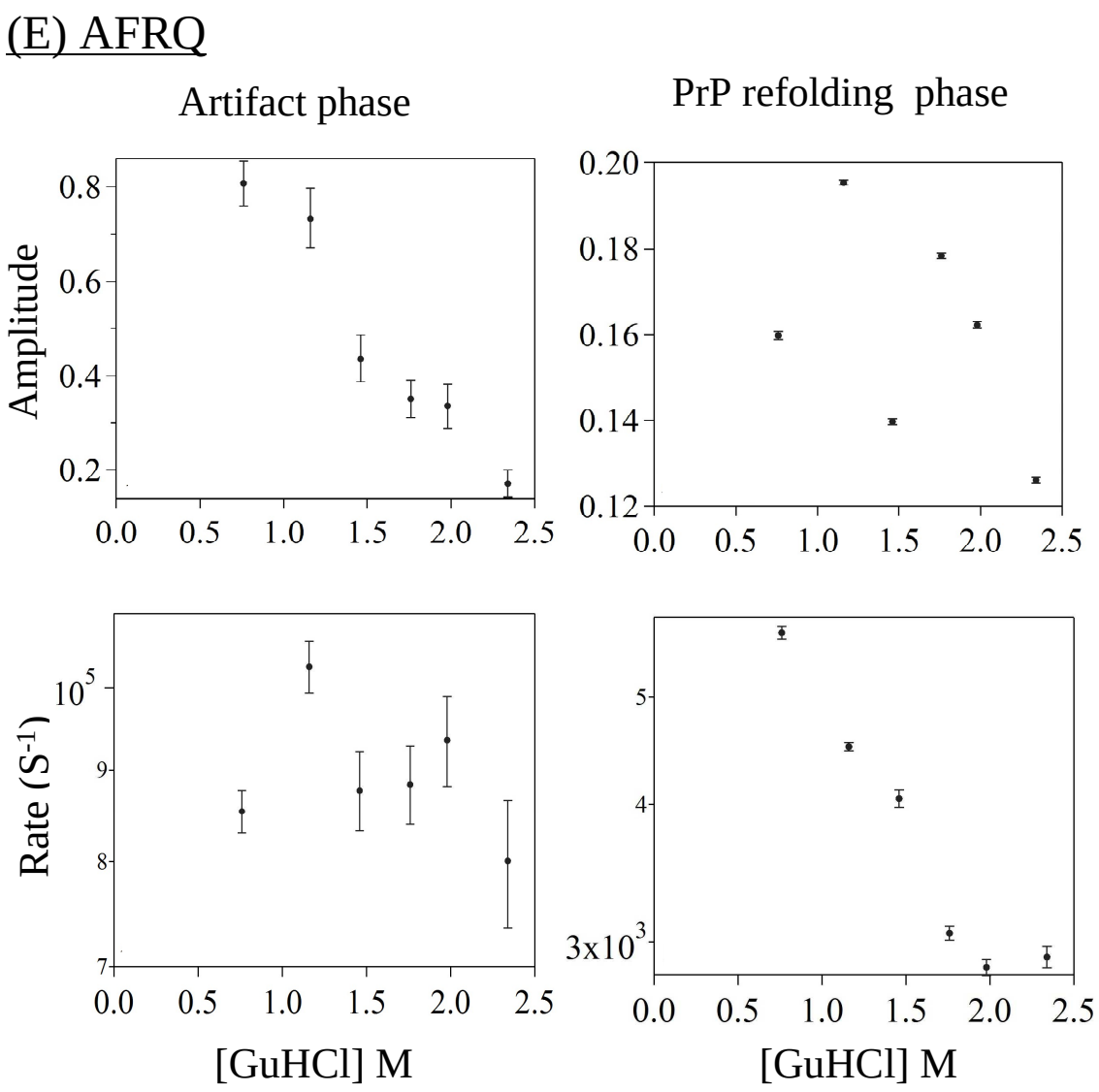

Figure S1. (cont'd)

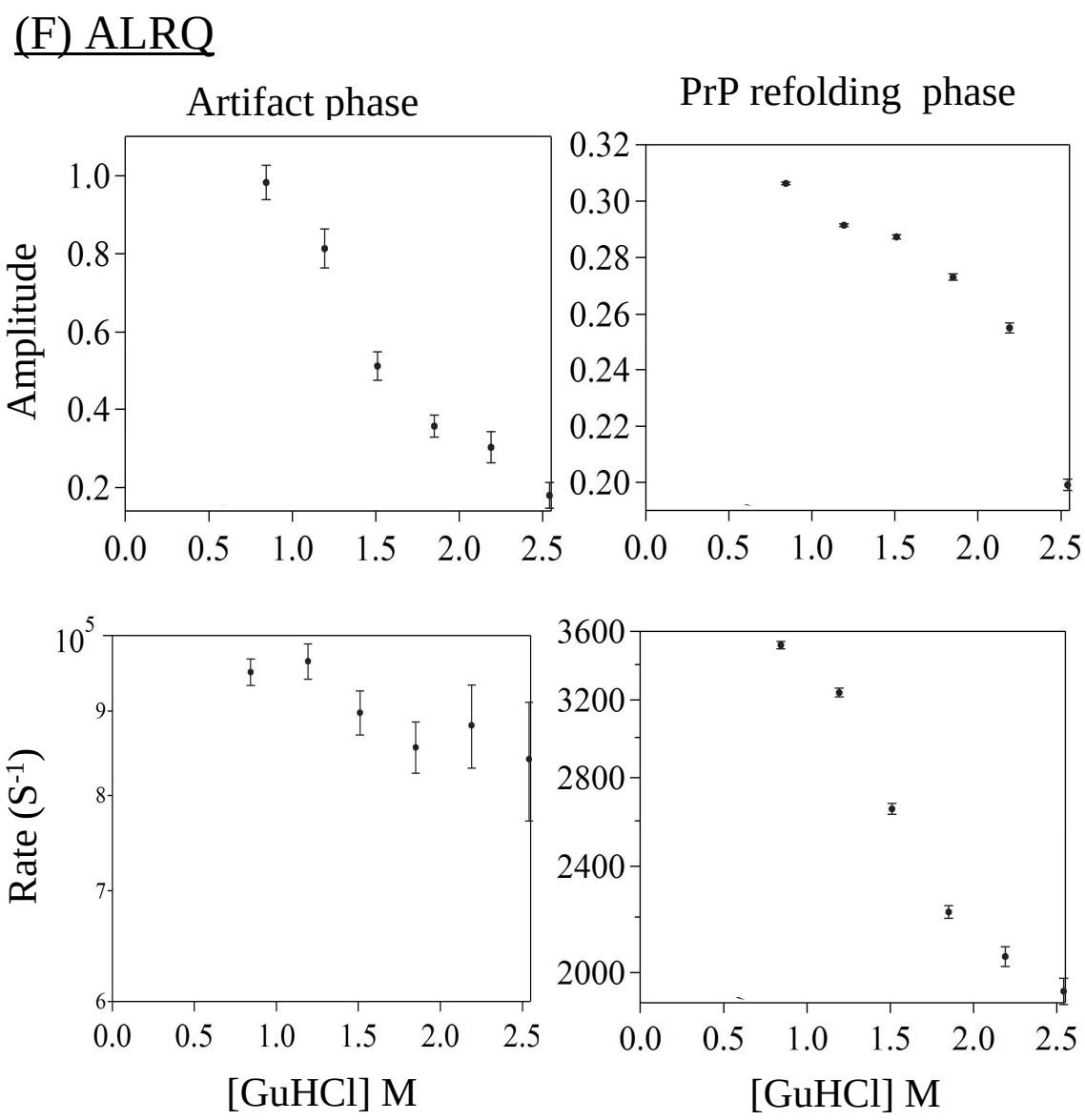

Figure S1. (cont'd)

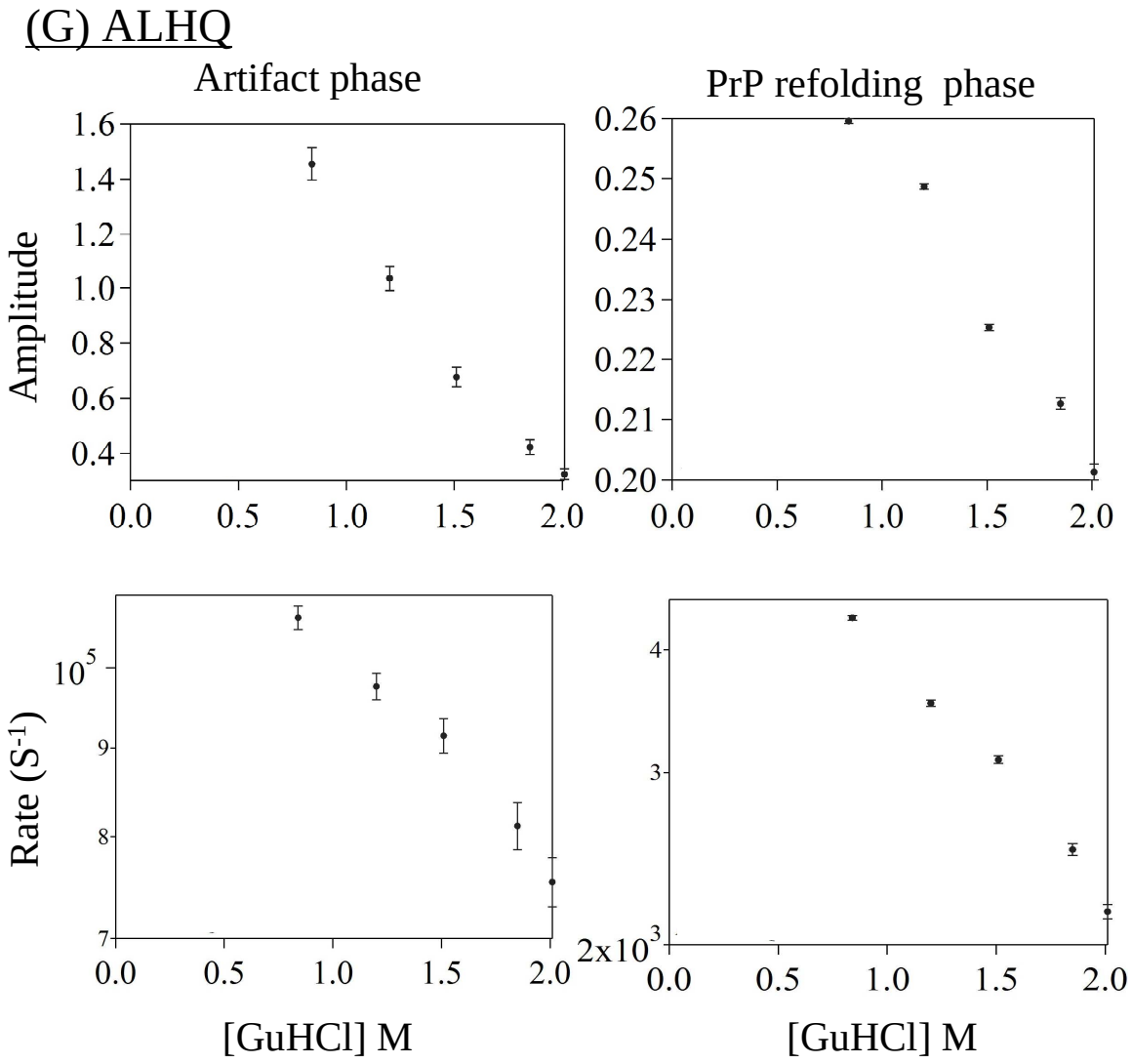

Figure S1. (cont'd)

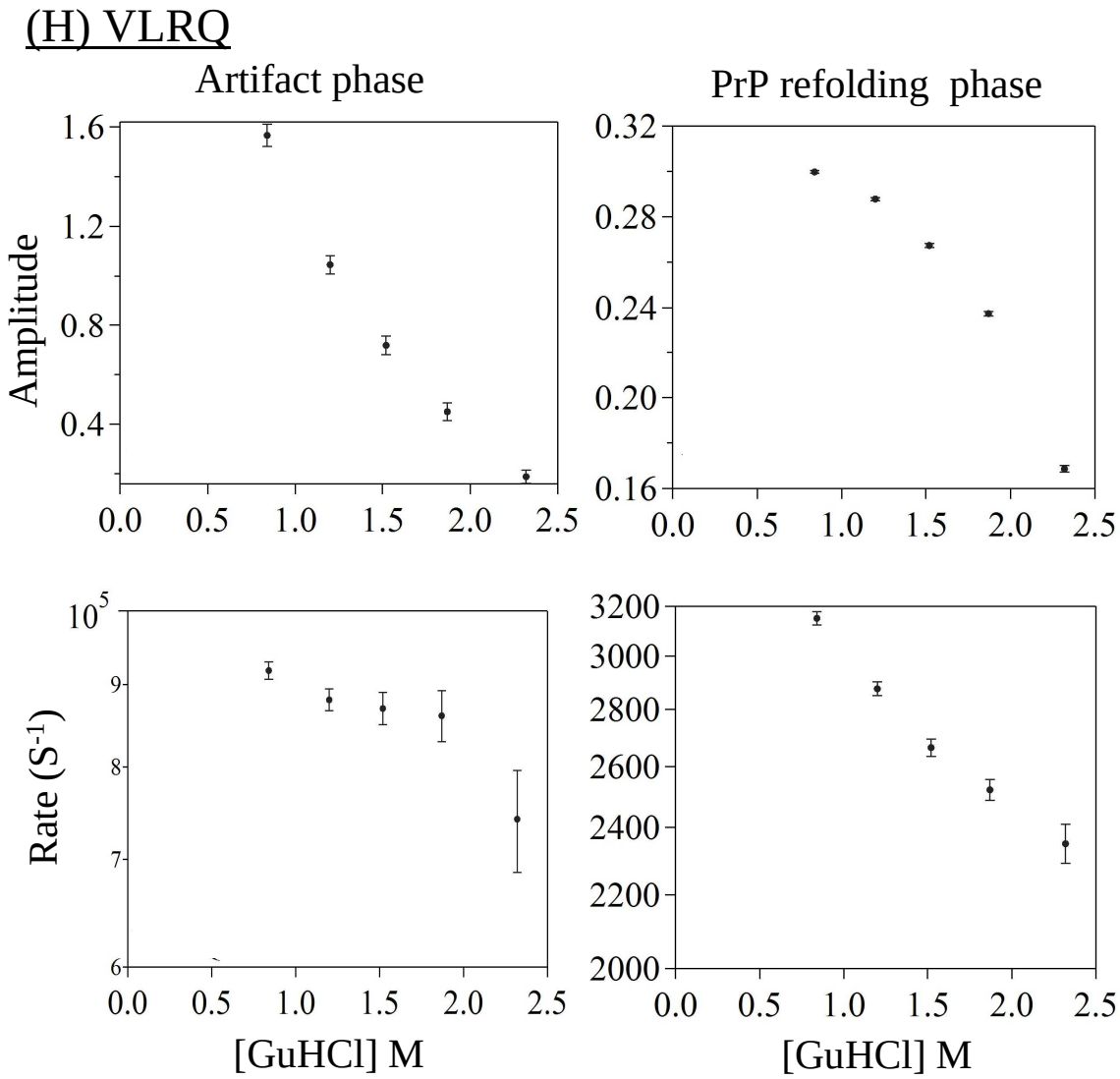

Figure S1. (cont'd)

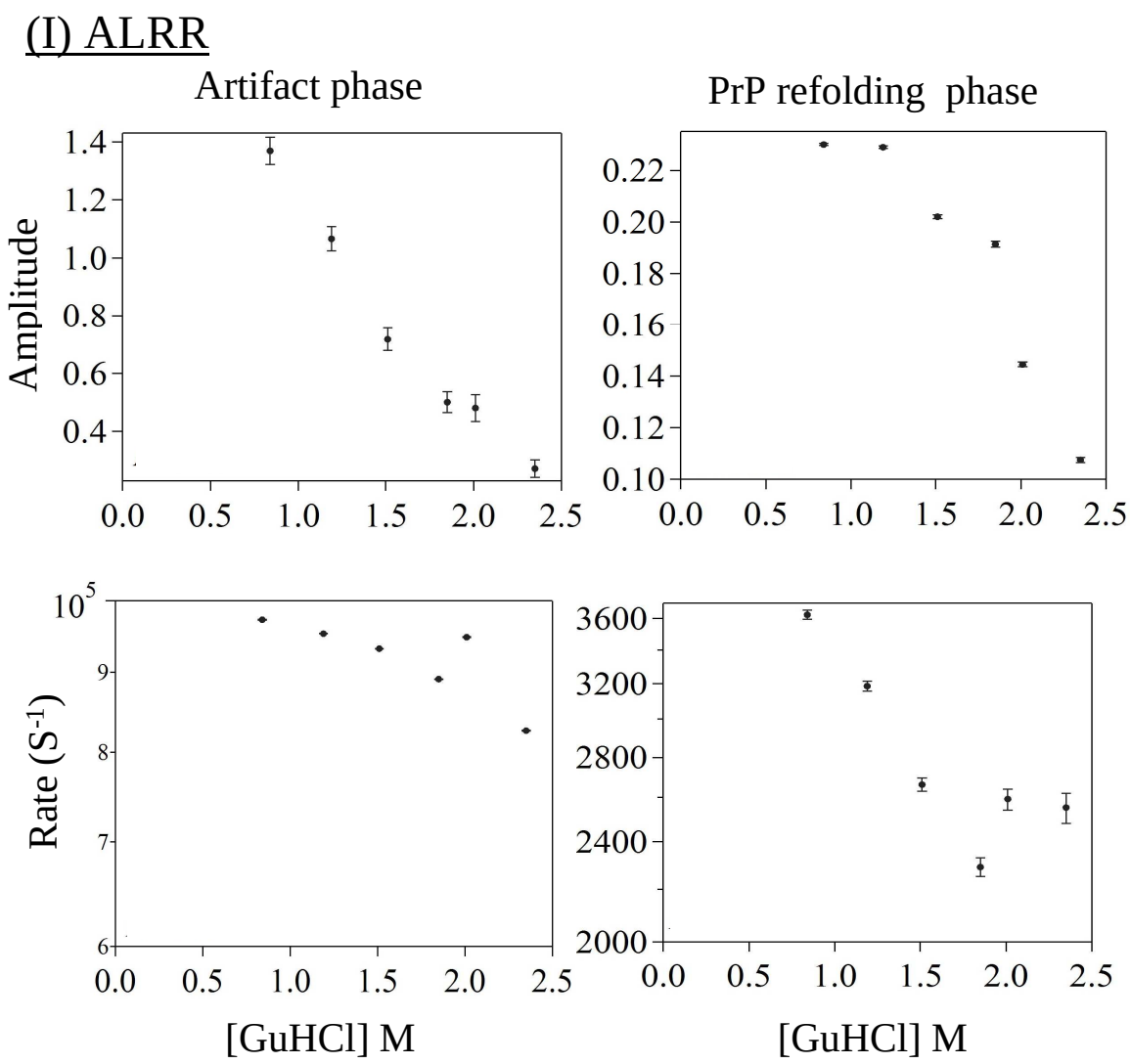

Figure S2. Amplitudes and rate constants from the best fit to refolding kinetic traces. Rate constants were plotted on semilogarithmic scale. Traces were taken in (A): 50 mM imidazole with various concentrations of urea, at pH 7 and 5^{o}C; (B): 50 mM sodium acetate with various concentrations of urea, at pH 5 and 15 ^{o}C; (C): 50 mM imidazole with various concentrations of GuHCl, at pH 7 and 5^{o}C.

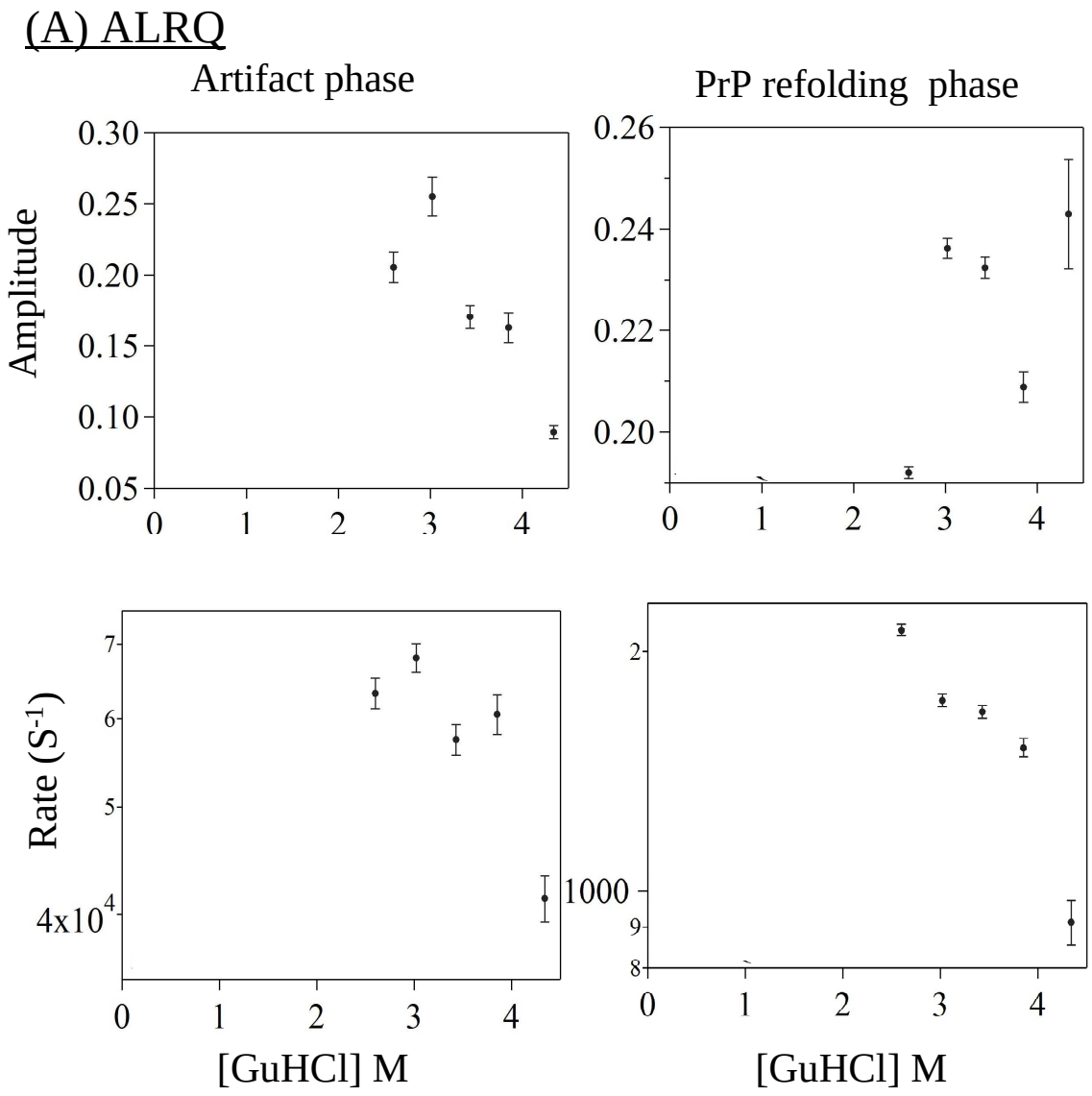

Figure S2. (cont'd)

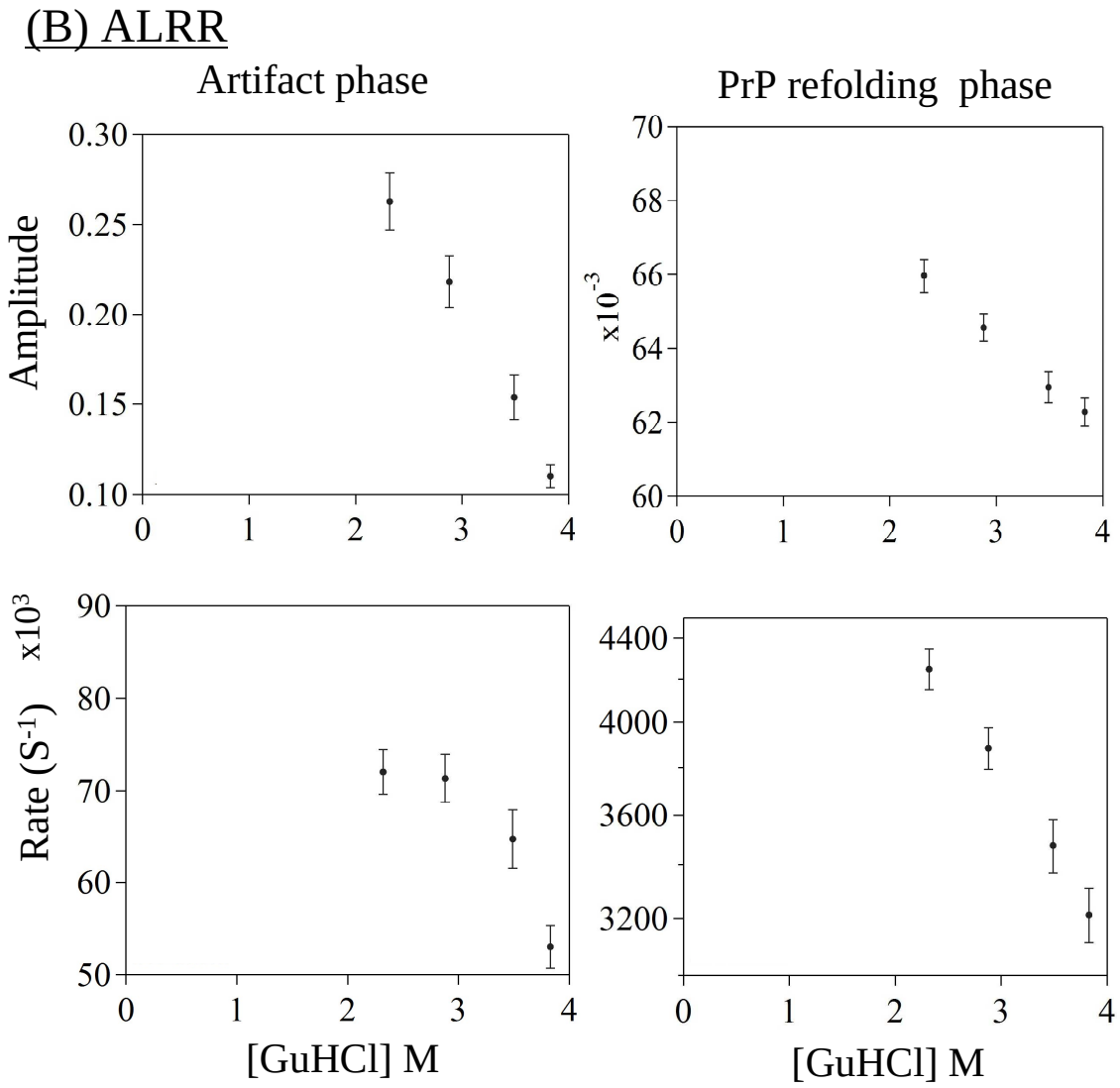

Figure S2. (cont'd)

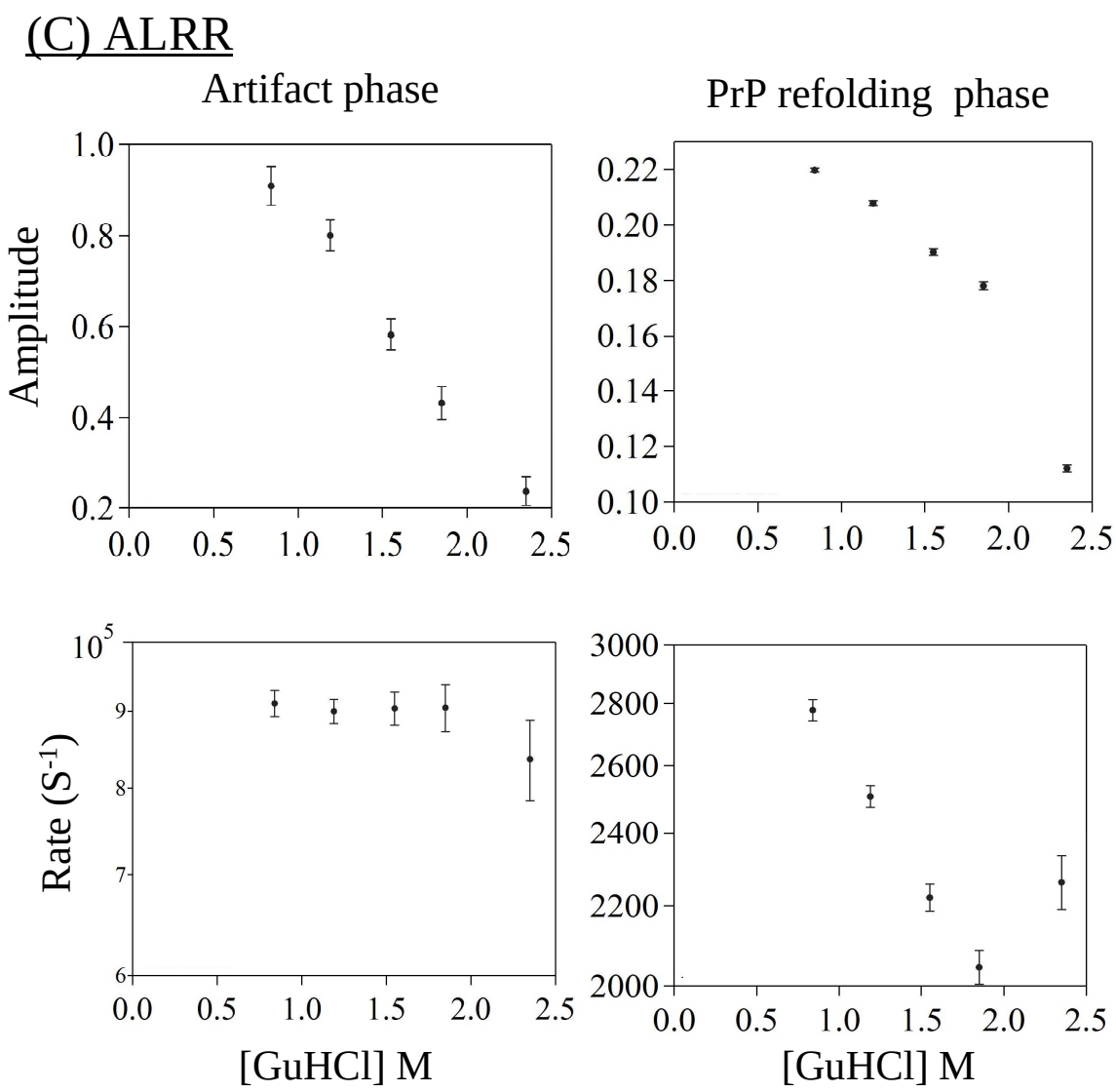

Chapter 5.Role of the Disulfide Bond in Stabilizing the Folding Intermediate

5.1. Introduction. Several studies argue for the importance of the sole disulfide bond of PrP (Figure 5.1.A) in prion diseases. Previous reports indicate that the disulfide-free PrP is destabilized, and exhibits a PrP^{Sc}-like conformation(*251, 272*). However, mutant PrPs in a reduced form, or with mutations that inhibit formation of a disulfide bond, are unable to be converted into PrP^{Sc} (*247-249*). The reshuffling of this disulfide bond from intramolecular to intermolecular forms has been proposed as a step in the PrP^{C}-to-PrP^{Sc} conversion (*239, 250-253*), although a later study (*240*) suggests that disulfide bond reshuffling is not required for PrP^{Sc} propagation. A very recent report has shown that the disulfide bond restricts the motion of the putative transmembrane domain (residues 111-135) of Syrian hamster PrP, thus modulating the initiation of misfolding by regulating membrane binding(*254*). Despite intensive studies, the mechanisms underlying the influence of this disulfide bond on prion diseases remain elusive.

Since a disulfide bond imposes conformational constraints on its neighboring residues and stabilizes its local structure(*149*), it may stabilize the formation of the PrP folding intermediate observed in the *Chapter Four*. If so, and if the intermediate is indeed the PrP^{Sc} precursor, then the intramolecular disulfide bond may regulate the conversion to PrP^{C} and PrP^{Sc} through the same folding nucleus. To examine whether the interactions in the vicinity of the disulfide bond suffice to form the folding intermediate of PrP, I used a

peptide model flanking the disulfide bond to measure the local folding using circular dichroism (CD) and hydrogen/deuterium exchange (HDX). Folding in the vicinity of a disulfide bond has been observed in several other model peptides using this method(*151-154*).

Figure 5.1. Positions of the disulfide bond and the selected model peptides. (A) Ribbon representation of the structure of ovPrP (PDB entry: 1UW3). The disulfide bond is shown in yellow. P1 and P2 are shown in blue and red, respectively. (B) Sequence alignment of homologous PrP. The symbols α and β correspond to α-helix and β-sheet structure in PrPs, respectively.

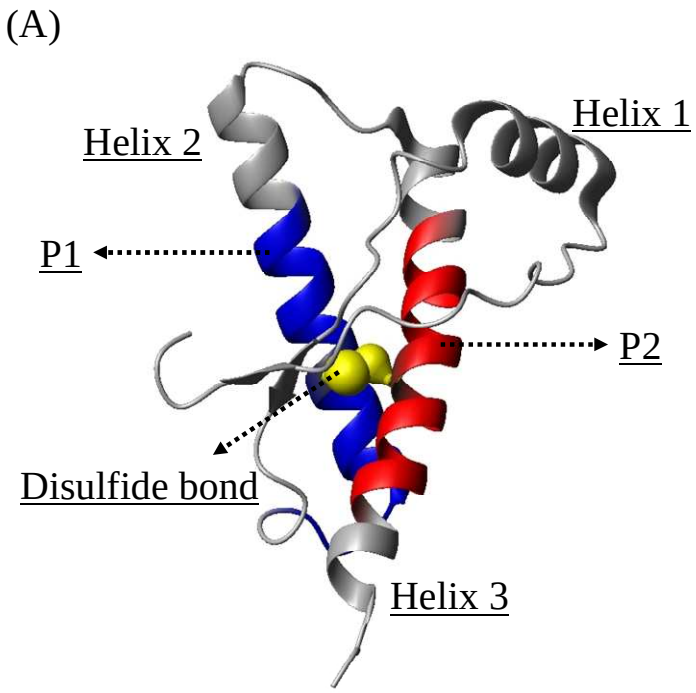

Figure 5.1. (cont'd)

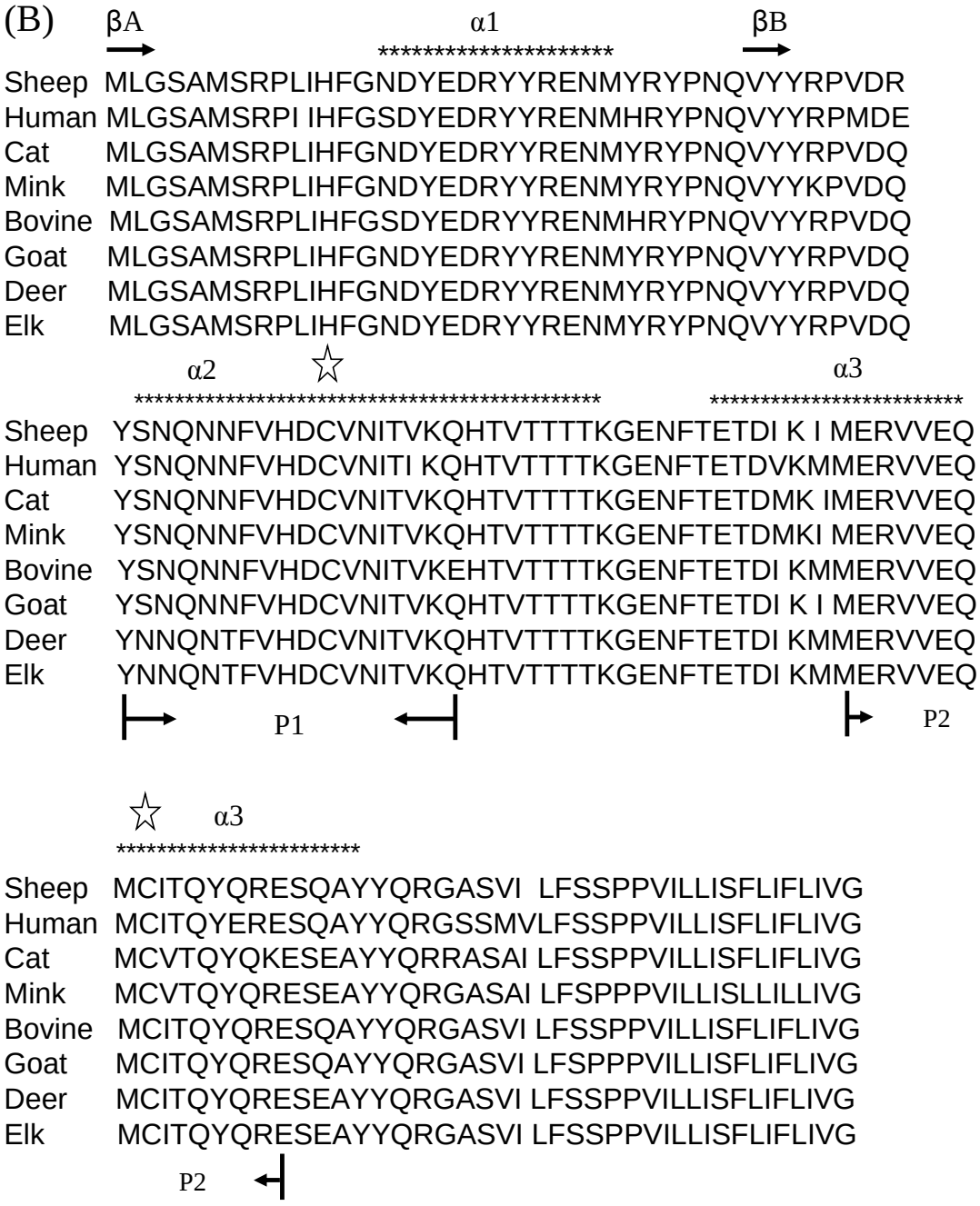

5.2. Materials and methods.

5.2.1. Materials. The tris-(2-carboxyethyl) phosphine hydrochloride (TCEP) solutions were freshly prepared before use. NaH_2PO_4 was purchased from Mallinckrodt Baker (Phillipsburg, NJ). Guanidine hydrochloride (GuHCl) and sodium citrate were obtained from Invitrogen (Carlsbad, CA) and Spectrum Quality Products (Gardena, CA). Acetonitrile was obtained from EMD Chemicals (Gibbstown, NJ). Immobilized pepsin was obtained from Pierce (Rockford, IL). C18 ZipTip was purchased from Millipore (Bedford, MA). All other chemicals were obtained from Sigma-Aldrich.

5.2.2. Construction of peptide models. Multiple sequence alignment and structural alignment were performed to identify the key conserved residues stabilizing this local structure. The homologous sequences of ovine PrP were identified through several rounds of NCBI PsiBLAST (http://www.ncbi.nih.gov/BLAST/Blast.cgi), and the mature homologous sequences were aligned using ESPript server (http://espript.ibcp.fr/ESPript/cgi-bin/ESPript.cgi). Based on the alignment result, two peptide sequences involved in this disulfide bond were selected: (P1) YSNQNNFVHDCVNITVKQH (residues 169-187), and (P2) MERVVEQMCITQYQRE (residues 206-221) (Figure 5.1).

5.2.3. Preparation of peptide models. P1 and P2 were synthesized by SynPep Corporation. Purification was carried out with 5% - 100% acetonitrile gradient in the presence of 0.1% trifluoro-acetic acid in 90 minutes on Vydac C4 and C18 columns coupled with reverse-phase high-performance liquid chromatography (RP-HPLC) system (Waters) detected at

205 nm. Matrix-assisted laser-desorption/ionization time-of-flight mass spectrometry (MALDI-TOF-MS) measurements were performed to identify the two model peptides (Figure 5.2). To prepare P1P1, P2P2, and P1P2 peptide pairs, roughly equal amount of purified monomers were mixed in a solution containing 5 M GuHCl, 0.2 M Tris-HCl, and 10 mM NaH_2PO_4 (pH 8), then air-oxidized overnight at room temperature. Separation and identification of these dimeric peptides were carried out by RP-HPLC purification and MALDI-TOF-MS measurement as mentioned above. The combination of RP-HPLC and MALDI-TOF-MS confirms that the P1P1, P2P2, and P1P2 peptides are indeed disulfide-bonded, since these methods cause non-covalent complexes to dissociate.

Figure 5.2. Identification of P1 and P2. (A) and (C): Chromatograms of P1 and P2, respectively. (B) and (D) MALDI mass spectra of P1 and P2, respectively.

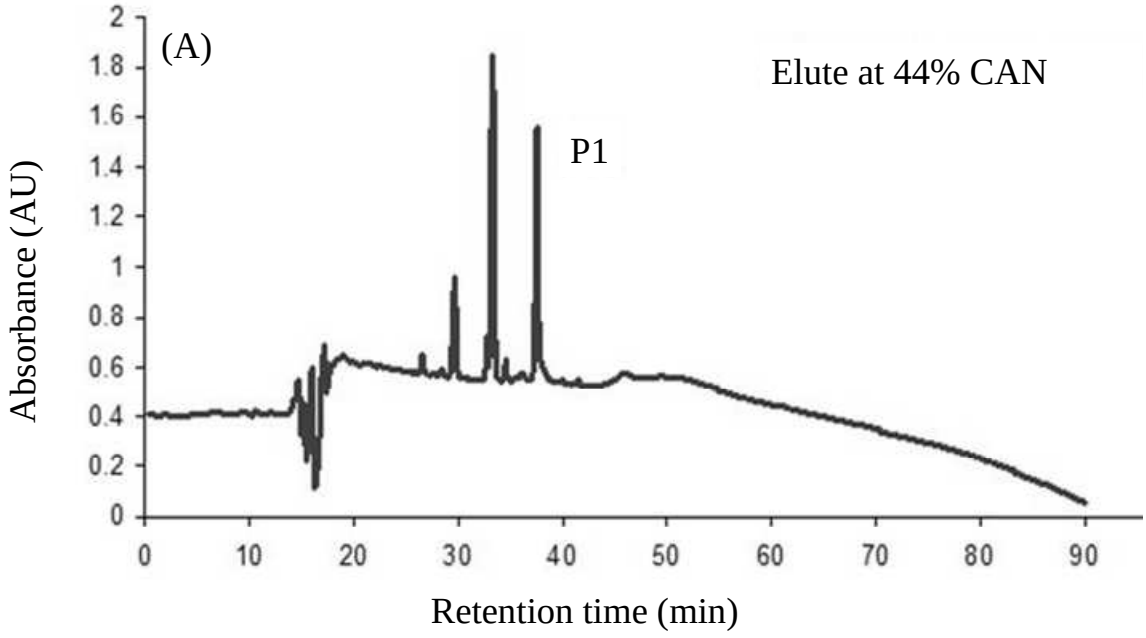

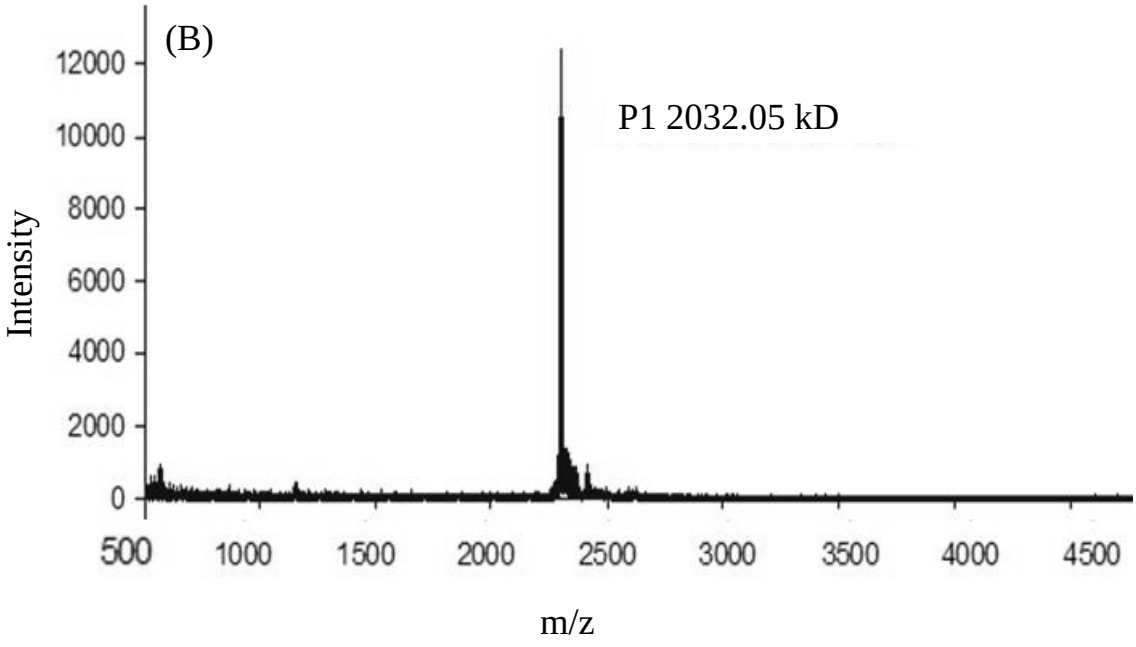

Figure 5.2. (cont'd)

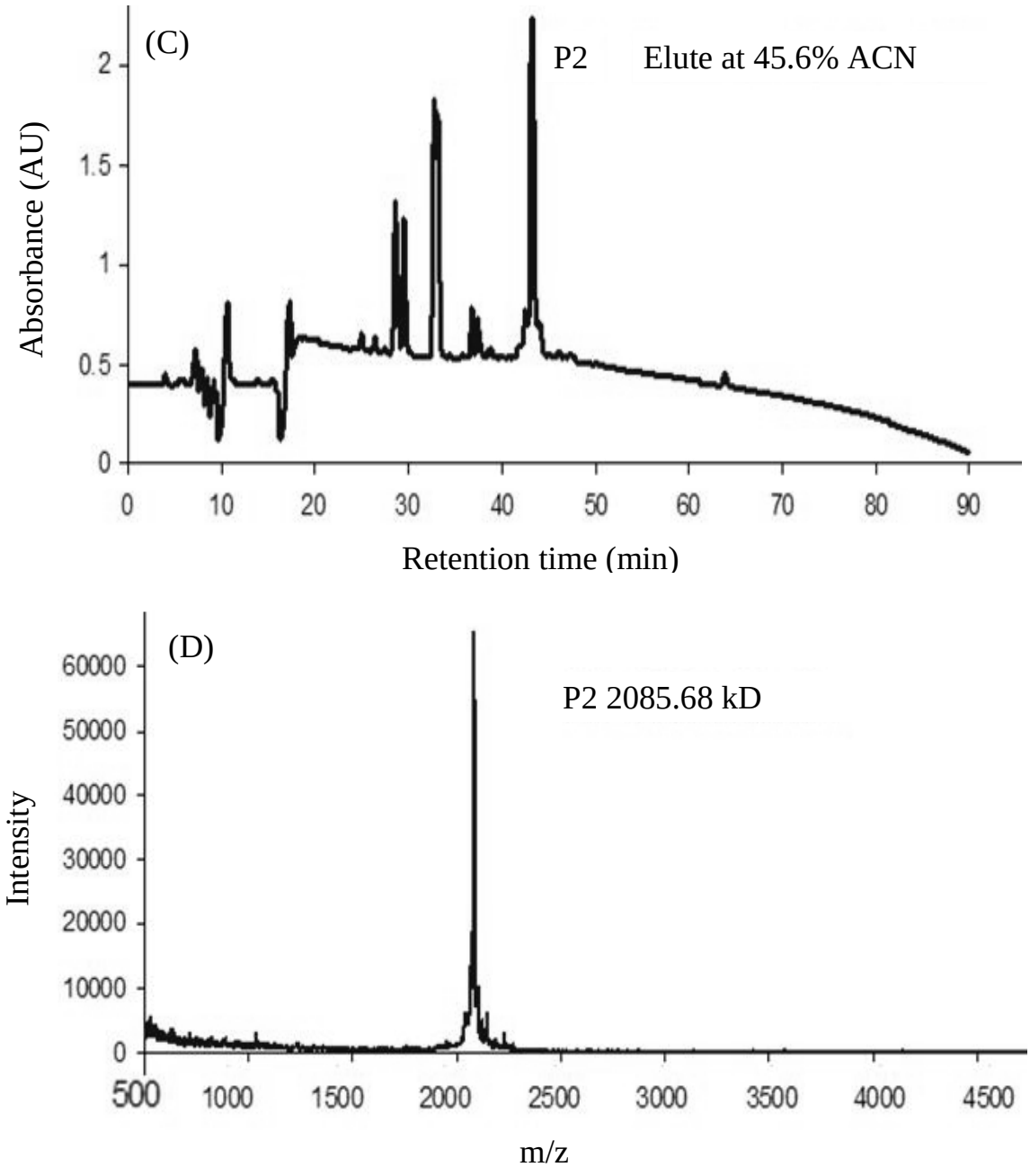

5.2.4. Hydrogen/deuterium exchange.

(1) Technical background of hydrogen/deuterium exchange. Hydrogen/deuterium exchange (HDX) has been applied to probe hydrogen bonding and solvent accessibility in several proteins and peptides. In an unfolded protein or polypeptide, hydrogen exchange

is a relatively fast process. However, exchange of amide protons in a native form is often much slower due to these hydrogen being protected from the solvent by secondary and tertiary structure(*134*, *273*).

The rate of HDX reaction depends strongly on the temperature and the pH of the reacting system(*274*). The reaction is catalyzed by both acidic and basic conditions (Figure 5.3.A), with the reaction rate reaching its minimum at roughly pH 2.5(*274*) (Figure 5.3.B). By utilizing these two characteristics of HDX reactions, exchange can be slowed down significantly for MS measurements by lowering the pH to 2.5 and the temperature to 0^{o}C.

Figure 5.3. Mechanism of HDX reaction and its reaction rates plotted as a function of pH for polyalanine. (A) HDX reactions at neutral pH involve base-catalyzed proton abstraction and acid-catalyzed deuterium transfer from solvent. (B) Figure was adopted from Smith, D.L. et al. (1997) *J. Mass Spectrom.* **32**, 135-146.

(A) $\mathbf{A\text{-}H + OD^-} \xrightarrow{\mathbf{OD^-}} \mathbf{A^- + H\text{-}OD}$

$\mathbf{A^- + D_3O^+} \longrightarrow \mathbf{D_2O + A\text{-}D}$

(B)

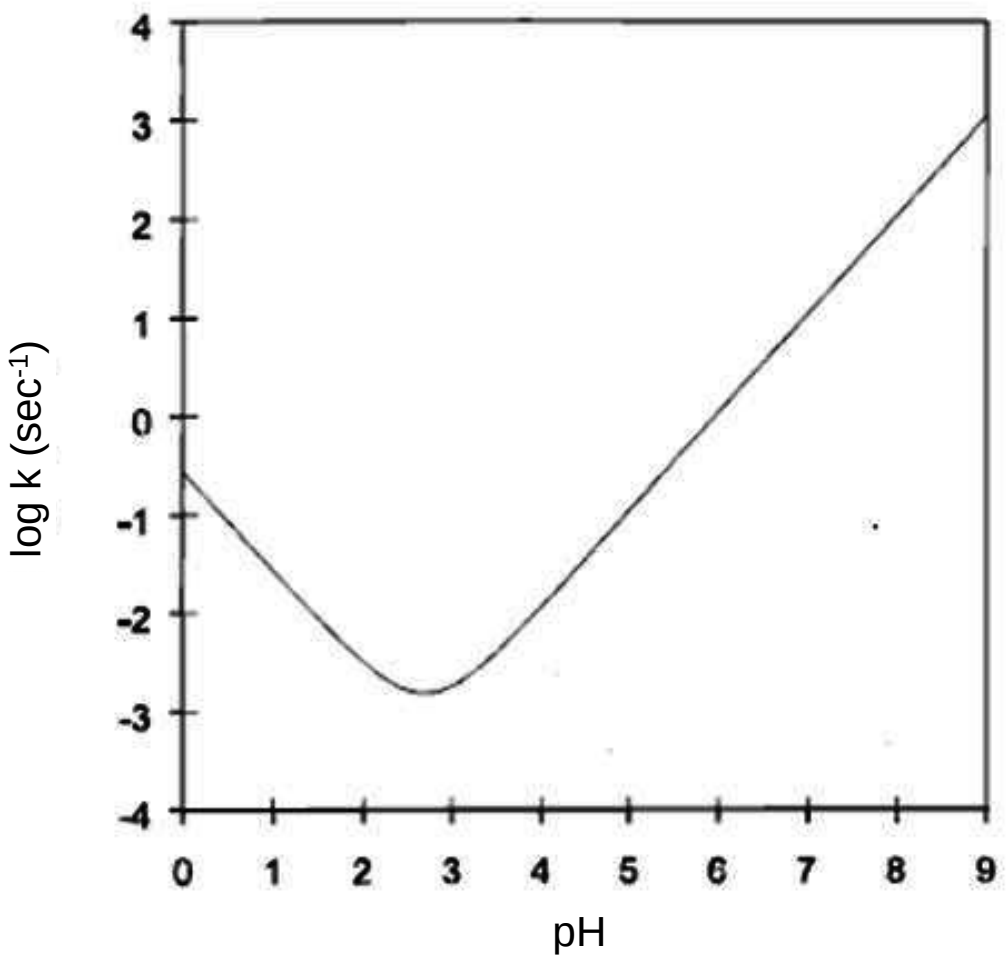

(2) Experimental procedure. Samples were equilibrated in 20 mM phosphate buffer/H_2O (pH 7.0) for one hour. 1 µL of equilibrated peptide solution (~100 pmol/µL) was added to 19 µL of 20 mM phosphate buffer either in D_2O (pD 6.8) or in H_2O (pH 7.0) at 4 ^oC. After 15 seconds, 19 µL of 0.1 M citrate buffer containing 0.5 M tris-(2-carboxyethyl) phosphine hydrochloride (pH 2.5) was added to quench the exchange reaction and reduce the disulfide bonds. Reduction of the disulfide bond makes it feasible to compare the exchange in a dimeric peptide to its monomeric peptide components. The sample was desalted using a C18 ZipTip (Millipore), and eluted with a matrix solution, followed by being spotted on a pre-chilled MALDI plate. The target plate was immediately dried in a desiccator for 1-2 minutes, then transferred to the MALDI mass spectrometer under vacuum.

5.2.5. Circular dichroism (CD) spectroscopy.

Far-UV CD spectroscopy was carried out to detect the secondary structure of these five model peptides (P1, P2, P1P1, P2P2, and P1P2) in a buffer containing 10 mM NaH_2PO_4 and 10 mM NaF (pH 7.5). The CD spectra were acquired on a Jasco J-810 CD spectropolarimeter using a 1-mm path-length cell from 190 nm to 250 nm with a scanning speed of 1 nm/min at 4 ^oC.

5.3. Results.

CD and HDX measurements were carried out to examine two hypotheses. *First*, if the local interactions around the disulfide bond suffice to form a PrP folding intermediate, the isolated P1P2 model peptide should adopt the same secondary structure as its

counterpart in a native protein, which is α-helical. *Second*, the association of any two peptides may increase the secondary-structure content of both peptides, since intramolecular hydrogen bonds within a peptide pair will have less competition from intermolecular hydrogen bonds between its monomeric peptide component and water(*151*). Therefore, the structure induced in the homodimeric P1P1 and P2P2 peptide pairs was also measured, in addition to the heterodimeric P1P2 pair. A control experiment was carried out on their monomeric components (P1 and P2) to determine whether the observations result from the interactions stabilizing by the disulfide bond.

As shown in Figure 5.4, CD spectra of these model peptides (P1P1, P2P2, and P1P2) exhibit a single minima at near 200 nm, as expected for random-coil structure(*275*). A similar situation was observed for their monomeric peptide components (P1 and P2). This observation indicates that interactions within P1P2 peptide pair do not suffice to stabilize a folding intermediate, and that association of the monomeric peptides (P1P1, P2P2, and P1P2) does not provoke significant secondary-structure formation. Consistent with CD measurements, the covalent linkage of two model peptides does not protect them from HDX reactions, suggesting that stable hydrogen bonding does not form within the peptide pair (Figure 5.5).

Figure 5.4. CD spectra of the five peptide models. (A) and (B): Monomeric P1 and P2, respectively. (C)-(E): Disulfide-bonded P1P1, P2P2, and P1P2, respectively. Measurements were made in buffer containing 10 mM NaH_2PO_4 and 10 mM NaF at pH 7.5, 4°C.

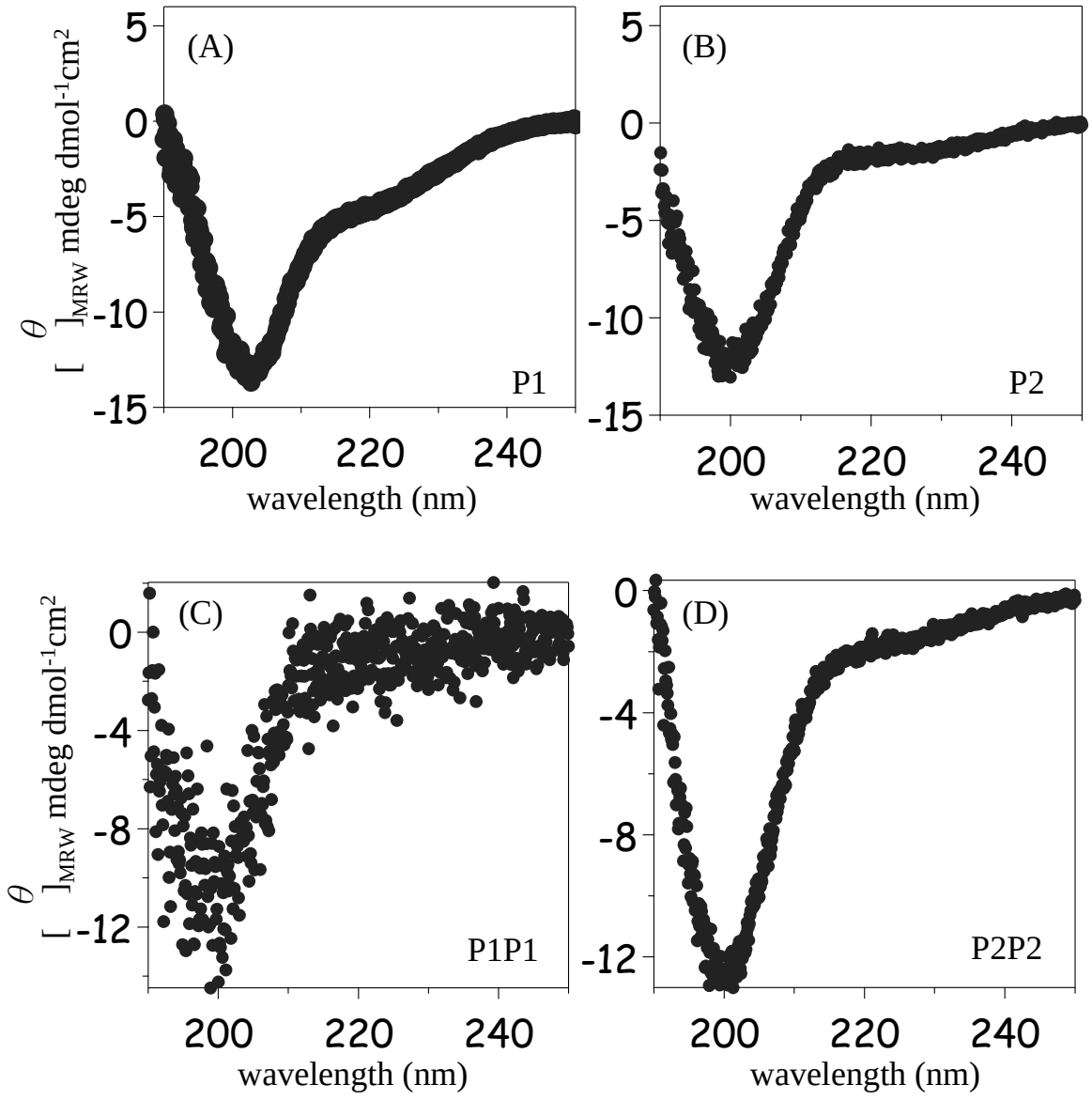

Figure 5.4. (cont'd)

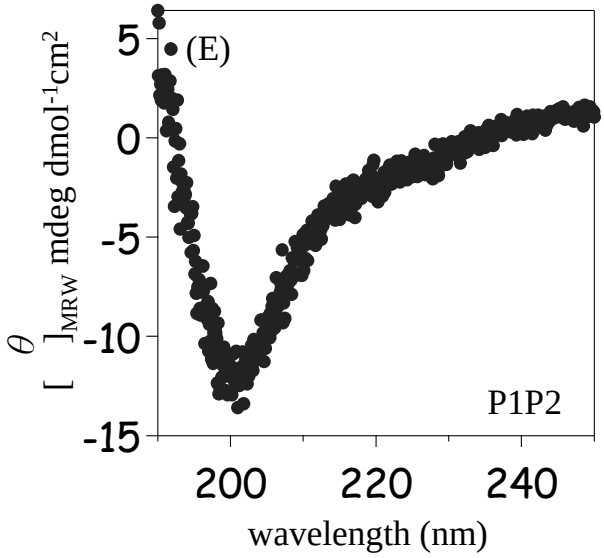

Figure 5.5. HDX reactions for the model peptides. Mass shifts calculated for the monomeric P2 and dimeric P2P2 are 6.2 and 6.45, respectively.

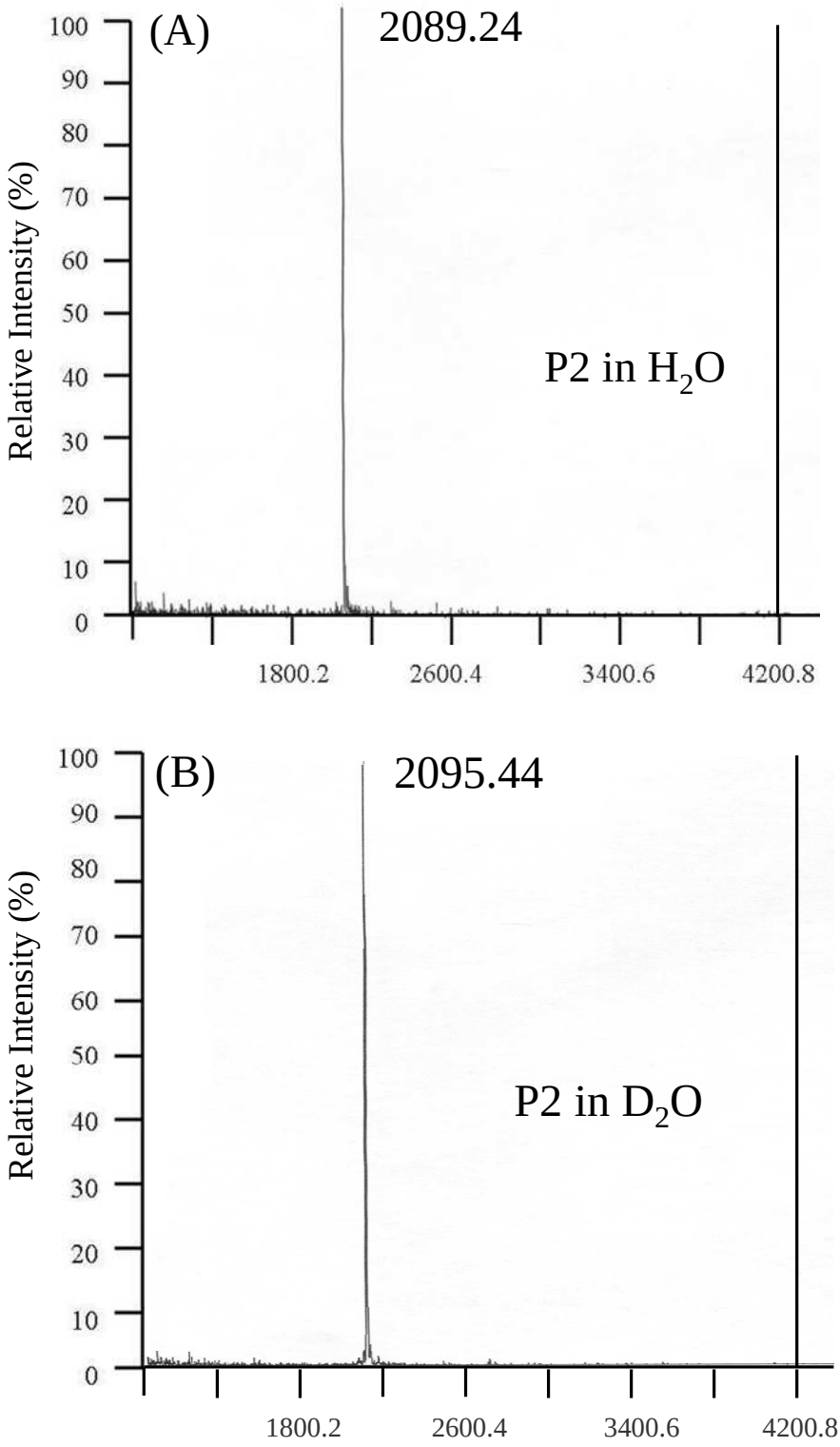

Figure 5.5. (cont'd)

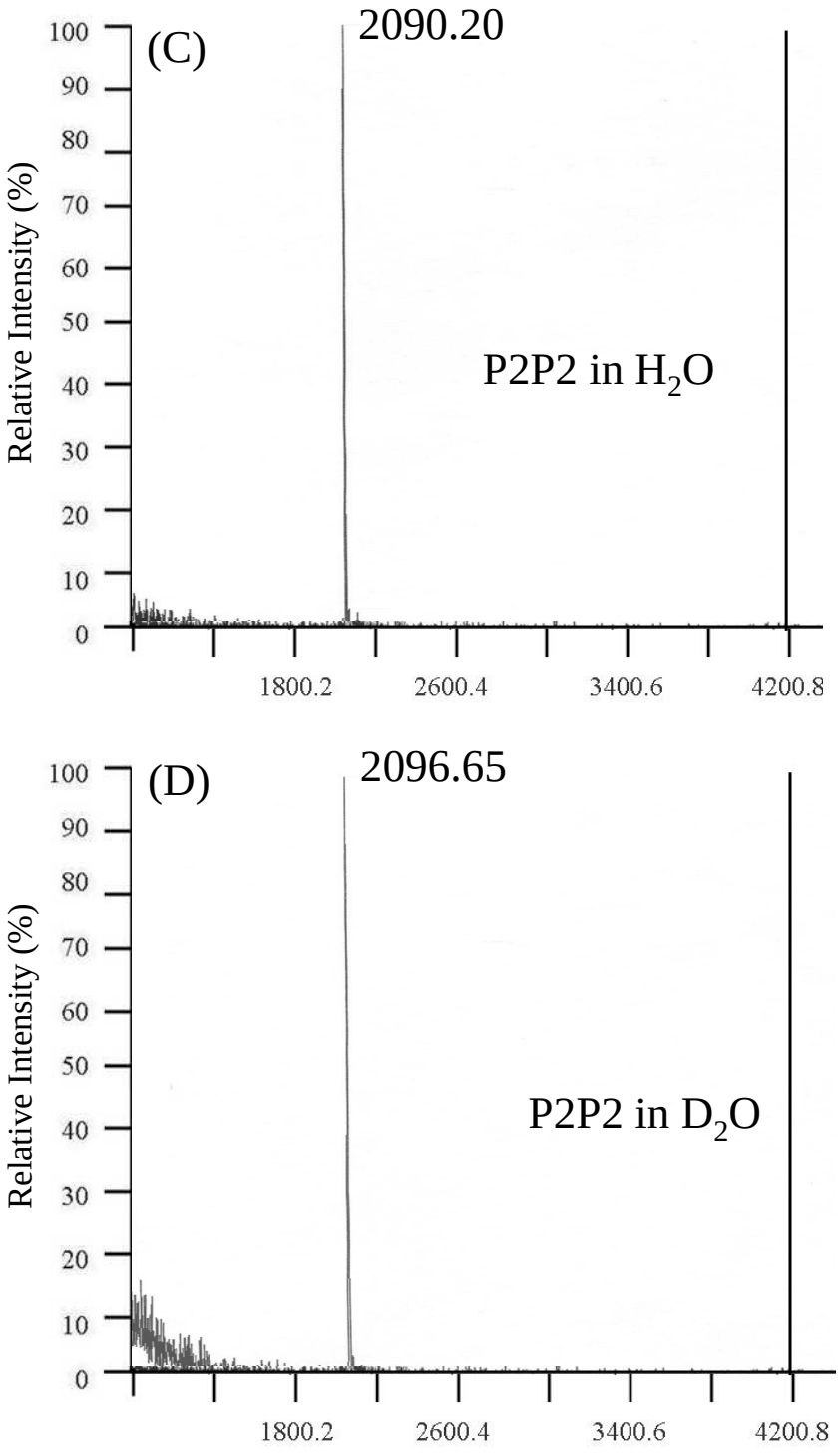

5.4. Discussion.

Hosszu *et al*. observed that a hyper-stable region involving helices 2 and 3 is retained around the disulfide bond in the C-terminal huPrP upon unfolding(*276*), suggesting its importance in initiating PrP folding. Presumably, the interactions stabilizing this structured core are essential to form a folding intermediate. Thus, a peptide pair was designed to assess the contribution of the disulfide bond and its local interactions to the formation of this folding nucleus. The data presented here indicate that interactions stabilized by the disulfide bond do not suffice to form this local structure.

Although the peptide corresponding to helix 3 (residue 202-230) exhibits high intrinsic α-helical propensity, the peptide corresponding to helix 2 (residue 175-197) shows a strong propensity to adopt random-coil (N-terminus) and β-sheet (C-terminus) structure, instead of the α-helical structure exhibited by its counterpart in a full-length folded PrP. Consequently, non-local interactions between helix 2 and the rest of the protein are required to stabilize its helical conformation. Since the disulfide bond brings residues distant in the primary structure into proximity and strengthens its local interactions, it may play a determining role in helical formation in this region (i.e. helices 2 and 3) (Figure 5.1), particularly for helix 2. Such stabilizing effect of the disulfide bond on PrP has been reported previously(*251, 272*). Nevertheless, the present data indicate that interactions from other part of the protein, besides those stabilized by the disulfide bond, are required for forming helices 2 and 3.

Even if association of P1 and P2 does not suffice to form helical structure, an increased secondary-structure content might be expected in any dimeric peptide pair, as compared to its monomeric components. However, I found that the covalent linkage of these model peptides (P1P1, P2P2, and P1P2) does not provoke secondary-structure formation, stable hydrogen bonding, and burial of solvent-accessible surface area.

Polymorphisms of ovine PrPs (ovPrPs) have been associated with differing susceptibility to classical scrapie, particularly at positions 136 (A/V), 154 (H/R), and 171 (Q/R). This genetic modulation has been shown to affect the structural stability of the folding intermediate in *Specific Aim Two* (see *Chapter Four*). Since these residues are distant from the disulfide bond, long-range interactions may contribute to the formation of this intermediate, if the folding nucleus is formed around the disulfide bond, as suggested by Hosszu *et al*.(*276*). This is in good agreement with the present data.

5.5. Future directions.

The present data show that the local structure around the disulfide bond in PrP does not suffice for the formation of the folding intermediate; in other words, interactions involving other parts of PrP are required for folding nucleus formation. To sort out the contribution of interactions to intermediate formation, cleavable GST-tagged constructs were engineered to produce P1 and P2 in *E. coli*. Based on these constructs, peptides of different lengths flanking the disulfide bond can be easily produced. These constructs also allow the studies on the synthesized peptides from SynPeP Corporation to be repeated and confirmed.

5.5.1. Preparation of GST-tagged peptides. PGEX-4T-1 (Amersham Biosciences) was digested with *Bam*HI and *Xho*I. Oligomers corresponding to the DNA sequences encoding P1 and P2 were designed and cloned into two digested PGEX-4T-1 vectors separately (Figure 5.6):

P1: 5'-GAT CCT ATA GCA ACC AGA ACA ACT TTG TGC ATG ATT GCG TGA ACA TTA CCG TGA AAC AAC ATT GAT AAC-3' and 5'- TCG AGT TAT CAA TGT TGT TTC ACG GTA ATG TTC ACG CAA TCA TGC ACA AAG TTG TTC TGG TTG CTA TAG -3'

P2: 5'- GAT CCA TGG AAC GCG TGG TGG AAC AGA TGT GCA TTA CCC AGT ATC AGC GCG AAT GAT AAC -3' and 5'- TCG AGT TAT CAT TCG CGC TGA TAC TGG GTA ATG CAC ATC TGT TCC ACC ACG CGT TCC ATG -3'

DNA sequencing was utilized to confirm the validity of these two constructs.

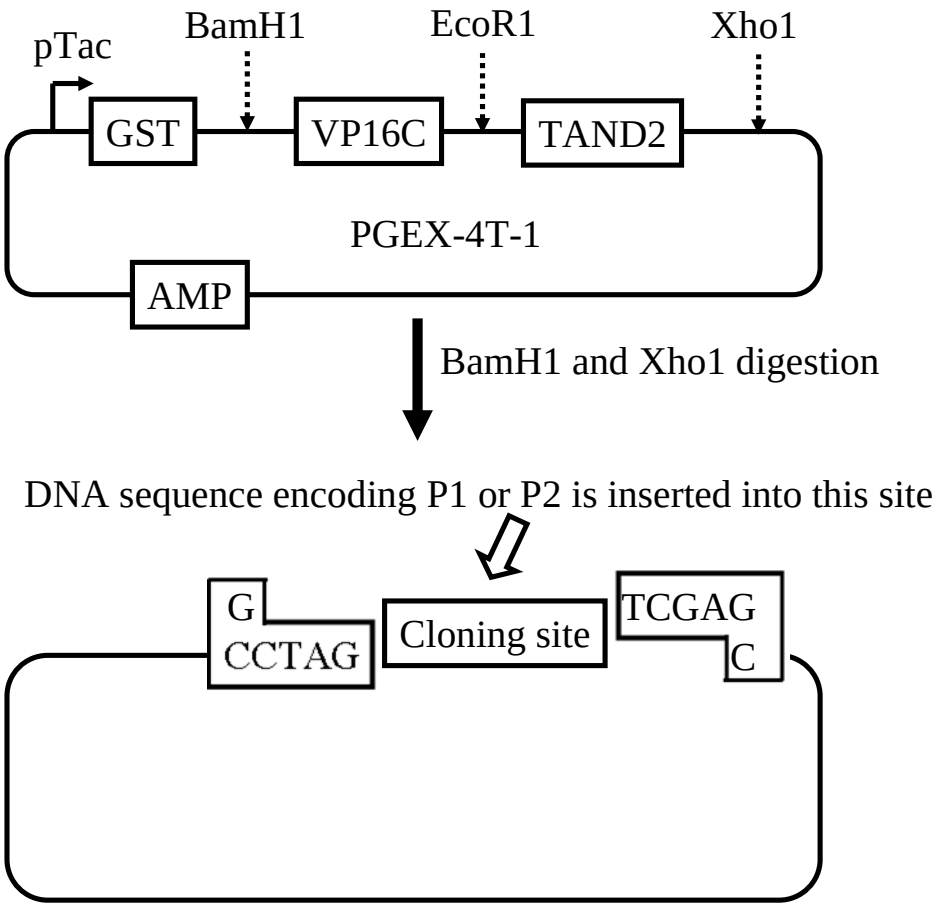

Figure 5.6. DNA encoding P1 and P2 were cloned into PGEX-4T-1.

These plasmids were transformed into competent *E. coli* BL21 (DE3) cells. To express GST-tagged peptides, *E. coli* cells containing the desired plasmid were grown in LB medium containing 100 µg/ml ampicillin with shaking at 250 rpm at 37 ^{o}C. Based on induction studies, once the optical density reaches 0.6 – 1.0, expression is induced by adding isopropyl β-D-1-thiogalactopyranoside (IPTG) to a final concentration of 1 mM. Purification was carried out using glutathione resin, followed by ion-exchange and gel-filtration chromatography. These two GST-tagged peptides have been identified with SDS-PAGE and Western blotting (Figure 5.7).

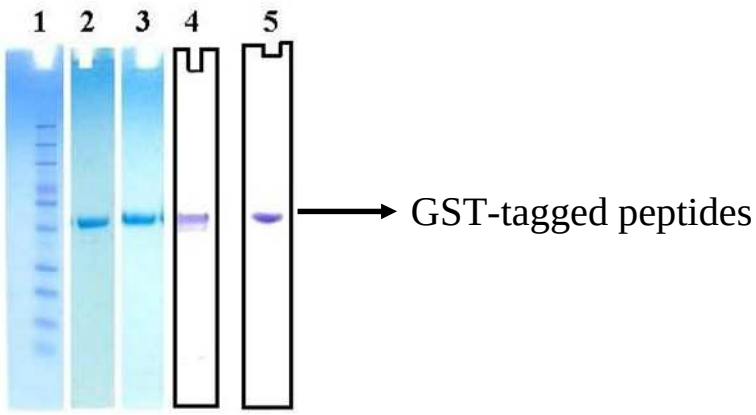

Figure 5.7. SDS-PAGE and Western blotting show the purified GST-P1 and GST-P2. Lane 1-3, SDS-PAGE (12%) analysis. Lane 4-5, Western blotting analysis using anti-GST as the primary antibody. Lanes 1: Invitrogen protein ladder. Lanes 2 and 4: GST-P1. Lanes 3 and 5: GST-P2.

5.5.2. Future work. Peptides flanking the disulfide bond with various lengths will be produced based on the engineered constructs described here. HDX and CD measurements will be carried out as described previously on disulfide-bridged peptide pairs and their monomeric components to assess whether the interactions within a peptide pair are able to form the folding nucleus.

Conclusions and Future Directions

I observed a native-like intermediate in ovPrP refolding and unfolding. This intermediate is denoted as $\boldsymbol{I_\alpha}$ because, being similar to the native species ***N***, its secondary structure is largely α-helical. I found that the ***population*** and ***structure*** of $\boldsymbol{I_\alpha}$ in the variants correlate with their differing propensities towards classical scrapie. Variants with higher classical scrapie propensity are characterized by higher populations and more stable tertiary structure in $\boldsymbol{I_\alpha}$. Thus, I argue that this partially unfolded, native-like intermediate $\boldsymbol{I_\alpha}$ is a plausible PrP^{Sc} precursor. Consistent with this model, an α-helix-rich species has been observed during the PrP^{C}-to-PrP^{Sc} conversion(*222-225*, *261*).

In agreement with the theoretical ***refolding model*** (*5, 255*), the present data suggest a model to explain PrP^{Sc} propagation in classical scrapie:

$$\textit{Conformational folding of } PrP^{C}\textit{: } N \leftrightarrow I_\alpha \leftrightarrow U$$

$$\textit{Assembly of } PrP^{Sc} \textit{ oligomers: } (PrP^{Sc})_n + I_\alpha \rightarrow (PrP^{Sc})_{n+1}$$

where polymorphisms determine disease susceptibilities by modulating the population and structure of $\boldsymbol{I_\alpha}$. In the absence of denaturant (i.e. under folding conditions), the relative population of $\boldsymbol{I_\alpha}$ in the susceptible variant (ALRQ) is about 10 times higher than that in the resistant variant (ALRR). The higher population of $\boldsymbol{I_\alpha}$ in the susceptible variants gives them more opportunities for the PrP^{C}-to-PrP^{Sc} conversion.

$\boldsymbol{I_\alpha}$ exhibits differing degree of surface exposure in the four variants: the ALRQ variant shows ~77% of surface-burial in its intermediate relative to its native state, in contrast with ~42% for the ALRR variant, indicating that the intermediate of the ALRQ variant is more folded and structurally closer to its native state, as compared to the ALRR variant. The correlation between the scrapie susceptibility of a variant and the structure of its intermediate suggests the conformation of $\boldsymbol{I_\alpha}$ is crucial to PrP misfolding. According to my model, a poorly populated and/or weakly structured intermediate has difficulty in folding onto a preexisting PrP^{Sc} seed. Therefore, variants with such intermediates are more resistant to scrapie. By contrast, this model predicts that a well-populated and/or mostly folded $\boldsymbol{I_\alpha}$ is more likely to convert to PrP^{Sc} and incorporate into a preexisting PrP^{Sc} oligomer; therefore, variants with such $\boldsymbol{I_\alpha}$ are more susceptible to scrapie.

If indeed PrP^{Sc} is formed by absorption of a native-like intermediate, such as $\boldsymbol{I_\alpha}$, onto an preexisting PrP^{Sc} seed, then it is biophysically more plausible that the formed PrP^{Sc} conformation should likewise have native-like structure. This picture seems to be consistent with the ***β-helical*** *and* ***spiral models***(48, 50) of the PrP^{Sc} conformation, where most of the helical structure is conserved during the PrP^{C}-to-PrP^{Sc} conversion. Such structural conservation is also in agreement with an antibody study, in which α-helices 2 and 3 in PrP^{C} remain largely conserved in PrP^{Sc} (*49*).

Since the residues (136, 154, and 171) involved in the classical scrapie are distant from each other in the primary structure, I conjectured that genetic modulation exerts its effects

on this intermediate through long-range interactions. Consistent with this idea, a peptide model indicated that long-range interactions within PrPs are required for intermediate formation.

Future directions.

Initiation of protein folding depends on the diffusion-driven contact formation between different regions of an unfolded polypeptide chain. This process sets an upper *speed limit* on a folding reaction, and is determined by the solvent conditions and the protein sequence(*148*). Since formation of an intermediate is the first step for ovPrP folding, and long-range interactions likely contribute to the differing stability of the I_α in these allelic variants, the formation of long-range interactions in the initial stage likely differs among these allelic variants. In particular, these allelic variants should exhibit differing rates of contact formation in the unfolded state.

To test this hypothesis, the rates of contact formation in the unfolded state can be measured using the tryptophan/cystine (Trp/Cys) triplet quenching method(*277*). In this method, Trp is excited to its triplet state by pulse laser, and its gradual quenching is monitored. Quenching occurs when the excited Trp encounters the disulfide bond (cystine) in a diffusion-limited process (FigureC1). By measuring the quenching rate, the dynamics of the unfolded protein can be characterized. The cystine has a much higher efficiency of quenching the Trp triplet than other elements of the protein; this, and the long lifetime of the Trp triplet excited state in the absence of quencher, allow the rate of Trp-Cys contact formation to be measured(*278-280*).

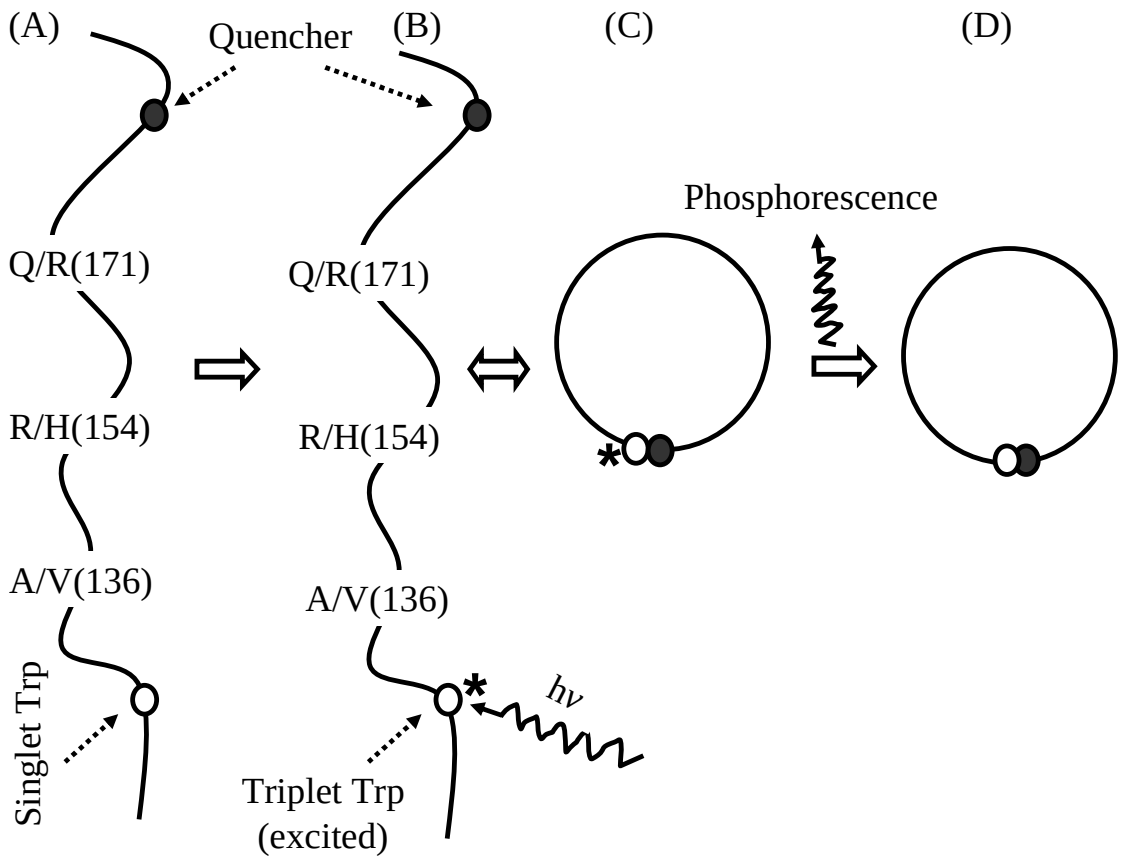

Figure C1. Schematic illustration for quenching reaction. (A) Trp is in the singlet ground state. (B) Trp is excited to its triplet state. (C) The excited Trp contacts the quencher. (D) Trp goes back to the singlet state from the triplet state and releases phosphorescence.

Preliminary data has been taken in the laboratory of Dr. Lisa Lapidus of the MSU Physics department. The loop length between the sole Trp and the sole cystine is 80 residues in the wild-type ovPrP (Figure C2). ['Loop length' is defined as the distance along the backbone (counted in residues) between Trp and the quencher.] The initial conditions were set to pH 5 at five different temperatures ranging from 0^{o}C to 40^{o}C. Two decay

phases with time constants of ~1 and ~15 μs were observed for wild-type ALRQ variant (Figure C3). Similar experiments will be carried out on the other three variants.

(A)

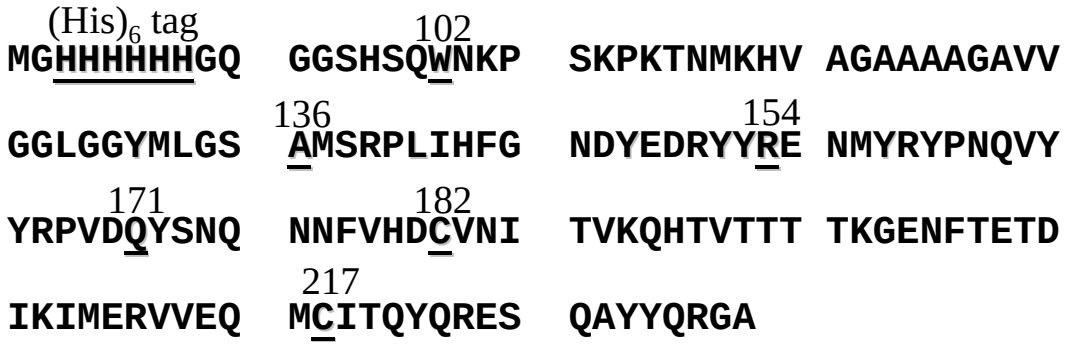

(B)

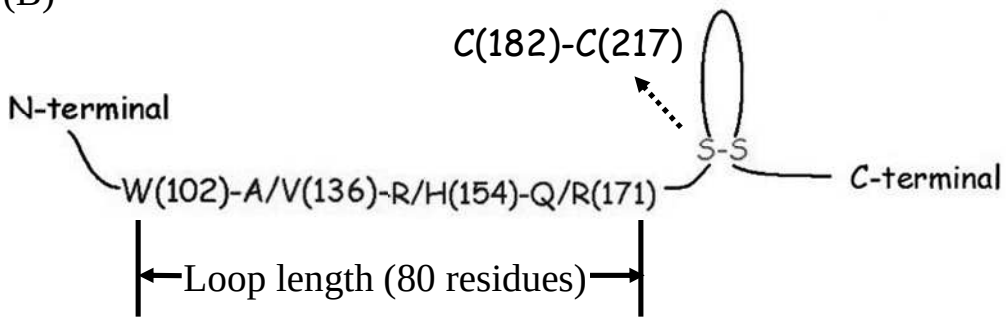

Figure C2. The positions of quenchers, Trp, and residues involved in sheep polymorphisms. (A) Primary structure of wild-type ALRQ variant. (B) Schematic representation showing the relative positions of Trp , the disulfide bond, and residues involved in sheep polymorphisms.

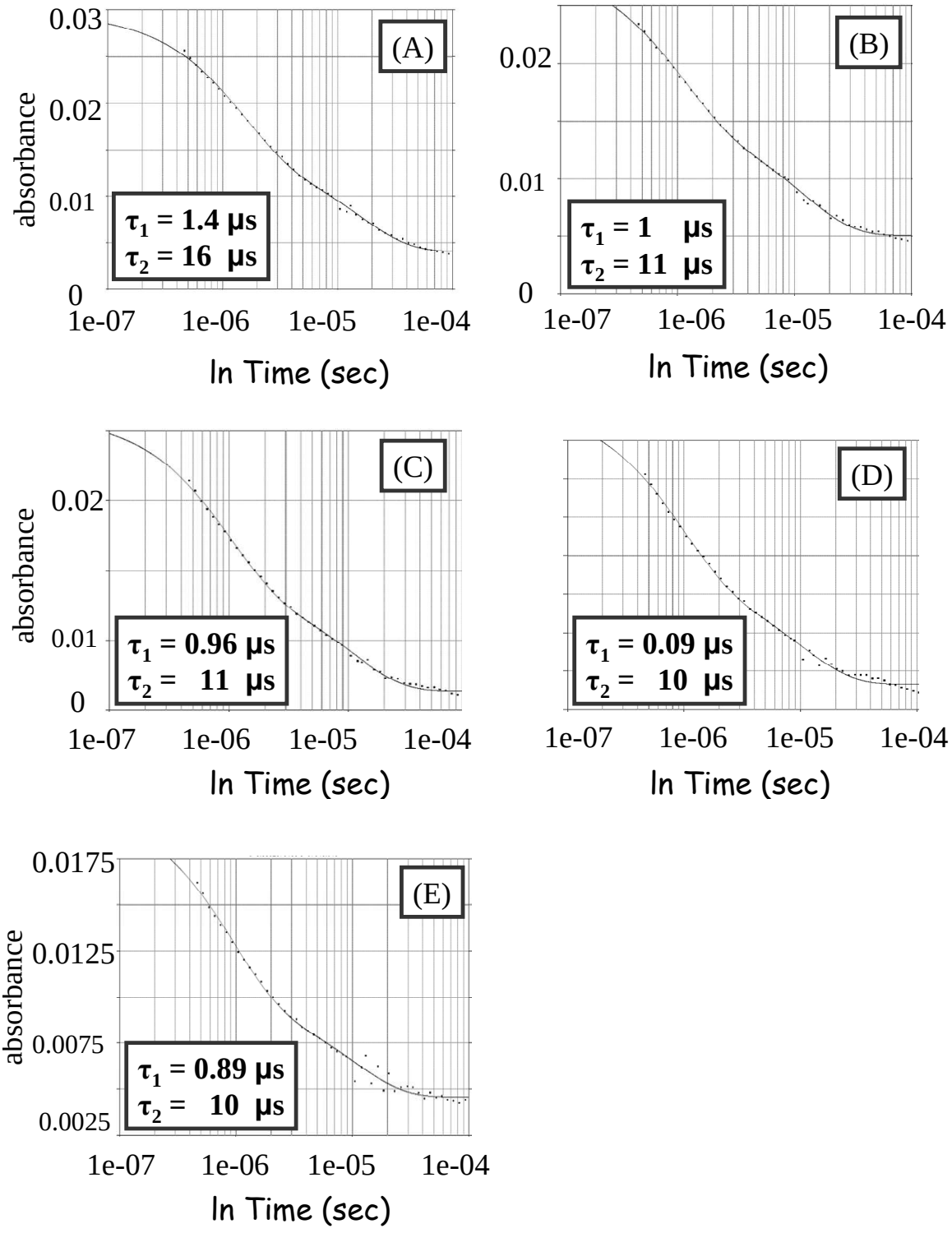

Figure C3. Quenching reactions of the Trp/Cys pair. Experiments were carried out in 50 mM sodium acetate (pH 5) at (A) 0°C, (B) 10°C, (C) 20°C, (D) 30°C, and (E) 40°C. Time constants for triplet decay are indicated in the plots.

If more than one quencher is involved in the observed quenching reactions, interpretation of the data could become complicated. Therefore, additional control experiments were carried out to determine whether another quencher, such as the $(His)_6$ tag upstream of Trp (Figure C2), contributes to the observed quenching reactions. Although the quenching rate of a free His is about 10 times slower than that of a free cystine at pH 5, the $(His)_6$ tag may compete with cystine in the quenching reaction due to the shorter loop length of the Trp/$(His)_6$ pair (9 residues) and the higher quencher concentration, as compared to the Trp/Cys pair. Since the quenching rate of a free His becomes about 100 times slower in its deprotonated form(*280*), a pH value higher than its pK_a (~6) should be able to slow down the quenching reaction of Trp/$(His)_6$ significantly. Thus, experiments mentioned above were repeated at pH 7, 8, and 9. A pH dependence was not observed in the range of pH 5 to 9, indicating that quenching reactions of Trp/$(His)_6$ are negligible. More control experiments should be carried out on the disulfide-disrupted mutant with *Cys* → *Ala* mutations to confirm that the observed quenching rate derives only from Trp/Cys contact formation.

APPENDIX

GLOSSARY

Folding nucleus: *Folding nucleus* is defined here as a specific subset of native interactions required for stabilizing an intermediate state.

Kinetic Species: Kinetic states occurring at a particular stage of protein folding or unfolding.

Misfolding: *Misfolding* is defined here as structural conversion from PrP^{C} to PrP^{Sc}.

Pathway: A *pathway* is denoted to the kinetically most accessible route for folding throughout this dissertation.

State: A *state* is defined as a conformational ensemble at a specified stage of protein folding or unfolding.

Transition state: The highest free-energy conformational ensemble along the reaction coordinate.

REFERENCES

1. Weissmann, C. (2004) The state of the prion, *Nat Rev Microbiol 2*, 861-871.

2. Prusiner, S. B. (2004) *Prion biology and diseases*, 2nd ed., Cold Spring Harbor Laboratory Press, Cold Spring Harbor, N.Y.

3. Aguzzi, A., and Glatzel, M. (2006) Prion infections, blood and transfusions, *Nat Clin Pract Neurol 2*, 321-329.

4. Alper, T., Cramp, W. A., Haig, D. A., and Clarke, M. C. (1967) Does the agent of scrapie replicate without nucleic acid?, *Nature 214*, 764-766.

5. Griffith, J. S. (1967) Self-replication and scrapie, *Nature 215*, 1043-1044.

6. Prusiner, S. B. (1982) Novel proteinaceous infectious particles cause scrapie, *Science 216*, 136-144.

7. Oesch, B., Westaway, D., Walchli, M., McKinley, M. P., Kent, S. B., Aebersold, R., Barry, R. A., Tempst, P., Teplow, D. B., Hood, L. E., and et al. (1985) A cellular gene encodes scrapie PrP 27-30 protein, *Cell 40*, 735-746.

8. Basler, K., Oesch, B., Scott, M., Westaway, D., Walchli, M., Groth, D. F., McKinley, M. P., Prusiner, S. B., and Weissmann, C. (1986) Scrapie and cellular PrP isoforms are encoded by the same chromosomal gene, *Cell 46*, 417-428.

9. Hope, J., Morton, L. J., Farquhar, C. F., Multhaup, G., Beyreuther, K., and Kimberlin, R. H. (1986) The major polypeptide of scrapie-associated fibrils (SAF) has the same size, charge distribution and N-terminal protein sequence as predicted for the normal brain protein (PrP), *EMBO J 5*, 2591-2597.

10. Stahl, N., Baldwin, M. A., Teplow, D. B., Hood, L., Gibson, B. W., Burlingame, A. L., and Prusiner, S. B. (1993) Structural studies of the scrapie prion protein using mass spectrometry and amino acid sequencing, *Biochemistry 32*, 1991-2002.

11. Gill, A. C., Ritchie, M. A., Hunt, L. G., Steane, S. E., Davies, K. G., Bocking, S. P., Rhie, A. G., Bennett, A. D., and Hope, J. (2000) Post-translational hydroxylation at the N-terminus of the prion protein reveals presence of PPII structure in vivo, *EMBO J 19*, 5324-5331.

12. Jang, B., Jin, J. K., Jeon, Y. C., Cho, H. J., Ishigami, A., Choi, K. C., Carp, R. I., Maruyama, N., Kim, Y. S., and Choi, E. K. (2010) Involvement of peptidylarginine deiminase-mediated post-translational citrullination in pathogenesis of sporadic Creutzfeldt-Jakob disease, *Acta Neuropathol 119*, 199-210.

13. Caughey, B. W., Dong, A., Bhat, K. S., Ernst, D., Hayes, S. F., and Caughey, W. S. (1991) Secondary structure analysis of the scrapie-associated protein PrP 27-30 in water by infrared spectroscopy, *Biochemistry 30*, 7672-7680.

14. Gasset, M., Baldwin, M. A., Fletterick, R. J., and Prusiner, S. B. (1993) Perturbation of the secondary structure of the scrapie prion protein under conditions that alter infectivity, *Proc Natl Acad Sci U S A 90*, 1-5.

15. Pan, K. M., Baldwin, M., Nguyen, J., Gasset, M., Serban, A., Groth, D., Mehlhorn, I., Huang, Z., Fletterick, R. J., Cohen, F. E., and et al. (1993) Conversion of alpha-helices into beta-sheets features in the formation of the scrapie prion proteins, *Proc Natl Acad Sci U S A 90*, 10962-10966.

16. Gabizon, R., McKinley, M. P., Groth, D., and Prusiner, S. B. (1988) Immunoaffinity purification and neutralization of scrapie prion infectivity, *Proc Natl Acad Sci U S A 85*, 6617-6621.

17. Enari, M., Flechsig, E., and Weissmann, C. (2001) Scrapie prion protein accumulation by scrapie-infected neuroblastoma cells abrogated by exposure to a prion protein antibody, *Proc Natl Acad Sci U S A 98*, 9295-9299.

18. Peretz, D., Williamson, R. A., Kaneko, K., Vergara, J., Leclerc, E., Schmitt-Ulms, G., Mehlhorn, I. R., Legname, G., Wormald, M. R., Rudd, P. M., Dwek, R. A., Burton, D. R., and Prusiner, S. B. (2001) Antibodies inhibit prion propagation and clear cell cultures of prion infectivity, *Nature 412*, 739-743.

19. Hsiao, K. K., Groth, D., Scott, M., Yang, S. L., Serban, H., Rapp, D., Foster, D., Torchia, M., Dearmond, S. J., and Prusiner, S. B. (1994) Serial transmission in rodents of neurodegeneration from transgenic mice expressing mutant prion protein, *Proc Natl Acad Sci U S A 91*, 9126-9130.

20. Bueler, H., Aguzzi, A., Sailer, A., Greiner, R. A., Autenried, P., Aguet, M., and Weissmann, C. (1993) Mice devoid of PrP are resistant to scrapie, *Cell 73*, 1339-1347.

21. Race, R. E., Fadness, L. H., and Chesebro, B. (1987) Characterization of scrapie infection in mouse neuroblastoma cells, *J Gen Virol 68 (Pt 5)*, 1391-1399.

22. Rubenstein, R., Merz, P. A., Kascsak, R. J., Carp, R. I., Scalici, C. L., Fama, C. L., and Wisniewski, H. M. (1987) Detection of scrapie-associated fibrils (SAF) and SAF proteins from scrapie-affected sheep, *J Infect Dis 156*, 36-42.

23. Ryou, C., and Mays, C. E. (2008) Prion propagation in vitro: are we there yet?, *Int J Med Sci 5*, 347-353.

24. Kocisko, D. A., Come, J. H., Priola, S. A., Chesebro, B., Raymond, G. J., Lansbury, P. T., and Caughey, B. (1994) Cell-free formation of protease-resistant prion protein, *Nature 370*, 471-474.

25. Saborio, G. P., Permanne, B., and Soto, C. (2001) Sensitive detection of pathological prion protein by cyclic amplification of protein misfolding, *Nature 411*, 810-813.

26. Deleault, N. R., Harris, B. T., Rees, J. R., and Supattapone, S. (2007) Formation of native prions from minimal components in vitro, *Proc Natl Acad Sci U S A 104*, 9741-9746.

27. Wang, F., Wang, X., Yuan, C. G., and Ma, J. (2010) Generating a prion with bacterially expressed recombinant prion protein, *Science 327*, 1132-1135.

28. Kim, J. I., Cali, I., Surewicz, K., Kong, Q., Raymond, G. J., Atarashi, R., Race, B., Qing, L., Gambetti, P., Caughey, B., and Surewicz, W. K. (2010) Mammalian prions generated from bacterially expressed prion protein in the absence of any mammalian cofactors, *J Biol Chem*.

29. Caughey, B., and Lansbury, P. T. (2003) Protofibrils, pores, fibrils, and neurodegeneration: separating the responsible protein aggregates from the innocent bystanders, *Annu Rev Neurosci 26*, 267-298.

30. Cronier, S., Laude, H., and Peyrin, J. M. (2004) Prions can infect primary cultured neurons and astrocytes and promote neuronal cell death, *Proc Natl Acad Sci U S A 101*, 12271-12276.

31. Kristiansen, M., Messenger, M. J., Klohn, P. C., Brandner, S., Wadsworth, J. D., Collinge, J., and Tabrizi, S. J. (2005) Disease-related prion protein forms aggresomes in neuronal cells leading to caspase activation and apoptosis, *J Biol Chem 280*, 38851-38861.

32. Muller, W. E., Ushijima, H., Schroder, H. C., Forrest, J. M., Schatton, W. F., Rytik, P. G., and Heffner-Lauc, M. (1993) Cytoprotective effect of NMDA receptor antagonists on prion protein (PrionSc)-induced toxicity in rat cortical cell cultures, *Eur J Pharmacol 246*, 261-267.

33. Sailer, A., Bueler, H., Fischer, M., Aguzzi, A., and Weissmann, C. (1994) No propagation of prions in mice devoid of PrP, *Cell 77*, 967-968.

34. Brandner, S., Isenmann, S., Raeber, A., Fischer, M., Sailer, A., Kobayashi, Y., Marino, S., Weissmann, C., and Aguzzi, A. (1996) Normal host prion protein necessary for scrapie-induced neurotoxicity, *Nature 379*, 339-343.

35. Collinge, J., Palmer, M. S., Sidle, K. C., Gowland, I., Medori, R., Ironside, J., and Lantos, P. (1995) Transmission of fatal familial insomnia to laboratory animals, *Lancet 346*, 569-570.

36. Hsiao, K. K., Scott, M., Foster, D., Groth, D. F., DeArmond, S. J., and Prusiner, S. B. (1990) Spontaneous neurodegeneration in transgenic mice with mutant prion protein, *Science 250*, 1587-1590.

37. Lasmezas, C. I., Deslys, J. P., Robain, O., Jaegly, A., Beringue, V., Peyrin, J. M., Fournier, J. G., Hauw, J. J., Rossier, J., and Dormont, D. (1997) Transmission of the BSE agent to mice in the absence of detectable abnormal prion protein, *Science 275*, 402-405.

38. Medori, R., Montagna, P., Tritschler, H. J., LeBlanc, A., Cortelli, P., Tinuper, P., Lugaresi, E., and Gambetti, P. (1992) Fatal familial insomnia: a second kindred with mutation of prion protein gene at codon 178, *Neurology 42*, 669-670.

39. Hill, A. F., and Collinge, J. (2003) Subclinical prion infection, *Trends Microbiol 11*, 578-584.

40. Hill, A. F., and Collinge, J. (2003) Subclinical prion infection in humans and animals, *Br Med Bull 66*, 161-170.

41. Prusiner, S. B., McKinley, M. P., Bowman, K. A., Bolton, D. C., Bendheim, P. E., Groth, D. F., and Glenner, G. G. (1983) Scrapie prions aggregate to form amyloid-like birefringent rods, *Cell 35*, 349-358.

42. Haire, L. F., Whyte, S. M., Vasisht, N., Gill, A. C., Verma, C., Dodson, E. J., Dodson, G. G., and Bayley, P. M. (2004) The crystal structure of the globular domain of sheep prion protein, *J Mol Biol 336*, 1175-1183.

43. Knaus, K. J., Morillas, M., Swietnicki, W., Malone, M., Surewicz, W. K., and Yee, V. C. (2001) Crystal structure of the human prion protein reveals a mechanism for oligomerization, *Nat Struct Biol 8*, 770-774.

44. Riek, R., Hornemann, S., Wider, G., Billeter, M., Glockshuber, R., and Wuthrich, K. (1996) NMR structure of the mouse prion protein domain PrP(121-321), *Nature 382*, 180-182.

45. Riek, R., Hornemann, S., Wider, G., Glockshuber, R., and Wuthrich, K. (1997) NMR characterization of the full-length recombinant murine prion protein, mPrP(23-231), *FEBS Lett 413*, 282-288.

46. Zhang, H., Stockel, J., Mehlhorn, I., Groth, D., Baldwin, M. A., Prusiner, S. B., James, T. L., and Cohen, F. E. (1997) Physical studies of conformational plasticity in a recombinant prion protein, *Biochemistry 36*, 3543-3553.

47. Koradi, R., Billeter, M., and Wuthrich, K. (1996) MOLMOL: a program for display and analysis of macromolecular structures, *J Mol Graph 14*, 51-55, 29-32.

48. Govaerts, C., Wille, H., Prusiner, S. B., and Cohen, F. E. (2004) Evidence for assembly of prions with left-handed beta-helices into trimers, *Proc Natl Acad Sci U S A 101*, 8342-8347.

49. Eghiaian, F., Grosclaude, J., Lesceu, S., Debey, P., Doublet, B., Treguer, E., Rezaei, H., and Knossow, M. (2004) Insight into the PrPC-->PrPSc conversion from the structures of antibody-bound ovine prion scrapie-susceptibility variants, *Proc Natl Acad Sci U S A 101*, 10254-10259.

50. DeMarco, M. L., and Daggett, V. (2004) From conversion to aggregation: protofibril formation of the prion protein, *Proc Natl Acad Sci U S A 101*, 2293-2298.

51. Lu, X., Wintrode, P. L., and Surewicz, W. K. (2007) Beta-sheet core of human prion protein amyloid fibrils as determined by hydrogen/deuterium exchange, *Proc Natl Acad Sci U S A 104*, 1510-1515.

52. Aguzzi, A., and Calella, A. M. (2009) Prions: protein aggregation and infectious diseases, *Physiol Rev 89*, 1105-1152.

53. Peretz, D., Scott, M. R., Groth, D., Williamson, R. A., Burton, D. R., Cohen, F. E., and Prusiner, S. B. (2001) Strain-specified relative conformational stability of the scrapie prion protein, *Protein Sci 10*, 854-863.

54. Collinge, J., Sidle, K. C., Meads, J., Ironside, J., and Hill, A. F. (1996) Molecular analysis of prion strain variation and the aetiology of 'new variant' CJD, *Nature 383*, 685-690.

55. Kuczius, T., and Groschup, M. H. (1999) Differences in proteinase K resistance and neuronal deposition of abnormal prion proteins characterize bovine spongiform encephalopathy (BSE) and scrapie strains, *Mol Med 5*, 406-418.

56. Bessen, R. A., and Marsh, R. F. (1992) Biochemical and physical properties of the prion protein from two strains of the transmissible mink encephalopathy agent, *J Virol 66*, 2096-2101.

57. Telling, G. C., Parchi, P., DeArmond, S. J., Cortelli, P., Montagna, P., Gabizon, R., Mastrianni, J., Lugaresi, E., Gambetti, P., and Prusiner, S. B. (1996) Evidence for the conformation of the pathologic isoform of the prion protein enciphering and propagating prion diversity, *Science 274*, 2079-2082.

58. Beringue, V., Vilotte, J. L., and Laude, H. (2008) Prion agent diversity and species barrier, *Vet Res 39*, 47.

59. Pattison, I. H. (1965) Scrapie in the welsh mountain breed of sheep and its experimental transmission to goats, *Vet Rec 77*, 1388-1390.

60. Collinge, J. (2001) Prion diseases of humans and animals: their causes and molecular basis, *Annu Rev Neurosci 24*, 519-550.

61. Collinge, J., and Clarke, A. R. (2007) A general model of prion strains and their pathogenicity, *Science 318*, 930-936.

62. Beringue, V., Mallinson, G., Kaisar, M., Tayebi, M., Sattar, Z., Jackson, G., Anstee, D., Collinge, J., and Hawke, S. (2003) Regional heterogeneity of cellular prion protein isoforms in the mouse brain, *Brain 126*, 2065-2073.

63. Li, J., Browning, S., Mahal, S. P., Oelschlegel, A. M., and Weissmann, C. (2010) Darwinian evolution of prions in cell culture, *Science 327*, 869-872.

64. Harris, D. A. (2003) Trafficking, turnover and membrane topology of PrP, *Br Med Bull 66*, 71-85.

65. Linden, R., Martins, V. R., Prado, M. A., Cammarota, M., Izquierdo, I., and Brentani, R. R. (2008) Physiology of the prion protein, *Physiol Rev 88*, 673-728.

66. Shyng, S. L., Huber, M. T., and Harris, D. A. (1993) A prion protein cycles between the cell surface and an endocytic compartment in cultured neuroblastoma cells, *J Biol Chem 268*, 15922-15928.

67. Horiuchi, M., Yamazaki, N., Ikeda, T., Ishiguro, N., and Shinagawa, M. (1995) A cellular form of prion protein (PrPC) exists in many non-neuronal tissues of sheep, *J Gen Virol 76 (Pt 10)*, 2583-2587.

68. Fournier, J. G., Escaig-Haye, F., Billette de Villemeur, T., Robain, O., Lasmezas, C. I., Deslys, J. P., Dormont, D., and Brown, P. (1998) Distribution and submicroscopic immunogold localization of cellular prion protein (PrPc) in extracerebral tissues, *Cell Tissue Res 292*, 77-84.

69. Fournier, J. G., Escaig-Haye, F., and Grigoriev, V. (2000) Ultrastructural localization of prion proteins: physiological and pathological implications, *Microsc Res Tech 50*, 76-88.

70. Herms, J., Tings, T., Gall, S., Madlung, A., Giese, A., Siebert, H., Schurmann, P., Windl, O., Brose, N., and Kretzschmar, H. (1999) Evidence of presynaptic location and function of the prion protein, *J Neurosci 19*, 8866-8875.

71. Mironov, A., Jr., Latawiec, D., Wille, H., Bouzamondo-Bernstein, E., Legname, G., Williamson, R. A., Burton, D., DeArmond, S. J., Prusiner, S. B., and Peters, P. J. (2003) Cytosolic prion protein in neurons, *J Neurosci 23*, 7183-7193.

72. Laine, J., Marc, M. E., Sy, M. S., and Axelrad, H. (2001) Cellular and subcellular morphological localization of normal prion protein in rodent cerebellum, *Eur J Neurosci 14*, 47-56.

73. Collinge, J., Whittington, M. A., Sidle, K. C., Smith, C. J., Palmer, M. S., Clarke, A. R., and Jefferys, J. G. (1994) Prion protein is necessary for normal synaptic function, *Nature 370*, 295-297.

74. Nishida, N., Tremblay, P., Sugimoto, T., Shigematsu, K., Shirabe, S., Petromilli, C., Erpel, S. P., Nakaoke, R., Atarashi, R., Houtani, T., Torchia, M., Sakaguchi, S., DeArmond, S. J., Prusiner, S. B., and Katamine, S. (1999) A mouse prion protein transgene rescues mice deficient for the prion protein gene from purkinje cell degeneration and demyelination, *Lab Invest 79*, 689-697.

75. Tobler, I., Gaus, S. E., Deboer, T., Achermann, P., Fischer, M., Rulicke, T., Moser, M., Oesch, B., McBride, P. A., and Manson, J. C. (1996) Altered circadian activity rhythms and sleep in mice devoid of prion protein, *Nature 380*, 639-642.

76. Roucou, X., Gains, M., and LeBlanc, A. C. (2004) Neuroprotective functions of prion protein, *J Neurosci Res 75*, 153-161.

77. Rachidi, W., Mange, A., Senator, A., Guiraud, P., Riondel, J., Benboubetra, M., Favier, A., and Lehmann, S. (2003) Prion infection impairs copper binding of cultured cells, *J Biol Chem 278*, 14595-14598.

78. Rachidi, W., Vilette, D., Guiraud, P., Arlotto, M., Riondel, J., Laude, H., Lehmann, S., and Favier, A. (2003) Expression of prion protein increases cellular copper binding and antioxidant enzyme activities but not copper delivery, *J Biol Chem 278*, 9064-9072.

79. Brown, D. R. (2001) Copper and prion disease, *Brain Res Bull 55*, 165-173.

80. Vassallo, N., and Herms, J. (2003) Cellular prion protein function in copper homeostasis and redox signalling at the synapse, *J Neurochem 86*, 538-544.

81. Kretzschmar, H. A., Tings, T., Madlung, A., Giese, A., and Herms, J. (2000) Function of PrP(C) as a copper-binding protein at the synapse, *Arch Virol Suppl*, 239-249.

82. Colling, S. B., Collinge, J., and Jefferys, J. G. (1996) Hippocampal slices from prion protein null mice: disrupted Ca(2+)-activated K+ currents, *Neurosci Lett 209*, 49-52.

83. Steele, A. D., Emsley, J. G., Ozdinler, P. H., Lindquist, S., and Macklis, J. D. (2006) Prion protein (PrPc) positively regulates neural precursor proliferation during developmental and adult mammalian neurogenesis, *Proc Natl Acad Sci U S A 103*, 3416-3421.

84. Zhang, C. C., Steele, A. D., Lindquist, S., and Lodish, H. F. (2006) Prion protein is expressed on long-term repopulating hematopoietic stem cells and is important for their self-renewal, *Proc Natl Acad Sci U S A 103*, 2184-2189.

85. Benestad, S. L., Sarradin, P., Thu, B., Schonheit, J., Tranulis, M. A., and Bratberg, B. (2003) Cases of scrapie with unusual features in Norway and designation of a new type, Nor98, *Vet Rec 153*, 202-208.

86. Benestad, S. L., Arsac, J. N., Goldmann, W., and Noremark, M. (2008) Atypical/Nor98 scrapie: properties of the agent, genetics, and epidemiology, *Vet Res 39*, 19.

87. Kimberlin, R. H. (1990) Transmissible encephalopathies in animals, *Can J Vet Res 54*, 30-37.

88. Goldmann, W. (2008) PrP genetics in ruminant transmissible spongiform encephalopathies, *Vet Res 39*, 30.

89. Luhken, G., Buschmann, A., Brandt, H., Eiden, M., Groschup, M. H., and Erhardt, G. (2007) Epidemiological and genetical differences between classical and atypical scrapie cases, *Vet Res 38*, 65-80.

90. Onnasch, H., Gunn, H. M., Bradshaw, B. J., Benestad, S. L., and Bassett, H. F. (2004) Two Irish cases of scrapie resembling Nor98, *Vet Rec 155*, 636-637.

91. Buschmann, A., Biacabe, A. G., Ziegler, U., Bencsik, A., Madec, J. Y., Erhardt, G., Luhken, G., Baron, T., and Groschup, M. H. (2004) Atypical scrapie cases in Germany and France are identified by discrepant reaction patterns in BSE rapid tests, *J Virol Methods 117*, 27-36.

92. Vidal, E., Tortosa, R., Costa, C., Benavides, J., Francino, O., Sanchez-Robert, E., Perez, V., and Pumarola, M. (2008) Lack of PrP(sc) immunostaining in intracranial ectopic lymphoid follicles in a sheep with concomitant non-suppurative encephalitis and Nor98-like atypical scrapie: a case report, *Vet J 177*, 283-288.

93. Bartz, J. C., Dejoia, C., Tucker, T., Kincaid, A. E., and Bessen, R. A. (2005) Extraneural prion neuroinvasion without lymphoreticular system infection, *J Virol 79*, 11858-11863.

94. Belt, P. B., Muileman, I. H., Schreuder, B. E., Bos-de Ruijter, J., Gielkens, A. L., and Smits, M. A. (1995) Identification of five allelic variants of the sheep PrP gene and their association with natural scrapie, *J Gen Virol 76 (Pt 3)*, 509-517.

95. Clouscard, C., Beaudry, P., Elsen, J. M., Milan, D., Dussaucy, M., Bounneau, C., Schelcher, F., Chatelain, J., Launay, J. M., and Laplanche, J. L. (1995) Different allelic effects of the codons 136 and 171 of the prion protein gene in sheep with natural scrapie, *J Gen Virol 76 (Pt 8)*, 2097-2101.

96. Tranulis, M. A., Osland, A., Bratberg, B., and Ulvund, M. J. (1999) Prion protein gene polymorphisms in sheep with natural scrapie and healthy controls in Norway, *J Gen Virol 80 (Pt 4)*, 1073-1077.

97. Goldmann, W., Hunter, N., Smith, G., Foster, J., and Hope, J. (1994) PrP genotype and agent effects in scrapie: change in allelic interaction with different isolates of agent in sheep, a natural host of scrapie, *J Gen Virol 75 (Pt 5)*, 989-995.

98. Hope, J., Wood, S. C., Birkett, C. R., Chong, A., Bruce, M. E., Cairns, D., Goldmann, W., Hunter, N., and Bostock, C. J. (1999) Molecular analysis of ovine prion protein identifies similarities between BSE and an experimental isolate of natural scrapie, CH1641, *J Gen Virol 80 (Pt 1)*, 1-4.

99. Foster, J. D., Parnham, D. W., Hunter, N., and Bruce, M. (2001) Distribution of the prion protein in sheep terminally affected with BSE following experimental oral transmission, *J Gen Virol 82*, 2319-2326.

100. Moum, T., Olsaker, I., Hopp, P., Moldal, T., Valheim, M., and Benestad, S. L. (2005) Polymorphisms at codons 141 and 154 in the ovine prion protein gene are associated with scrapie Nor98 cases, *J Gen Virol 86*, 231-235.

101. Saunders, G. C., Cawthraw, S., Mountjoy, S. J., Hope, J., and Windl, O. (2006) PrP genotypes of atypical scrapie cases in Great Britain, *J Gen Virol 87*, 3141-3149.

102. Masters, C. L., Gajdusek, D. C., and Gibbs, C. J., Jr. (1981) The familial occurrence of Creutzfeldt-Jakob disease and Alzheimer's disease, *Brain 104*, 535-558.

103. Beck, J. A., Mead, S., Campbell, T. A., Dickinson, A., Wientjens, D. P., Croes, E. A., Van Duijn, C. M., and Collinge, J. (2001) Two-octapeptide repeat deletion of prion protein associated with rapidly progressive dementia, *Neurology 57*, 354-356.

104. Mead, S., Poulter, M., Beck, J., Webb, T. E., Campbell, T. A., Linehan, J. M., Desbruslais, M., Joiner, S., Wadsworth, J. D., King, A., Lantos, P., and Collinge,

J. (2006) Inherited prion disease with six octapeptide repeat insertional mutation--molecular analysis of phenotypic heterogeneity, *Brain 129*, 2297-2317.

105. Aguzzi, A., Baumann, F., and Bremer, J. (2008) The prion's elusive reason for being, *Annu Rev Neurosci 31*, 439-477.

106. Mead, S. (2006) Prion disease genetics, *Eur J Hum Genet 14*, 273-281.

107. Jansen, C., Parchi, P., Capellari, S., Vermeij, A. J., Corrado, P., Baas, F., Strammiello, R., van Gool, W. A., van Swieten, J. C., and Rozemuller, A. J. (2010) Prion protein amyloidosis with divergent phenotype associated with two novel nonsense mutations in PRNP, *Acta Neuropathol 119*, 189-197.

108. Hill, A. F., Joiner, S., Wadsworth, J. D., Sidle, K. C., Bell, J. E., Budka, H., Ironside, J. W., and Collinge, J. (2003) Molecular classification of sporadic Creutzfeldt-Jakob disease, *Brain 126*, 1333-1346.

109. Palmer, M. S., Dryden, A. J., Hughes, J. T., and Collinge, J. (1991) Homozygous prion protein genotype predisposes to sporadic Creutzfeldt-Jakob disease, *Nature 352*, 340-342.

110. Dlouhy, S. R., Hsiao, K., Farlow, M. R., Foroud, T., Conneally, P. M., Johnson, P., Prusiner, S. B., Hodes, M. E., and Ghetti, B. (1992) Linkage of the Indiana kindred of Gerstmann-Straussler-Scheinker disease to the prion protein gene, *Nat Genet 1*, 64-67.

111. Goldfarb, L. G., Petersen, R. B., Tabaton, M., Brown, P., LeBlanc, A. C., Montagna, P., Cortelli, P., Julien, J., Vital, C., Pendelbury, W. W., and et al. (1992) Fatal familial insomnia and familial Creutzfeldt-Jakob disease: disease phenotype determined by a DNA polymorphism, *Science 258*, 806-808.

112. Goldfarb, L. G., Haltia, M., Brown, P., Nieto, A., Kovanen, J., McCombie, W. R., Trapp, S., and Gajdusek, D. C. (1991) New mutation in scrapie amyloid precursor gene (at codon 178) in Finnish Creutzfeldt-Jakob kindred, *Lancet 337*, 425.

113. Zarranz, J. J., Digon, A., Atares, B., Rodriguez-Martinez, A. B., Arce, A., Carrera, N., Fernandez-Manchola, I., Fernandez-Martinez, M., Fernandez-Maiztegui, C., Forcadas, I., Galdos, L., Gomez-Esteban, J. C., Ibanez, A., Lezcano, E., Lopez de Munain, A., Marti-Masso, J. F., Mendibe, M. M., Urtasun, M., Uterga, J. M., Saracibar, N., Velasco, F., and de Pancorbo, M. M. (2005) Phenotypic variability in familial prion diseases due to the D178N mutation, *J Neurol Neurosurg Psychiatry 76*, 1491-1496.

114. Jarrett, J. T., and Lansbury, P. T., Jr. (1993) Seeding "one-dimensional crystallization" of amyloid: a pathogenic mechanism in Alzheimer's disease and scrapie?, *Cell 73*, 1055-1058.

115. Kisilevsky, R. (2005) Preparation and propagation of amyloid-enhancing factor, *Methods Mol Biol 299*, 237-241.

116. Zhang, B., Une, Y., Fu, X., Yan, J., Ge, F., Yao, J., Sawashita, J., Mori, M., Tomozawa, H., Kametani, F., and Higuchi, K. (2008) Fecal transmission of AA amyloidosis in the cheetah contributes to high incidence of disease, *Proc Natl Acad Sci U S A 105*, 7263-7268.

117. Manuelidis, E. E., de Figueiredo, J. M., Kim, J. H., Fritch, W. W., and Manuelidis, L. (1988) Transmission studies from blood of Alzheimer disease patients and healthy relatives, *Proc Natl Acad Sci U S A 85*, 4898-4901.

118. Baker, H. F., Ridley, R. M., Duchen, L. W., Crow, T. J., and Bruton, C. J. (1994) Induction of beta (A4)-amyloid in primates by injection of Alzheimer's disease brain homogenate. Comparison with transmission of spongiform encephalopathy, *Mol Neurobiol 8*, 25-39.

119. Meyer-Luehmann, M., Coomaraswamy, J., Bolmont, T., Kaeser, S., Schaefer, C., Kilger, E., Neuenschwander, A., Abramowski, D., Frey, P., Jaton, A. L., Vigouret, J. M., Paganetti, P., Walsh, D. M., Mathews, P. M., Ghiso, J., Staufenbiel, M., Walker, L. C., and Jucker, M. (2006) Exogenous induction of cerebral beta-amyloidogenesis is governed by agent and host, *Science 313*, 1781-1784.

120. Brown, P., Gibbs, C. J., Jr., Rodgers-Johnson, P., Asher, D. M., Sulima, M. P., Bacote, A., Goldfarb, L. G., and Gajdusek, D. C. (1994) Human spongiform encephalopathy: the National Institutes of Health series of 300 cases of experimentally transmitted disease, *Ann Neurol 35*, 513-529.

121. Munson, L., Terio, K. A., Worley, M., Jago, M., Bagot-Smith, A., and Marker, L. (2005) Extrinsic factors significantly affect patterns of disease in free-ranging and captive cheetah (Acinonyx jubatus) populations, *J Wildl Dis 41*, 542-548.

122. Caughey, B., Baron, G. S., Chesebro, B., and Jeffrey, M. (2009) Getting a grip on prions: oligomers, amyloids, and pathological membrane interactions, *Annu Rev Biochem 78*, 177-204.

123. Forman, M. S., Trojanowski, J. Q., and Lee, V. M. (2004) Neurodegenerative diseases: a decade of discoveries paves the way for therapeutic breakthroughs, *Nat Med 10*, 1055-1063.

124. Calhoun, M. E., Burgermeister, P., Phinney, A. L., Stalder, M., Tolnay, M., Wiederhold, K. H., Abramowski, D., Sturchler-Pierrat, C., Sommer, B., Staufenbiel, M., and Jucker, M. (1999) Neuronal overexpression of mutant amyloid precursor protein results in prominent deposition of cerebrovascular amyloid, *Proc Natl Acad Sci U S A 96*, 14088-14093.

125. Wong, P. C., Cai, H., Borchelt, D. R., and Price, D. L. (2002) Genetically engineered mouse models of neurodegenerative diseases, *Nat Neurosci 5*, 633-639.

126. Jarrett, J. T., Berger, E. P., and Lansbury, P. T., Jr. (1993) The carboxy terminus of the beta amyloid protein is critical for the seeding of amyloid formation: implications for the pathogenesis of Alzheimer's disease, *Biochemistry 32*, 4693-4697.

127. Klement, I. A., Skinner, P. J., Kaytor, M. D., Yi, H., Hersch, S. M., Clark, H. B., Zoghbi, H. Y., and Orr, H. T. (1998) Ataxin-1 nuclear localization and aggregation: role in polyglutamine-induced disease in SCA1 transgenic mice, *Cell 95*, 41-53.

128. Koistinaho, M., Ort, M., Cimadevilla, J. M., Vondrous, R., Cordell, B., Koistinaho, J., Bures, J., and Higgins, L. S. (2001) Specific spatial learning deficits become severe with age in beta -amyloid precursor protein transgenic mice that harbor diffuse beta -amyloid deposits but do not form plaques, *Proc Natl Acad Sci U S A 98*, 14675-14680.

129. Zerbinatti, C. V., Wozniak, D. F., Cirrito, J., Cam, J. A., Osaka, H., Bales, K. R., Zhuo, M., Paul, S. M., Holtzman, D. M., and Bu, G. (2004) Increased soluble amyloid-beta peptide and memory deficits in amyloid model mice overexpressing the low-density lipoprotein receptor-related protein, *Proc Natl Acad Sci U S A 101*, 1075-1080.

130. Koistinaho, M., Kettunen, M. I., Goldsteins, G., Keinanen, R., Salminen, A., Ort, M., Bures, J., Liu, D., Kauppinen, R. A., Higgins, L. S., and Koistinaho, J. (2002) Beta-amyloid precursor protein transgenic mice that harbor diffuse A beta deposits but do not form plaques show increased ischemic vulnerability: role of inflammation, *Proc Natl Acad Sci U S A 99*, 1610-1615.

131. Walsh, D. M., Klyubin, I., Fadeeva, J. V., Cullen, W. K., Anwyl, R., Wolfe, M. S., Rowan, M. J., and Selkoe, D. J. (2002) Naturally secreted oligomers of amyloid beta protein potently inhibit hippocampal long-term potentiation in vivo, *Nature 416*, 535-539.

132. Lambert, M. P., Viola, K. L., Chromy, B. A., Chang, L., Morgan, T. E., Yu, J., Venton, D. L., Krafft, G. A., Finch, C. E., and Klein, W. L. (2001) Vaccination with soluble Abeta oligomers generates toxicity-neutralizing antibodies, *J Neurochem 79*, 595-605.

133. Creighton, T. E. (1990) *Protein structure : a practical approach*, IRL Press, Oxford, England ; New York.

134. Pain, R. H. (2000) *Mechanisms of protein folding*, 2nd ed., Oxford University Press, Oxford ; New York.

135. Lee, B. C., Kumauchi, M., and Hoff, W. D. (2010) Modulating native-like residual structure in the fully denatured state of photoactive yellow protein affects its refolding, *J Biol Chem*.

136. Shan, B., Eliezer, D., and Raleigh, D. P. (2009) The unfolded state of the C-terminal domain of the ribosomal protein L9 contains both native and non-native structure, *Biochemistry 48*, 4707-4719.

137. Cortajarena, A. L., Lois, G., Sherman, E., O'Hern, C. S., Regan, L., and Haran, G. (2008) Non-random-coil behavior as a consequence of extensive PPII structure in the denatured state, *J Mol Biol 382*, 203-212.

138. Mok, K. H., Kuhn, L. T., Goez, M., Day, I. J., Lin, J. C., Andersen, N. H., and Hore, P. J. (2007) A pre-existing hydrophobic collapse in the unfolded state of an ultrafast folding protein, *Nature 447*, 106-109.

139. Robic, S., Guzman-Casado, M., Sanchez-Ruiz, J. M., and Marqusee, S. (2003) Role of residual structure in the unfolded state of a thermophilic protein, *Proc Natl Acad Sci U S A 100*, 11345-11349.

140. Klein-Seetharaman, J., Oikawa, M., Grimshaw, S. B., Wirmer, J., Duchardt, E., Ueda, T., Imoto, T., Smith, L. J., Dobson, C. M., and Schwalbe, H. (2002) Long-range interactions within a nonnative protein, *Science 295*, 1719-1722.

141. Roder, H., and Colon, W. (1997) Kinetic role of early intermediates in protein folding, *Curr Opin Struct Biol 7*, 15-28.

142. Shakhnovich, E. I. (1997) Theoretical studies of protein-folding thermodynamics and kinetics, *Curr Opin Struct Biol 7*, 29-40.

143. Abkevich, V. I., Gutin, A. M., and Shakhnovich, E. I. (1994) Specific nucleus as the transition state for protein folding: evidence from the lattice model, *Biochemistry 33*, 10026-10036.

144. Faisca, P. F., Travasso, R. D., Ball, R. C., and Shakhnovich, E. I. (2008) Identifying critical residues in protein folding: Insights from phi-value and P(fold) analysis, *J Chem Phys 129*, 095108.

145. De Prat Gay, G., Ruiz-Sanz, J., Neira, J. L., Itzhaki, L. S., and Fersht, A. R. (1995) Folding of a nascent polypeptide chain in vitro: cooperative formation of structure in a protein module, *Proc Natl Acad Sci U S A 92*, 3683-3686.

146. Lopez-Hernandez, E., and Serrano, L. (1996) Structure of the transition state for folding of the 129 aa protein CheY resembles that of a smaller protein, CI-2, *Fold Des 1*, 43-55.

147. Viguera, A. R., Serrano, L., and Wilmanns, M. (1996) Different folding transition states may result in the same native structure, *Nat Struct Biol 3*, 874-880.

148. Karplus, M., and Weaver, D. L. (1994) Protein folding dynamics: the diffusion-collision model and experimental data, *Protein Sci 3*, 650-668.

149. Wedemeyer, W. J., Welker, E., Narayan, M., and Scheraga, H. A. (2000) Disulfide bonds and protein folding, *Biochemistry 39*, 4207-4216.

150. Narayan, M., Welker, E., Wedemeyer, W. J., and Scheraga, H. A. (2000) Oxidative folding of proteins, *Acc Chem Res 33*, 805-812.

151. Li, X., Hood, R. J., Wedemeyer, W. J., and Watson, J. T. (2005) Characterization of peptide folding nuclei by hydrogen/deuterium exchange-mass spectrometry, *Protein Sci 14*, 1922-1928.

152. Oas, T. G., and Kim, P. S. (1988) A peptide model of a protein folding intermediate, *Nature 336*, 42-48.

153. Hua, Q. X., Mayer, J. P., Jia, W., Zhang, J., and Weiss, M. A. (2006) The folding nucleus of the insulin superfamily: a flexible peptide model foreshadows the native state, *J Biol Chem 281*, 28131-28142.

154. Feige, M. J., Hagn, F., Esser, J., Kessler, H., and Buchner, J. (2007) Influence of the internal disulfide bridge on the folding pathway of the CL antibody domain, *J Mol Biol 365*, 1232-1244.

155. Wedemeyer, W. J., Welker, E., and Scheraga, H. A. (2002) Proline cis-trans isomerization and protein folding, *Biochemistry 41*, 14637-14644.

156. Schmid, F. X., and Blaschek, H. (1981) A native-like intermediate on the ribonuclease A folding pathway. 2. Comparison of its properties to native ribonuclease A, *Eur J Biochem 114*, 111-117.

157. Schmid, F. X. (1982) Proline isomerization in unfolded ribonuclease A. The equilibrium between fast-folding and slow-folding species is independent of temperature, *Eur J Biochem 128*, 77-80.

158. Schmid, F. X., and Baldwin, R. L. (1978) Acid catalysis of the formation of the slow-folding species of RNase A: evidence that the reaction is proline isomerization, *Proc Natl Acad Sci U S A 75*, 4764-4768.

159. Brandts, J. F., Halvorson, H. R., and Brennan, M. (1975) Consideration of the Possibility that the slow step in protein denaturation reactions is due to cis-trans isomerism of proline residues, *Biochemistry 14*, 4953-4963.

160. Jackson, S. E. (1998) How do small single-domain proteins fold?, *Fold Des 3*, R81-91.

161. O'Brien, E. P., Dima, R. I., Brooks, B., and Thirumalai, D. (2007) Interactions between hydrophobic and ionic solutes in aqueous guanidinium chloride and urea solutions: lessons for protein denaturation mechanism, *J Am Chem Soc 129*, 7346-7353.

162. Lim, W. K., Rosgen, J., and Englander, S. W. (2009) Urea, but not guanidinium, destabilizes proteins by forming hydrogen bonds to the peptide group, *Proc Natl Acad Sci U S A 106*, 2595-2600.

163. Chalikian, T. V., and Bresiauer, K. J. (1996) On volume changes accompanying conformational transitions of biopolymers, *Biopolymers 39*, 619-626.

164. Prehoda, K. E., Mooberry, E. S., and Markley, J. L. (1998) Pressure denaturation of proteins: evaluation of compressibility effects, *Biochemistry 37*, 5785-5790.

165. Dill, K. A. (1990) Dominant forces in protein folding, *Biochemistry 29*, 7133-7155.

166. Shastry, M. C., Luck, S. D., and Roder, H. (1998) A continuous-flow capillary mixing method to monitor reactions on the microsecond time scale, *Biophys J 74*, 2714-2721.

167. Lapidus, L. J., Yao, S., McGarrity, K. S., Hertzog, D. E., Tubman, E., and Bakajin, O. (2007) Protein hydrophobic collapse and early folding steps observed in a microfluidic mixer, *Biophys J 93*, 218-224.

168. Nölting, B. (1999) *Protein folding kinetics : biophysical methods*, Springer, Berlin ; New York.

169. Uversky, V. N., Winter, S., and Lober, G. (1996) Use of fluorescence decay times of 8-ANS-protein complexes to study the conformational transitions in proteins which unfold through the molten globule state, *Biophys Chem 60*, 79-88.

170. Ptitsyn, O. B. (1995) Molten globule and protein folding, *Adv Protein Chem 47*, 83-229.

171. Latypov, R. F., Liu, D., Gunasekaran, K., Harvey, T. S., Razinkov, V. I., and Raibekas, A. A. (2008) Structural and thermodynamic effects of ANS binding to human interleukin-1 receptor antagonist, *Protein Sci 17*, 652-663.

172. Kumar, T. K., Jayaraman, G., Lin, W. Y., and Yu, C. (1996) Effect of chaotropic denaturant on the binding of 1-anilino-8-naphthalene sulfonic acid to proteins, *Biochim Biophys Acta 1294*, 103-105.

173. Engelhard, M., and Evans, P. A. (1995) Kinetics of interaction of partially folded proteins with a hydrophobic dye: evidence that molten globule character is maximal in early folding intermediates, *Protein Sci 4*, 1553-1562.

174. Kelly, S. M., Jess, T. J., and Price, N. C. (2005) How to study proteins by circular dichroism, *Biochim Biophys Acta 1751*, 119-139.

175. Garcia, R. A., Pantazatos, D., and Villarreal, F. J. (2004) Hydrogen/deuterium exchange mass spectrometry for investigating protein-ligand interactions, *Assay Drug Dev Technol 2*, 81-91.

176. Katta, V., and Chait, B. T. (1991) Conformational changes in proteins probed by hydrogen-exchange electrospray-ionization mass spectrometry, *Rapid Commun Mass Spectrom 5*, 214-217.

177. Fersht, A. R., Matouschek, A., and Serrano, L. (1992) The folding of an enzyme. I. Theory of protein engineering analysis of stability and pathway of protein folding, *J Mol Biol 224*, 771-782.

178. Matouschek, A., and Fersht, A. R. (1991) Protein engineering in analysis of protein folding pathways and stability, *Methods Enzymol 202*, 82-112.

179. Matouschek, A., Kellis, J. T., Jr., Serrano, L., and Fersht, A. R. (1989) Mapping the transition state and pathway of protein folding by protein engineering, *Nature 340*, 122-126.

180. Grantcharova, V., Alm, E. J., Baker, D., and Horwich, A. L. (2001) Mechanisms of protein folding, *Curr Opin Struct Biol 11*, 70-82.

181. Plaxco, K. W., Simons, K. T., and Baker, D. (1998) Contact order, transition state placement and the refolding rates of single domain proteins, *J Mol Biol 277*, 985-994.

182. Friel, C. T., Capaldi, A. P., and Radford, S. E. (2003) Structural analysis of the rate-limiting transition states in the folding of Im7 and Im9: similarities and differences in the folding of homologous proteins, *J Mol Biol 326*, 293-305.

183. Moran, L. B., Schneider, J. P., Kentsis, A., Reddy, G. A., and Sosnick, T. R. (1999) Transition state heterogeneity in GCN4 coiled coil folding studied by using multisite mutations and crosslinking, *Proc Natl Acad Sci U S A 96*, 10699-10704.

184. Kim, D. E., Fisher, C., and Baker, D. (2000) A breakdown of symmetry in the folding transition state of protein L, *J Mol Biol 298*, 971-984.

185. McCallister, E. L., Alm, E., and Baker, D. (2000) Critical role of beta-hairpin formation in protein G folding, *Nat Struct Biol 7*, 669-673.

186. Fersht, A. R. (1995) Optimization of rates of protein folding: the nucleation-condensation mechanism and its implications, *Proc Natl Acad Sci U S A 92*, 10869-10873.

187. Gutin, A. M., Abkevich, V. I., and Shakhnovich, E. I. (1995) Evolution-like selection of fast-folding model proteins, *Proc Natl Acad Sci U S A 92*, 1282-1286.

188. Irback, A., Peterson, C., and Potthast, F. (1996) Evidence for nonrandom hydrophobicity structures in protein chains, *Proc Natl Acad Sci U S A 93*, 9533-9538.

189. Gutin, A. M., Abkevich, V. I., and Shakhnovich, E. I. (1995) Is burst hydrophobic collapse necessary for protein folding?, *Biochemistry 34*, 3066-3076.

190. Mirny, L. A., Abkevich, V., and Shakhnovich, E. I. (1996) Universality and diversity of the protein folding scenarios: a comprehensive analysis with the aid of a lattice model, *Fold Des 1*, 103-116.

191. Houry, W. A., Rothwarf, D. M., and Scheraga, H. A. (1995) The nature of the initial step in the conformational folding of disulphide-intact ribonuclease A, *Nat Struct Biol 2*, 495-503.

192. Parker, M. J., Spencer, J., and Clarke, A. R. (1995) An integrated kinetic analysis of intermediates and transition states in protein folding reactions, *J Mol Biol 253*, 771-786.

193. Khorasanizadeh, S., Peters, I. D., and Roder, H. (1996) Evidence for a three-state model of protein folding from kinetic analysis of ubiquitin variants with altered core residues, *Nat Struct Biol 3*, 193-205.

194. Sauder, J. M., MacKenzie, N. E., and Roder, H. (1996) Kinetic mechanism of folding and unfolding of Rhodobacter capsulatus cytochrome c2, *Biochemistry 35*, 16852-16862.

195. Yamasaki, K., Ogasahara, K., Yutani, K., Oobatake, M., and Kanaya, S. (1995) Folding pathway of Escherichia coli ribonuclease HI: a circular dichroism, fluorescence, and NMR study, *Biochemistry 34*, 16552-16562.

196. Kim, P. S., and Baldwin, R. L. (1982) Specific intermediates in the folding reactions of small proteins and the mechanism of protein folding, *Annu Rev Biochem 51*, 459-489.

197. Ptitsyn, O. B., and Rashin, A. A. (1975) A model of myoglobin self-organization, *Biophys Chem 3*, 1-20.

198. Epand, R. M., and Scheraga, H. A. (1968) The influence of long-range interactions on the structure of myoglobin, *Biochemistry 7*, 2864-2872.

199. Avbelj, F., and Baldwin, R. L. (2002) Role of backbone solvation in determining thermodynamic beta propensities of the amino acids, *Proc Natl Acad Sci U S A 99*, 1309-1313.

200. Creamer, T. P., and Rose, G. D. (1994) Alpha-helix-forming propensities in peptides and proteins, *Proteins 19*, 85-97.

201. Wetlaufer, D. B. (1973) Nucleation, rapid folding, and globular intrachain regions in proteins, *Proc Natl Acad Sci U S A 70*, 697-701.

202. Bennion, B. J., and Daggett, V. (2003) The molecular basis for the chemical denaturation of proteins by urea, *Proc Natl Acad Sci U S A 100*, 5142-5147.

203. Kauzmann, W. (1959) Some factors in the interpretation of protein denaturation, *Adv Protein Chem 14*, 1-63.

204. Daggett, V., and Fersht, A. R. (2003) Is there a unifying mechanism for protein folding?, *Trends Biochem Sci 28*, 18-25.

205. Ptitsyn, O. B. (1995) Structures of folding intermediates, *Curr Opin Struct Biol 5*, 74-78.

206. Fersht, A. R., and Daggett, V. (2002) Protein folding and unfolding at atomic resolution, *Cell 108*, 573-582.

207. Day, R., and Daggett, V. (2007) Direct observation of microscopic reversibility in single-molecule protein folding, *J Mol Biol 366*, 677-686.

208. Klimov, D. K., and Thirumalai, D. (2001) Multiple protein folding nuclei and the transition state ensemble in two-state proteins, *Proteins 43*, 465-475.

209. Onuchic, J. N., Socci, N. D., Luthey-Schulten, Z., and Wolynes, P. G. (1996) Protein folding funnels: the nature of the transition state ensemble, *Fold Des 1*, 441-450.

210. Anfinsen, C. B. (1973) Principles that govern the folding of protein chains, *Science 181*, 223-230.

211. Haber, E., and Anfinsen, C. B. (1962) Side-chain interactions governing the pairing of half-cystine residues in ribonuclease, *J Biol Chem 237*, 1839-1844.

212. Dill, K. A., Ozkan, S. B., Shell, M. S., and Weikl, T. R. (2008) The protein folding problem, *Annu Rev Biophys 37*, 289-316.

213. Leopold, P. E., Montal, M., and Onuchic, J. N. (1992) Protein folding funnels: a kinetic approach to the sequence-structure relationship, *Proc Natl Acad Sci U S A 89*, 8721-8725.

214. Bryngelson, J. D., Onuchic, J. N., Socci, N. D., and Wolynes, P. G. (1995) Funnels, pathways, and the energy landscape of protein folding: a synthesis, *Proteins 21*, 167-195.

215. Dinner, A. R., Sali, A., Smith, L. J., Dobson, C. M., and Karplus, M. (2000) Understanding protein folding via free-energy surfaces from theory and experiment, *Trends Biochem Sci 25*, 331-339.

216. Go, N. (1983) Theoretical studies of protein folding, *Annu Rev Biophys Bioeng 12*, 183-210.

217. Mallucci, G., and Collinge, J. (2005) Rational targeting for prion therapeutics, *Nat Rev Neurosci 6*, 23-34.

218. Wildegger, G., Liemann, S., and Glockshuber, R. (1999) Extremely rapid folding of the C-terminal domain of the prion protein without kinetic intermediates, *Nat Struct Biol 6*, 550-553.

219. Apetri, A. C., Maki, K., Roder, H., and Surewicz, W. K. (2006) Early intermediate in human prion protein folding as evidenced by ultrarapid mixing experiments, *J Am Chem Soc 128*, 11673-11678.

220. Apetri, A. C., and Surewicz, W. K. (2002) Kinetic intermediate in the folding of human prion protein, *J Biol Chem 277*, 44589-44592.

221. Apetri, A. C., Surewicz, K., and Surewicz, W. K. (2004) The effect of disease-associated mutations on the folding pathway of human prion protein, *J Biol Chem 279*, 18008-18014.

222. Stohr, J., Weinmann, N., Wille, H., Kaimann, T., Nagel-Steger, L., Birkmann, E., Panza, G., Prusiner, S. B., Eigen, M., and Riesner, D. (2008) Mechanisms of prion protein assembly into amyloid, *Proc Natl Acad Sci U S A 105*, 2409-2414.

223. Jansen, K., Schafer, O., Birkmann, E., Post, K., Serban, H., Prusiner, S. B., and Riesner, D. (2001) Structural intermediates in the putative pathway from the cellular prion protein to the pathogenic form, *Biol Chem 382*, 683-691.

224. Gerber, R., Tahiri-Alaoui, A., Hore, P. J., and James, W. (2007) Oligomerization of the human prion protein proceeds via a molten globule intermediate, *J Biol Chem 282*, 6300-6307.

225. Gerber, R., Tahiri-Alaoui, A., Hore, P. J., and James, W. (2008) Conformational pH dependence of intermediate states during oligomerization of the human prion protein, *Protein Sci 17*, 537-544.

226. El Moustaine, D., Perrier, V., Smeller, L., Lange, R., and Torrent, J. (2008) Full-length prion protein aggregates to amyloid fibrils and spherical particles by distinct pathways, *FEBS J 275*, 2021-2031.

227. O'Sullivan, D. B., Jones, C. E., Abdelraheim, S. R., Thompsett, A. R., Brazier, M. W., Toms, H., Brown, D. R., and Viles, J. H. (2007) NMR characterization of the pH 4 beta-intermediate of the prion protein: the N-terminal half of the protein remains unstructured and retains a high degree of flexibility, *Biochem J 401*, 533-540.

228. Moudjou, M., Treguer, E., Rezaei, H., Sabuncu, E., Neuendorf, E., Groschup, M. H., Grosclaude, J., and Laude, H. (2004) Glycan-controlled epitopes of prion protein include a major determinant of susceptibility to sheep scrapie, *J Virol 78*, 9270-9276.

229. Thackray, A. M., Fitzmaurice, T. J., Hopkins, L., and Bujdoso, R. (2006) Ovine plasma prion protein levels show genotypic variation detected by C-terminal epitopes not exposed in cell-surface PrPC, *Biochem J 400*, 349-358.

230. Tenzer, S., Stoltze, L., Schonfisch, B., Dengjel, J., Muller, M., Stevanovic, S., Rammensee, H. G., and Schild, H. (2004) Quantitative analysis of prion-protein degradation by constitutive and immuno-20S proteasomes indicates differences correlated with disease susceptibility, *J Immunol 172*, 1083-1091.

231. Bossers, A., Belt, P., Raymond, G. J., Caughey, B., de Vries, R., and Smits, M. A. (1997) Scrapie susceptibility-linked polymorphisms modulate the in vitro conversion of sheep prion protein to protease-resistant forms, *Proc Natl Acad Sci U S A 94*, 4931-4936.

232. Bossers, A., de Vries, R., and Smits, M. A. (2000) Susceptibility of sheep for scrapie as assessed by in vitro conversion of nine naturally occurring variants of PrP, *J Virol 74*, 1407-1414.

233. Rezaei, H., Choiset, Y., Eghiaian, F., Treguer, E., Mentre, P., Debey, P., Grosclaude, J., and Haertle, T. (2002) Amyloidogenic unfolding intermediates differentiate sheep prion protein variants, *J Mol Biol 322*, 799-814.

234. Sabuncu, E., Petit, S., Le Dur, A., Lan Lai, T., Vilotte, J. L., Laude, H., and Vilette, D. (2003) PrP polymorphisms tightly control sheep prion replication in cultured cells, *J Virol 77*, 2696-2700.

235. Wong, E., Thackray, A. M., and Bujdoso, R. (2004) Copper induces increased beta-sheet content in the scrapie-susceptible ovine prion protein PrPVRQ compared with the resistant allelic variant PrPARR, *Biochem J 380*, 273-282.

236. Kelly, J. W. (1998) The alternative conformations of amyloidogenic proteins and their multi-step assembly pathways, *Curr Opin Struct Biol 8*, 101-106.

237. Fitzmaurice, T. J., Burke, D. F., Hopkins, L., Yang, S., Yu, S., Sy, M. S., Thackray, A. M., and Bujdoso, R. (2008) The stability and aggregation of ovine prion protein associated with classical and atypical scrapie correlates with the ease of unwinding of helix-2, *Biochem J 409*, 367-375.

238. Rezaei, H., Marc, D., Choiset, Y., Takahashi, M., Hui Bon Hoa, G., Haertle, T., Grosclaude, J., and Debey, P. (2000) High yield purification and physico-chemical properties of full-length recombinant allelic variants of sheep prion protein linked to scrapie susceptibility, *Eur J Biochem 267*, 2833-2839.

239. Welker, E., Wedemeyer, W. J., and Scheraga, H. A. (2001) A role for intermolecular disulfide bonds in prion diseases?, *Proc Natl Acad Sci U S A 98*, 4334-4336.

240. Welker, E., Raymond, L. D., Scheraga, H. A., and Caughey, B. (2002) Intramolecular versus intermolecular disulfide bonds in prion proteins, *J Biol Chem 277*, 33477-33481.

241. Liemann, S., and Glockshuber, R. (1999) Influence of amino acid substitutions related to inherited human prion diseases on the thermodynamic stability of the cellular prion protein, *Biochemistry 38*, 3258-3267.

242. Swietnicki, W., Petersen, R. B., Gambetti, P., and Surewicz, W. K. (1998) Familial mutations and the thermodynamic stability of the recombinant human prion protein, *J Biol Chem 273*, 31048-31052.

243. Bae, S. H., Legname, G., Serban, A., Prusiner, S. B., Wright, P. E., and Dyson, H. J. (2009) Prion proteins with pathogenic and protective mutations show similar structure and dynamics, *Biochemistry 48*, 8120-8128.

244. Kremer, W., Kachel, N., Kuwata, K., Akasaka, K., and Kalbitzer, H. R. (2007) Species-specific differences in the intermediate states of human and Syrian hamster prion protein detected by high pressure NMR spectroscopy, *J Biol Chem 282*, 22689-22698.

245. Kuwata, K., Kamatari, Y. O., Akasaka, K., and James, T. L. (2004) Slow conformational dynamics in the hamster prion protein, *Biochemistry 43*, 4439-4446.

246. Kuwata, K., Li, H., Yamada, H., Legname, G., Prusiner, S. B., Akasaka, K., and James, T. L. (2002) Locally disordered conformer of the hamster prion protein: a crucial intermediate to PrPSc?, *Biochemistry 41*, 12277-12283.

247. Yanai, A., Meiner, Z., Gahali, I., Gabizon, R., and Taraboulos, A. (1999) Subcellular trafficking abnormalities of a prion protein with a disrupted disulfide loop, *FEBS Lett 460*, 11-16.

248. Herrmann, L. M., and Caughey, B. (1998) The importance of the disulfide bond in prion protein conversion, *Neuroreport 9*, 2457-2461.

249. Muramoto, T., Scott, M., Cohen, F. E., and Prusiner, S. B. (1996) Recombinant scrapie-like prion protein of 106 amino acids is soluble, *Proc Natl Acad Sci U S A 93*, 15457-15462.

250. Horiuchi, M., and Caughey, B. (1999) Prion protein interconversions and the transmissible spongiform encephalopathies, *Structure 7*, R231-240.

251. Jackson, G. S., Hosszu, L. L., Power, A., Hill, A. F., Kenney, J., Saibil, H., Craven, C. J., Waltho, J. P., Clarke, A. R., and Collinge, J. (1999) Reversible conversion of monomeric human prion protein between native and fibrilogenic conformations, *Science 283*, 1935-1937.

252. Tompa, P., Tusnady, G. E., Friedrich, P., and Simon, I. (2002) The role of dimerization in prion replication, *Biophys J 82*, 1711-1718.

253. Lee, S., and Eisenberg, D. (2003) Seeded conversion of recombinant prion protein to a disulfide-bonded oligomer by a reduction-oxidation process, *Nat Struct Biol 10*, 725-730.

254. Shin, J. Y., Shin, J. I., Kim, J. S., Yang, Y. S., Shin, Y. K., Kim, K. K., Lee, S., and Kweon, D. H. (2009) Disulfide bond as a structural determinant of prion protein membrane insertion, *Mol Cells 27*, 673-680.

255. Prusiner, S. B. (1998) Prions, *Proc Natl Acad Sci U S A 95*, 13363-13383.

256. Hill, A. F., Joiner, S., Linehan, J., Desbruslais, M., Lantos, P. L., and Collinge, J. (2000) Species-barrier-independent prion replication in apparently resistant species, *Proc Natl Acad Sci U S A 97*, 10248-10253.

257. Donne, D. G., Viles, J. H., Groth, D., Mehlhorn, I., James, T. L., Cohen, F. E., Prusiner, S. B., Wright, P. E., and Dyson, H. J. (1997) Structure of the recombinant full-length hamster prion protein PrP(29-231): the N terminus is highly flexible, *Proc Natl Acad Sci U S A 94*, 13452-13457.

258. Zahn, R., Liu, A., Luhrs, T., Riek, R., von Schroetter, C., Lopez Garcia, F., Billeter, M., Calzolai, L., Wider, G., and Wuthrich, K. (2000) NMR solution structure of the human prion protein, *Proc Natl Acad Sci U S A 97*, 145-150.

259. Thackray, A. M., Yang, S., Wong, E., Fitzmaurice, T. J., Morgan-Warren, R. J., and Bujdoso, R. (2004) Conformational variation between allelic variants of cell-surface ovine prion protein, *Biochem J 381*, 221-229.

260. Paludi, D., Thellung, S., Chiovitti, K., Corsaro, A., Villa, V., Russo, C., Ianieri, A., Bertsch, U., Kretzschmar, H. A., Aceto, A., and Florio, T. (2007) Different structural stability and toxicity of PrP(ARR) and PrP(ARQ) sheep prion protein variants, *J Neurochem 103*, 2291-2300.

261. De Simone, A., Zagari, A., and Derreumaux, P. (2007) Structural and hydration properties of the partially unfolded states of the prion protein, *Biophys J 93*, 1284-1292.

262. Peterman, B. F. (1979) Measurement of the dead time of a fluorescence stopped-flow instrument, *Anal Biochem 93*, 442-444.

263. Broering, J. M., and Bommarius, A. S. (2007) Cation and strong co-solute effects on protein kinetic stability, *Biochem Soc Trans 35*, 1602-1605.

264. Jackson, S. E., and Fersht, A. R. (1991) Folding of chymotrypsin inhibitor 2. 1. Evidence for a two-state transition, *Biochemistry 30*, 10428-10435.

265. Tanford, C. (1970) Protein denaturation. C. Theoretical models for the mechanism of denaturation, *Adv Protein Chem 24*, 1-95.

266. Chen, B. L., Baase, W. A., Nicholson, H., and Schellman, J. A. (1992) Folding kinetics of T4 lysozyme and nine mutants at 12 degrees C, *Biochemistry 31*, 1464-1476.

267. Bossers, A., Harders, F. L., and Smits, M. A. (1999) PrP genotype frequencies of the most dominant sheep breed in a country free from scrapie, *Arch Virol 144*, 829-834.

268. Hunter, N., and Cairns, D. (1998) Scrapie-free Merino and Poll Dorset sheep from Australia and New Zealand have normal frequencies of scrapie-susceptible PrP genotypes, *J Gen Virol 79 (Pt 8)*, 2079-2082.

269. Hunter, N., Cairns, D., Foster, J. D., Smith, G., Goldmann, W., and Donnelly, K. (1997) Is scrapie solely a genetic disease?, *Nature 386*, 137.

270. Hosszu, L. L., Jackson, G. S., Trevitt, C. R., Jones, S., Batchelor, M., Bhelt, D., Prodromidou, K., Clarke, A. R., Waltho, J. P., and Collinge, J. (2004) The residue 129 polymorphism in human prion protein does not confer susceptibility to Creutzfeldt-Jakob disease by altering the structure or global stability of PrPC, *J Biol Chem 279*, 28515-28521.

271. McCully, M. E., Beck, D. A., and Daggett, V. (2008) Microscopic reversibility of protein folding in molecular dynamics simulations of the engrailed homeodomain, *Biochemistry 47*, 7079-7089.

272. Maiti, N. R., and Surewicz, W. K. (2001) The role of disulfide bridge in the folding and stability of the recombinant human prion protein, *J Biol Chem 276*, 2427-2431.

273. Maity, H., Lim, W. K., Rumbley, J. N., and Englander, S. W. (2003) Protein hydrogen exchange mechanism: local fluctuations, *Protein Sci 12*, 153-160.

274. Smith, D. L., Deng, Y., and Zhang, Z. (1997) Probing the non-covalent structure of proteins by amide hydrogen exchange and mass spectrometry, *J Mass Spectrom 32*, 135-146.

275. Woody, R. W., Sugeta, H., and Kodama, T. S. (1996) [Circular dichroism of proteins: recent developments in analysis and prediction], *Tanpakushitsu Kakusan Koso 41*, 56-69.

276. Hosszu, L. L., Baxter, N. J., Jackson, G. S., Power, A., Clarke, A. R., Waltho, J. P., Craven, C. J., and Collinge, J. (1999) Structural mobility of the human prion protein probed by backbone hydrogen exchange, *Nat Struct Biol 6*, 740-743.

277. Lapidus, L. J., Eaton, W. A., and Hofrichter, J. (2000) Measuring the rate of intramolecular contact formation in polypeptides, *Proc Natl Acad Sci U S A 97*, 7220-7225.

278. Sudhakar, K., Phillips, C. M., Owen, C. S., and Vanderkooi, J. M. (1995) Dynamics of parvalbumin studied by fluorescence emission and triplet absorption spectroscopy of tryptophan, *Biochemistry 34*, 1355-1363.

279. Bent, D. V., and Hayon, E. (1975) Excited state chemistry of aromatic amino acids and related peptides. III. Tryptophan, *J Am Chem Soc 97*, 2612-2619.

280. Gonnelli, M., and Strambini, G. B. (1995) Phosphorescence lifetime of tryptophan in proteins, *Biochemistry 34*, 13847-13857.